MULTICOMPONENT SEISMIC ANALYSIS AND CALIBRATION TO IMPROVE RECOVERY FROM ALGAL MOUNDS: APPLICATION TO THE ROADRUNNER/TOWAOC AREA OF THE PARADOX BASIN, UTE MOUNTAIN UTE RESERVATION, COLORADO

Fifth Semi-Annual Technical Report – Nov. 1, 2004 through April 31, 2005

Paul La Pointe[1]
Claudia Rebne[2]
Steve Dobbs[3]
Colby VanDenberg[3]
Rich Van Dok[4]
Robert Benson[5]

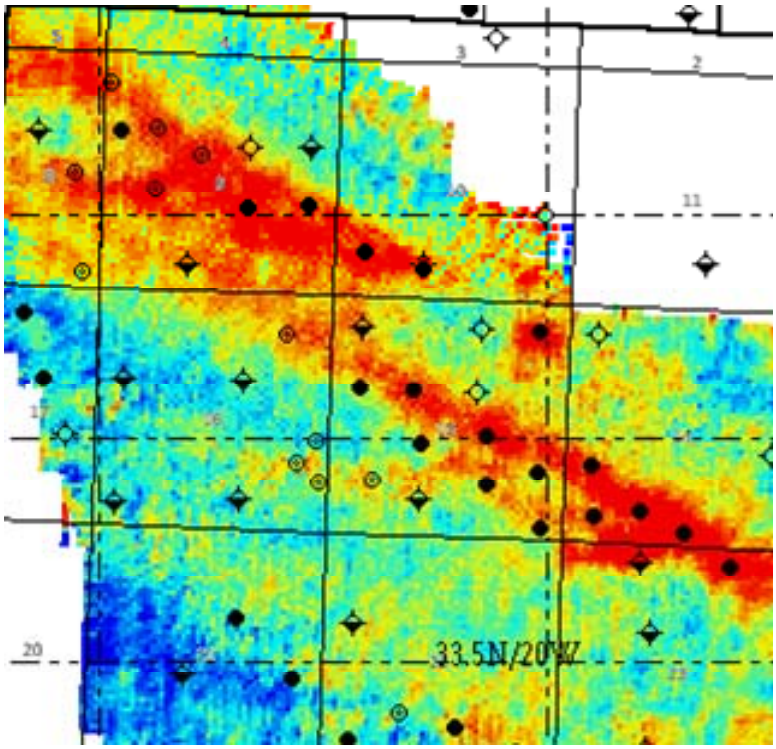

Interpreted P-Wave Data Showing Correspondence with Production

Report Date: July 18, 2005

DOE Award Number: DE-FG26-02NT15451

[1]Golder Associates Inc.
18300 NE Union Hill Road, Suite 200
Redmond, WA 98052

[2]Legacy Energy Corporation
P. O. Box 480272
Denver, CO 80248

[3]Red Willow Production Company
P.O. Box 737
Ignacio, Colorado 81137

[4]WesternGeco
1625 Broadway, Suite 1300
Denver, CO 80202

[5]Colorado School of Mines
Golden, CO 80401

"This report was prepared as an account of work sponsored by an agency of the United States Government. Neither the United States Government nor any agency thereof, nor any of their employees, make any warranty, express or implied, or assumes any legal liability or responsibility for the accuracy, completeness, or usefulness of any information, apparatus, product, or process disclosed, or represents that its use would not infringe privately owned rights. Reference herein to any specific commercial product, process, or service by trade name, trademark, manufacturer, or otherwise does not necessarily constitute or imply its endorsement, recommendation, or favoring by the United States Government or any agency thereof. The views and opinions of authors expressed herein do not necessarily state or reflect those of the United States Government or any agency thereof"

ABSTRACT

This report describes the results made in fulfillment of contract DE-FG26-02NT15451, "Multicomponent Seismic Analysis and Calibration to Improve Recovery from Algal Mounds: Application to the Roadrunner/Towaoc Area of the Paradox Basin, Ute Mountain Ute Reservation, Colorado", for the Fifth Semi-Annual Report covering the time period November 1, 2004 through April 31, 2005.

During this period, processing of the PS and SS wave data and final interpretation of the P-wave data were the project's primary focus. The P-wave interpretation was completed, as was a substantial portion of the PS- and SS-wave processing. Preliminary results are currently being used to locate wells in the survey area by Red Willow Production company.

Seismic attribute mapping, multivariate regressions analysis and resulting depth structure maps help in identifying current Ismay mound producing areas. Furthermore, based on the P-wave seismic interpretation, it appears that there are prospective undrilled Ismay mound areas within the 3D survey. The northwest portion of the 3D area contains the greatest undrilled potential. Red Mountain Energy, LLC, a company of the Southern Ute Indian Tribe, is currently permitting five drilling locations within the Roadrunner survey. Red Mountain is working closely with the Ute Mountain Ute Tribe to develop these potential resources. Red Mountain hopes to drill one or two of these proposed wells in the summer of 2005.

Interpretation of the PS- and SS-wave is currently underway, and will be used to locate additional drilling targets. Decision Point 3, regarding the decision to proceed with the PS- and SS-wave interpretation, was successfully passed.

Table of Contents

1 Introduction 1
2 Executive Summary 2
3 Experimental Methods 4
3.1 Acquisition Program Geometry & Parameters 4
3.2 Processing Workflow 5
3.3 Interpretation 6
4 Results and Discussion 9
4.1 Seismic Processing & Interpretation 9
4.1.1 Processing 9
4.1.2 PS – Wave processing 10
4.1.3 Azimuthal analysis 10
4.1.4 SS-Wave Processing 11
4.2 Interpretation 47
4.2.1 Map Generation 47
4.2.2 Time Structure Maps 48
4.2.3 Isopach Maps 69
4.2.4 Depth Structure Maps 69
4.3 P-Wave Seismic Interpretation – New Oil and Gas Drilling Proposed 70
4.4 Predicting Productive Properties of Wells from P-wave Data 70
4.5 Technology Transfer 75
4.5.1 Publications & Presentations 75
4.5.2 Project Website 75
4.6 Decision Points 76
5 Conclusions 77
References 78
6 List of Acronyms and Abbreviations 79
7 Appendices 80
7.1 81

List of Figures

Figure 3-1. Acquisition geometry for multicomponent seismic survey. 4
Figure 3-2. Correlation of lithostratigraphic boundaries with processed P-wave data..... 6
Figure 3-3. Detail of log expressions for the lithostratigraphic boundaries and their corresponding seismic picks. 7
Figure 4-1. Typical Shot Record: P source – Z detector..... 12
Figure 4-2. Typical Shot Record: P source – X detector. 13
Figure 4-3. Typical Shot Record: P source – Y detector. 14
Figure 4-4. Typical Shot Record: S1 source – Z detector..... 15
Figure 4-5. Typical Shot Record: S1 source – X detector. 16
Figure 4-6. Typical Shot Record: S1 source – Y detector. 17
Figure 4-7. Typical Shot Record: S2 source – Z detector..... 18
Figure 4-8. Typical Shot Record: S2 source – X detector. 19
Figure 4-9 Typical Shot Record: S2 source – Y detector. 20
Figure 4-10. Brute Stack: P source – Vertical component..... 21
Figure 4-11. Refraction Stack: P source – Vertical component..... 22
Figure 4-12. SCD Stack: P source – Vertical component..... 23
Figure 4-13. SCD/TVSW Stack: P source – Vertical component. 24
Figure 4-14. SCD/TVSW/ZAP Stack: P source – Vertical component..... 25
Figure 4-15. Reflection Statics Stack: P source – Vertical component 26
Figure 4-16. DMO Stack: P source – Vertical component. 27
Figure 4-17. Final Migration: P source – Vertical component. 28
Figure 4-18. Typical Shot Record: P source – Radial component..... 29
Figure 4-19. Typical Shot Record: P source – Transverse component..... 30
Figure 4-20. Brute Stack: P source – Radial component. 31
Figure 4-21. Preliminary Statics Stack: P source – Radial component. 32
Figure 4-22. SCD/TVSW/ZAP Stack: P source – Radial component. 33
Figure 4-23. Final CCP Stack: P source – Radial component. 34
Figure 4-24. Final Migration: P source – Radial component..... 35
Figure 4-25. Final Migration/FXY Dcn: P source – Radial component..... 36
Figure 4-26. Final Migration Comparison: PP to PS. 37
Figure 4-27. Source to Receiver Azimuth Limitation. 38
Figure 4-28. PS Input to 2Cx2C Layer Stripping. 39
Figure 4-29. S-wave Birefringence: Layer 1. 40
Figure 4-30. S-wave Birefringence: Layer 2. 41
Figure 4-31. Shot Record: Radial source – Radial detector..... 42
Figure 4-32. Shot Record: Radial source – Trans detector. 43
Figure 4-33. Shot Record: Trans source – Radial detector. 44
Figure 4-34. Shot Record: Trans source – Trans detector. 45
Figure 4-35. Source and receiver statics corrections. 46
Figure 4-36. Regression for the Isoapch Top Ismay to Top Upper Ismay Carbonate. 51
Figure 4-37. Regression for the Isoapch Top Ismay to Top Desert Creek, version 1. 52
Figure 4-38. Regression for the Isoapch Top Ismay to Top Desert Creek, version 2. 53
Figure 4-39. Regression for the Isoapch Top Upper Ismay to Top Lower Ismay. 54

Figure 4-40. Regression for the Isoapch Top Lower Ismay to Top Desert Creek, version 1 55
Figure 4-41. Regression for the Isoapch Top Lower Ismay to Top Desert Creek, version 2 56
Figure 4-42. Ismay Zero Crossing Time Structure Map. 57
Figure 4-43 Ismay Peak Time Structure Map. 58
Figure 4-44. Hovenweep Trough Time Structure Map. 59
Figure 4-45. Desert Creek Peak Time Structure Map. 60
Figure 4-46. Mississippian Peak Time Structure Map. 61
Figure 4-47. Top Ismay to Top Desert Creek Isopach Map. 62
Figure 4-48. Top Ismay to Top Upper Ismay Carbonate Isopach Map. 63
Figure 4-49. Top Lower Ismay to Top Desert Creek Isopach Map. 64
Figure 4-50. Top Ismay Depth Map CI = 20 ft 65
Figure 4-51. Top Desert Creek Depth Map, CI = 20 ft 66
Figure 4-52. Upper Ismay Carbonate Depth Map. 67
Figure 4-53. Lower Ismay Depth Map. 68
Figure 4-54. Principal component plot, showing groupings of underlying seismic variables into three components 71
Figure 4-55. Principal component plot showing groupings of underlying seismic and lithological isopach variables. 71
Figure 4-56. Screen shot of project web page with links to recent publications and presentations. 75

List of Tables

Table 3-1. Description of multicomponent acquisition program. 5
Table 3-2. List of wells used for calibration and cross-correlation between lithostratigraphic picks in wells and seismic picks in the P-wave data. 7
Table 3-3. List of variable acronyms used in statistical analysis. 8
Table 4-1. Spearman correlation coefficients for Western #1 seismic variables. 49
Table 4-2. Kendall correlation coefficients for Western #1 seismic variables. 50
Table 4-3. Spearman correlation coefficients between production variables and seismic & lithologic variables 74

1 INTRODUCTION

This report describes the activities, results and conclusions obtained during the Fifth SemiAnnual Project period. The work focused on completing the interpretation of the P-wave data and the processing of the PS- and SS-wave data to lay the groundwork for the interpretation of these data sets. The goal of this project is to develop and apply multicomponent seismic data to improve the exploration for and the exploitation of algal mounds in the Paradox Basin on the Ute Mountain Ute Reservation in southwestern Colorado. The technology, of course, is potentially beneficial to the exploration and exploitation of algal mounds elsewhere in the United States and abroad.

Algal mounds have little structural expression; advances in exploration success have parallel development of new seismic technology. Multicomponent seismic technology had not previously been applied to algal mounds. Because of the promise for improving economic success in this Basin, the Red Willow Production Co., a company owned by the Southern Ute tribe, upgraded the survey from a 3D3C study to a 3D9C study with the substantial additional cost born by Red Willow, who also decided to expand the P-wave coverage at their expense to an area immediately to the northwest of the 6 square miles comprising the 3D9C survey.

The interpretation approach consists of a multivariate analysis of seismic variables both within the reservoir facies and outside of it. This approach has proven successful for delineating the algal mound geometry, and has led to new drilling targets which are currently under discussion with the Ute Mountain Ute tribe for leasing.

This report contains an Executive Summary (Chapter 2), a description of the Experimental Methods (Chapter 3), a Discussion of the results (Chapter 4), Conclusions (Chapter 5), followed by references and an appendix. The Experimental Methods section focuses on the processing workflow used to complete the multicomponent processing, and the interpretation workflow and methodology. The primary focus of Chapter 4 is on the interpretation of the P-wave data and its use for selecting promising well locations.

2 EXECUTIVE SUMMARY

This report described the technical progress and accomplishements of the project entitled "Multicomponent Seismic Analysis And Calibration To Improve Recovery From Algal Mounds: Application To The Roadrunner/Towaoc Area Of The Paradox Basin, Ute Mountain Ute Reservation, Colorado", DOE Award Number: DE-FG26-02NT15451 during its fifth semiannual project period. The goal of this project is to develop and apply multicomponent seismic data to improve the exploration for and the exploitation of algal mounds in the Paradox Basin on the Ute Mountain Ute Reservation in southwestern Colorado for the benefit of the Ute Mountain Ute tribe. The technology, of course, will benefit the exploration and exploitation of algal mounds elsewhere in the US, and also help to develop 3D9C (three-dimensional, nine-component) seismic technology which is at the forefront of seismic imaging in the oil industry for many types of reservoirs besides algal mounds.

The overall technical approach is to use advanced multivariate statistical approaches for the interpretation of a wide range of seismic components extracted from the P-, PS- and SS-wave data for the target producing intervals as well as intervals above and below. This approach has several benefits:

- similar patterns that emerge from the analysis of different variables improve confidence that trends and anomalies are real and their boundaries are less uncertain, and important advantage in locating wells in subtle stratigraphic plays like algal mounds;

- use of multiple seismic attributes can reduce uncertainty in predicting mound geometry and properties, and at the same time, lead to a better geological exploration model; and

- inclusion of seismic data from intervals above and below the immediate target intervals can also reduce uncertainty and enhance geological understanding of mound development and how best to locate new wells.

The development, charging and preservation of oil and gas is rarely attributable to a single geological factor, and so the collection of several variables or surrogates, and an analytical approach that is tailored to developing predictive models from multiple attributes, is an appropriate method with better chances of improving exploration and exploitation.

During the fifth period, the project completed the interpretation of the P-wave data and nearly completed the processing of the PS- and SS-wave data. The P-wave data had been processed by two companies (WesternGeco and GMG/Axis) during the previous project period, and a particular processing workflow of the four tested was selected for interpretation based upon prediction success of lithostratigraphy in wells. In the current period, multivariate statistical techniques were applied to the data from the selected

WesterGeco #1 processing stream. Isopachs on key intervals were calculated from this data through multivariate methods.

The maps show that Ismay productive mound areas are associated with Ismay-Desert Creek isopach thicks. Some prospective isopach thicks were identified in the northwest portion of the survey. The Top Ismay to Top Upper Ismay Carbonate Isopach includes the Ismay Massive Anhydrite which is known to be thin in mound areas and thick in off-mound regions. Analysis showed that this isopach interval is anomalously thin in Ismay producing areas. The isopach thins are most dramatic in the Towaoc field area, which is located in the southern portion of the survey. It is possible that there may be at least one more new drilling location in the southern portion of the 3D P-wave survey based on this isopach. The Top Lower Ismay to Top Desert Creek Isopach is anomalously thick in producing areas, especially in the Marble Wash and Roadrunner fields, which are present in the the northwest and center of the 3D survey. This isopach map indicates undrilled Lower Ismay mound areas may exist in the northwest portion of the survey.

In summary, the new isopach maps derived from seismic regression analysis helped to identify prospective Upper Ismay and Lower Ismay mound areas, and have led to the selection of potential drilling locations that are currently being negotiated with the Ute Mountain Ute Tribe.

Technology transfer continued in the form of updates to the project website (http://utemountain.golder.com), oral presentations to a large industrial consortium meeting at the Colorado School of Mines in March, and the submission and acceptance of a paper on the multicomponent processing at an EAGE/SEG symposium.

3 EXPERIMENTAL METHODS

The experimental methods underlying the work in this report consist of the processing workflow for the multicomponent seismic and the methods used for interpreting the processed seismic data. In addition, the acquisition methods used to acquire the raw seismic data are briefly reviewed as these are germane to the processing workflow.

3.1 Acquisition Program Geometry & Parameters

Figure 3-1 shows the geometry of the sources and receivers. The S-wave source direction was parallel and perpendicular to source lines (NE/SW and NW/SE) while the horizontal geophones are aligned with the receiver line direction (E/W and N/S). This requires an additional rotation of the sensors to get all into same frame of reference.

Table 3-1 summarizes additional details of the acquisition program.

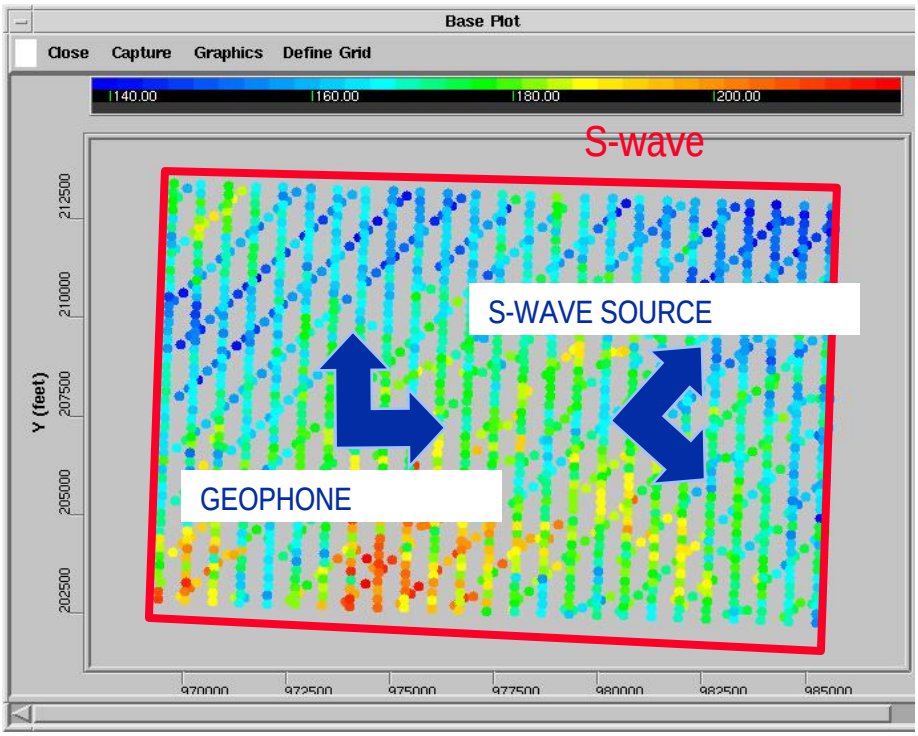

Figure 3-1. Acquisition geometry for multicomponent seismic survey.

Program Size:	6.0 square miles
Line Parameters	
Receiver point interval:	220 ft
Source point interval:	220 ft
Total receiver points:	1784
Total source points:	848
Source Type for programs	
P Waves:	4 sweeps x 10 seconds
Shear 1:	4 sweeps x 10 seconds
Shear 2:	4 sweeps x 10 seconds
Recording Parameters	
Record Length:	6 seconds
Geophone array:	6 over 45 ft
Live patch:	14 lines X 60 channels
Roll on / roll off:	Yes
Sample Rate:	2 ms

Table 3-1. Description of multicomponent acquisition program.

3.2 Processing Workflow

The data processing sequence for the P-wave data for the Western Geco processing is as follows:

1. Brute stack = raw data with regional velocity function and elevation statics.
2. Refraction stack = brute stack with refraction statics.
3. SCD stack = refraction stack with Surface-Consistent Deconvolution.
4. SCD/TVSW stack = SCD stack with Time-Variant Spectral Whitening (to broaden the bandwidth)
5. SCD/TVSW/ZAP stack = SCD/TVSW stack with Zone-Anomaly Processing (to get noise bursts and anomalous spikes)
6. Reflection stack = SCD/TVSW/ZAP with surface-consistent reflection statics.
7. DMO stack = Reflection stack with 3D common-offset DMO.
8. Final migration = DMO stack with FK extended Stolt migration.

The data processing sequence followed for the PS-wave (radial component) data for the WesternGeco processing is as follows:

1. Brute stack = radial component with regional velocity function, P-wave source statics and elevation detector statics.
2. Preliminary statics = Brute stack with detector hand statics (to match P-wave time structure)
3. SCD/TVSW/ZAP stack = same flow as P-wave version with adjusted time windows.
4. Final CCP stack = Common-Conversion Point stack (time variant correction of reflection point).
5. Final migration = CCP stack with Kirchhoff poststack time migration using PS-wave velocities.
6. Final migration/FXY Dcn = Final migration with 3D RNA (aka FXY deconvolution).

3.3 Interpretation

The fourth Semi-Annual Technical Report (La Pointe and others, 2004) has previously described the approach to picking lithostratigraphic horizons and isopachs. The work reported during that project period consisted of investigating which P-wave processing workflow produced the best correlations. Based upon this work, it was decided that the WesternGeco #1 processing scheme, which had Random Noise Attenuation applied, was preferable to second, which did not have the Random Noise Attenuation applied, but rather a Spectral Whitening.

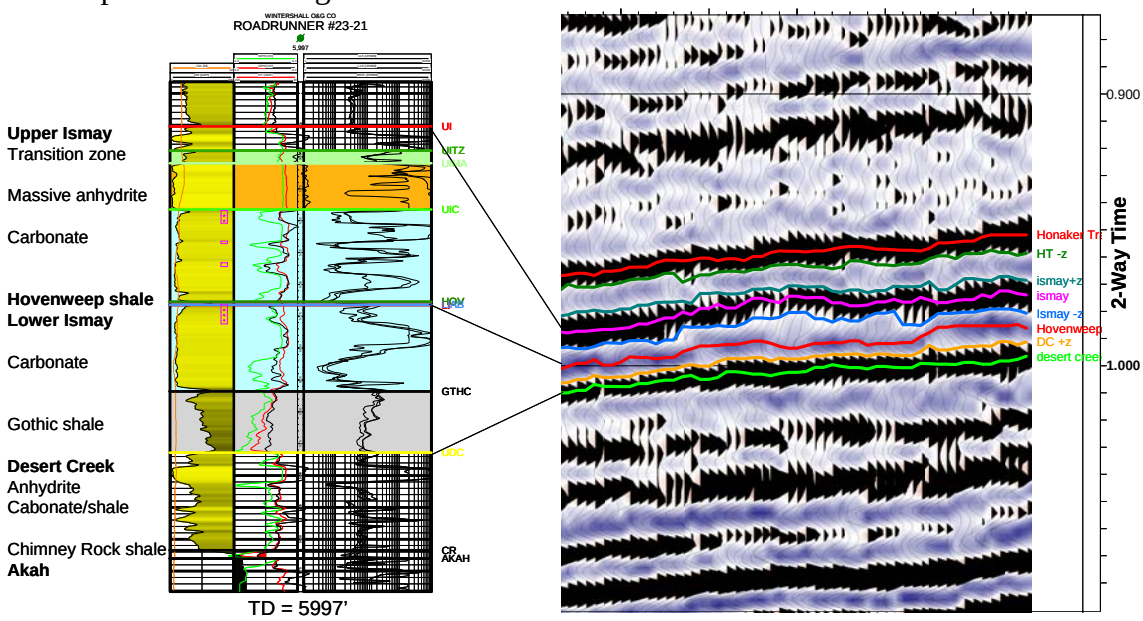

Figure 3-2. Correlation of lithostratigraphic boundaries with processed P-wave data.

The method used to construct the key horizons from seismic data is to calibrate the picks to the well logs (Figure 3-2) and then to extend the picks away from well control in the seismic volumes to map out the horizon throughout the region of interest.

The next step is to create isochron maps that are to be related to isopachs of various units. The isochron maps are created by subtracting the time horizon maps. Isopachs between

the units shown in Figure 3-2 and Figure 3-3 are calculated at wells where the requisite logging suite is available. In all, it was possible to calculate at least some of the horizon tops and isopachs for the forty-six wells listed in Table 3-2.

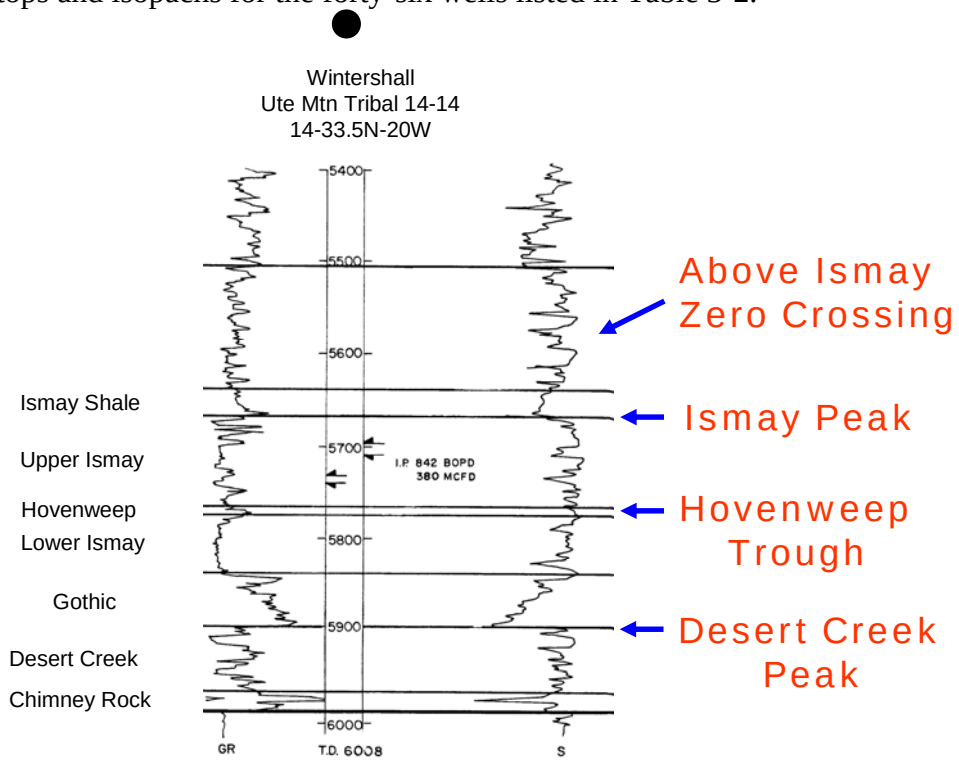

Figure 3-3. Detail of log expressions for the lithostratigraphic boundaries and their corresponding seismic picks.

API Number	Well Label	API Number	Well Label	API Number	Well Label
0508306332	SENTINEL PEAK #8-32	0508305104	CALCO-SUPERIOR-UTE #2	0508306331	SENTINEL PEAK #17-42
0508305137	UTE TRIBAL-GOVT #7	0508306420	UTE TRIBAL #6-15	0508306441	SENTINEL PEAK #17-2
0508306002	UTE-B #1	0508306421	UTE TRIBAL #11-15	0508305371	UTE MTN #1-17
0508305377	UTE A-GOVT #1	0508306424	UTE TRIBAL #5-15	0508305092	UTE MOUNTAIN TRIBAL #2
0508305111	CAL OIL-SUPERIOR #10	0508306406	UTE MTN UTE TRIBAL #15-43	0508305094	UTE MTN TRIBAL #1
0508306007	UTE-B #2	0508306410	ROADRUNNER #15-33	0508305091	UTE MTN TRIBAL #3
0508305138	UTE TRIBAL-GOVT #8	0508306445	ROAD RUNNER #15-34	0508306501	UTE #15-22
0508306005	UTE TRIBAL #9	0508306471	ROADRUNNER #15-44	0508306490	UTE #16-22
0508306008	UTE-AB #1	0508307002	UTE TRIBAL GOVT #9/11-1	0508306357	TOWAOC #1-22
0508306517	MARBLE UTE-AB #1	0508306015	UTE AB #2	0508305093	CALCO-SUPERIOR UTE #3
0508306399	UTE MOUNTAIN #14-13	0508306428	ROAD RUNNNER #15-32	0508306481	ROADRUNNER #23-21
0508306405	UTE MTN UTE TRIBAL #14-24	0508306440	UTE MTN TRIBAL #14-15	0508306419	ROADRUNNER UTE MTN #23-31
0508306467	ROADRUNNER #14-14	0508305102	UTE TRIBAL #1	0508305095	UTE-2 #1
0508306469	ROADRUNNER #14-34	0508306020	UTE D #1	0508307001	MCLISH-UTE TRIBAL #1-23
0508306026	UTE #76-1	0508305098	CALCO-SUPERIOR-UTE #4		
0508305427	UTE #1-14	0508306508	UTE #13-16		

Table 3-2. List of wells used for calibration and cross-correlation between lithostratigraphic picks in wells and seismic picks in the P-wave data.

A list of variable acronyms was developed for these picks and for the isopachs constructed from them (Table 3-3).

AbIS	Above Ismay
IS0	Ismay Zero Crossing
ISPeak	Ismay Peak
DCPeak	Desert Creek Peak
Miss	Mississippian
IS0_DCPeak	Ismay Zero Crossing to top of Desert Creek
ISPeak_DC	Ismay Peak to top of Desert Creek
IsAmp	Ismay Amplitude
IS_UIC	Ismay to top of Upper Ismay Carbonate
IS_DC	Ismay to top to Desert Creek
TUI_TLI	Top of Upper Ismay to top of Lower Ismay
TLI_TDC	Top of Lower Ismay to top of Desert Creek

Table 3-3. List of variable acronyms used in statistical analysis.

In this project period, final time structure and isopach maps were produced from the WesternGeco #1 processed data. The time structure maps for the Ismay Zero crossing, Ismay Peak, Hovenweep Trough, Desert Creek Peak and Mississippian Peak were created directly from the seismic picks. Isopachs were generated through multivariate regression for the Top Ismay to the Top Upper Ismay Carbonate, Top Ismay to Top Desert Creek, Top Upper Ismay to Top Lower Ismay and Top Lower Ismay to Top Desert Creek. Depth maps were calculated for the Top of the Ismay, Top Upper Ismay Carbonate, Top Lower Ismay and Top of the Desert Creek.

As part of the development of the multivariate regression, non-parametric correlation matrices using the Spearman and Kendall coefficients were generated for the dependent and independent variables. These matrices were used to help select the independent variables used in the regressions.

After selecting the variables, multivariate stepwise linear regressions were carried out. This procedure retains only the most significant variables. Independent variables that showed a high degree of correlation with one another, as evidenced from the correlation coefficients, were manually deleted prior to the stepwise regressions, since a strong correlation among “independent” variables invalidates the mathematical assumption of linear regression. For each regression found to be significant, defined as having a p-value of 0.05 or less for the F-test of variance, the residuals were examined for correlation and conformance to a Gaussian distribution. For the regressions to be useful and valid, residuals should approximate a Gaussian distribution and show no bias or correlation.

Depth maps were also constructed from seismic data. In constructing depth maps, velocity maps must first be generated. Horizon seismic times and actual horizon depth values at wells are used to calculate velocity. The velocity and seismic time grids are then used to create a depth structure map.

4 RESULTS AND DISCUSSION

4.1 Seismic Processing & Interpretation

4.1.1 PROCESSING

Processing of the P-wave data was largely completed during the previous (4th) semiannual project period. During the 5th period, processing of PS and S-wave data, initiated during the 4th period, was completed.

The following figures show the results of the processing workflows described in Section 2.2. Figure 4-1 through Figure 4-9 show typical shot records for the P-, S1- and S2-waves. Recall that there is an oblique relation between the sources and receivers (Figure 3-1), which makes it is difficult to draw conclusions from these shot records. The following processing steps were included:

- P-wave processing
  3D DMO, stack, 3D Random Noise Attenuation (RNA) and FK Stolt migration

- PS-wave processing
  CCP binning/post-stack time migration
  Limited-azimuth volumes
  Azimuthal anisotropy (splitting) analysis

- SS-wave processing
  Sh-Sh for statics and velocity
  Azimuthal anisotropy (splitting) analysis

The PS-wave processing included CCP binning to correct for the movement of the reflection point from the midpoint. This was followed by a Kirchhoff post-stack time migration flow using the appropriate PS-wave velocity field. P-Wave Processing

Figure 4-10 through Figure 4-17 show the progression of the P-wave data through the processing sequence. Figure 4-10 shows a brute stack, which is the raw data processed using the regional velocity function and elevation statics. Figure 4-11 is an example of a refraction stack, which incorporates the refractions statics. Figure 4-12 shows the SCD stack, which is the refraction stack incorporating the Surface-Consistent Deconvolution. Figure 4-13 is the SCD stack but with Time-Variant Spectral Whitening to broaden the bandwidth. Figure 4-14 contains Zone-Anomaly Processing to reduce noise bursts and anomalous spikes. Figure 4-15 is the reflection stack. Figure 4-16 is a DMO stack, which is the reflection stack with a 3D common-offset DMO. Figure 4-17 shows the final result after the DMO stack has had the FK extended Stolt migration.

4.1.2 PS – WAVE PROCESSING

Figure 4-18 and Figure 4-19 show the raw radial and transverse component shot records for the P-source. Figure 4-20 through Figure 4-25 illustrate the results of the PS-wave processing. Figure 4-20 is the brute stack for the radial component with the regional velocity function, P-wave source statics and elevation detector statics. Figure 4-21 are the brute stack with detector hand statics to match the P-wave time structure. Figure 4-22 is the SCD/TVSW/ZAP stack, which is essentially the same as the corresponding P-wave stack (Figure 4-14) with adjusted time windows. Figure 4-23 is the final CCP (Common-Conversion Point) stack with a time-varying correction of the reflection point. Figure 4-24 is the CCP stack with Kirchhoff post-stack time migration using the PS-wave velocities. Figure 4-25 is the final migration with 3D random noise attenuation (FXY deconvolution).

Figure 4-26 is a comparison of the PP and PS sections. The blue arrow shows the target. There is a reasonably good alignment of events.

4.1.3 AZIMUTHAL ANALYSIS

Figure 4-27 describes the azimuth sectors used to limit the PS data for azimuthal analysis. Both the radial and transverse components were used for this analysis. The transverse component data was processed using the parameters determined from the radial component.

Figure 4-28 shows one line from the survey (IL 1094) extracted for each of the 8 limited-azimuth sectors for both radial and transverse components. Note that the sectors ranged from 0 to 360 degrees in 10 degree increments. The purple arrows on the right show the analysis windows used. Layer 1 is considered the overburden and layer 2 includes the reservoir.

Figure 4-29 shows the result of the 2C x 2C Alford rotation and layer stripping procedure performed on the data in Figure 4-28. Note that the values are in percentage anisotropy and are relatively small (<2%). Also note that there seems to be a pattern that correlates roughly the weaker anisotropy with the isochron interpretation. It is not clear why this association might occur in the case of the overburden.

Figure 4-30 shows the results from the second layer which includes the reservoir. The overall level of anisotropy is smaller and less organized. It is possible, however, to see hints of a similar NW/SE feature of weaker anisotropy.

4.1.4 SS-WAVE PROCESSING

Figure 4-31 through Figure 4-34 show the shot records for the SS data as initially processed. These are believed to be in a radial and transverse orientation; however, subsequent analysis and discussion suggests that this is not the optimum orientation for processing.

Figure 4-35 shows the results of the S-wave statics calculation using the SS (transverse) data. The results are encouraging and when applied show improvement on the stack sections.

In summary, the processing results show that:

1) Algal mound feature is present on P-wave data
2) PS-wave data quality is good and the event correlation to the PP data is reasonable.
3) S-wave anisotropy measurements from the PS data are small but show a possible correlation to the reservoir structure.
4) SS refraction statics correlate well with PP statics.

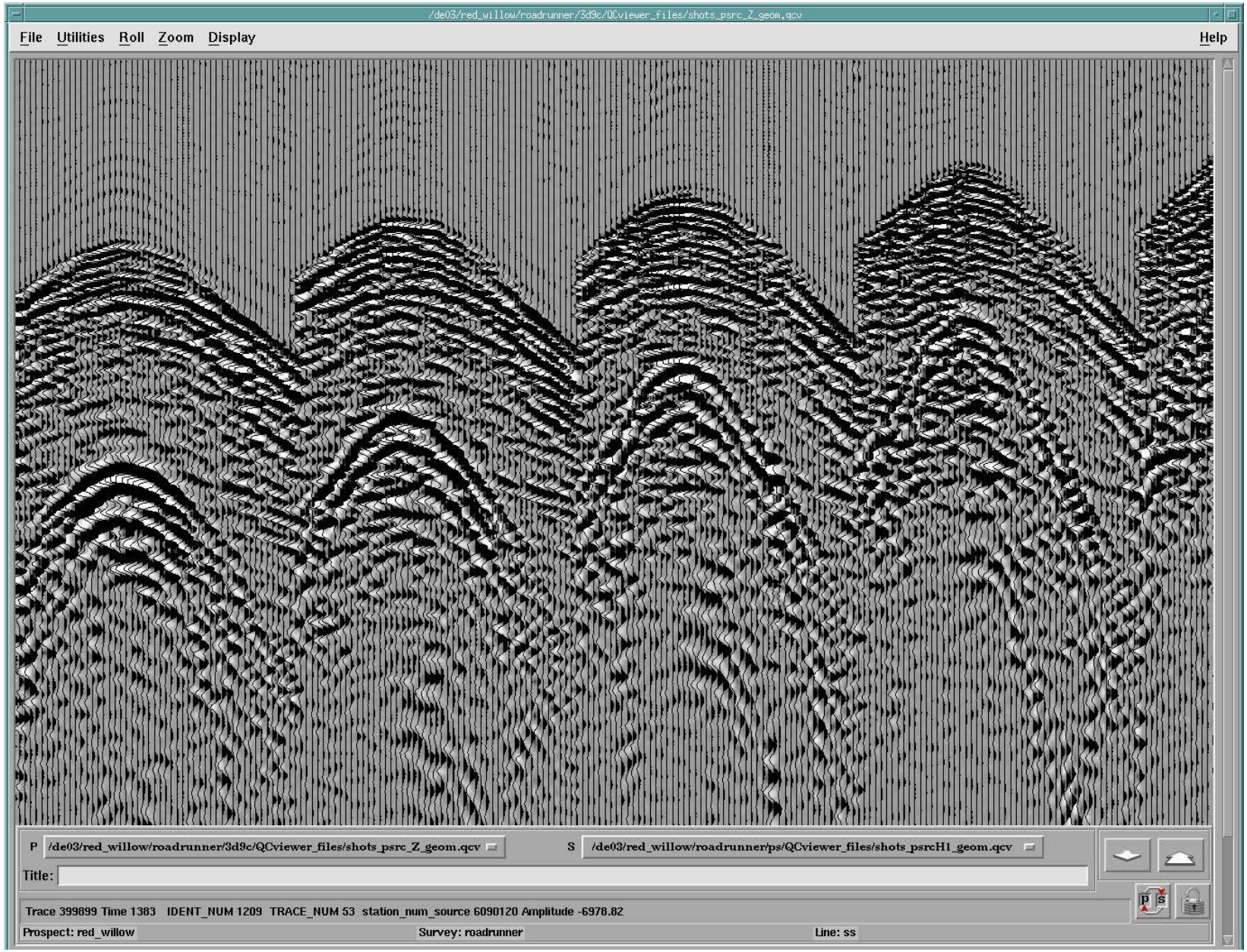

Figure 4-1. Typical Shot Record: P source – Z detector.

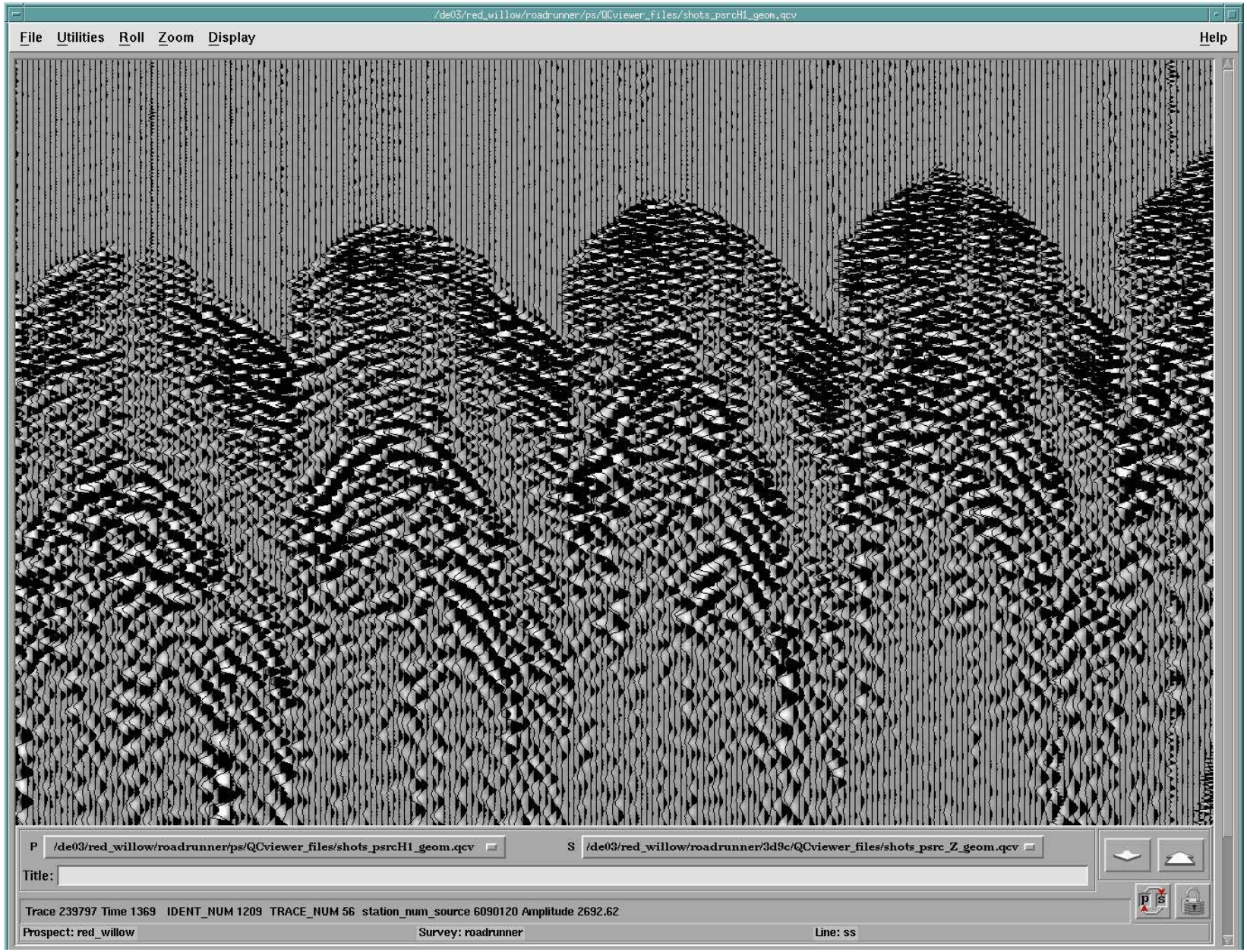

Figure 4-2. Typical Shot Record: P source – X detector.

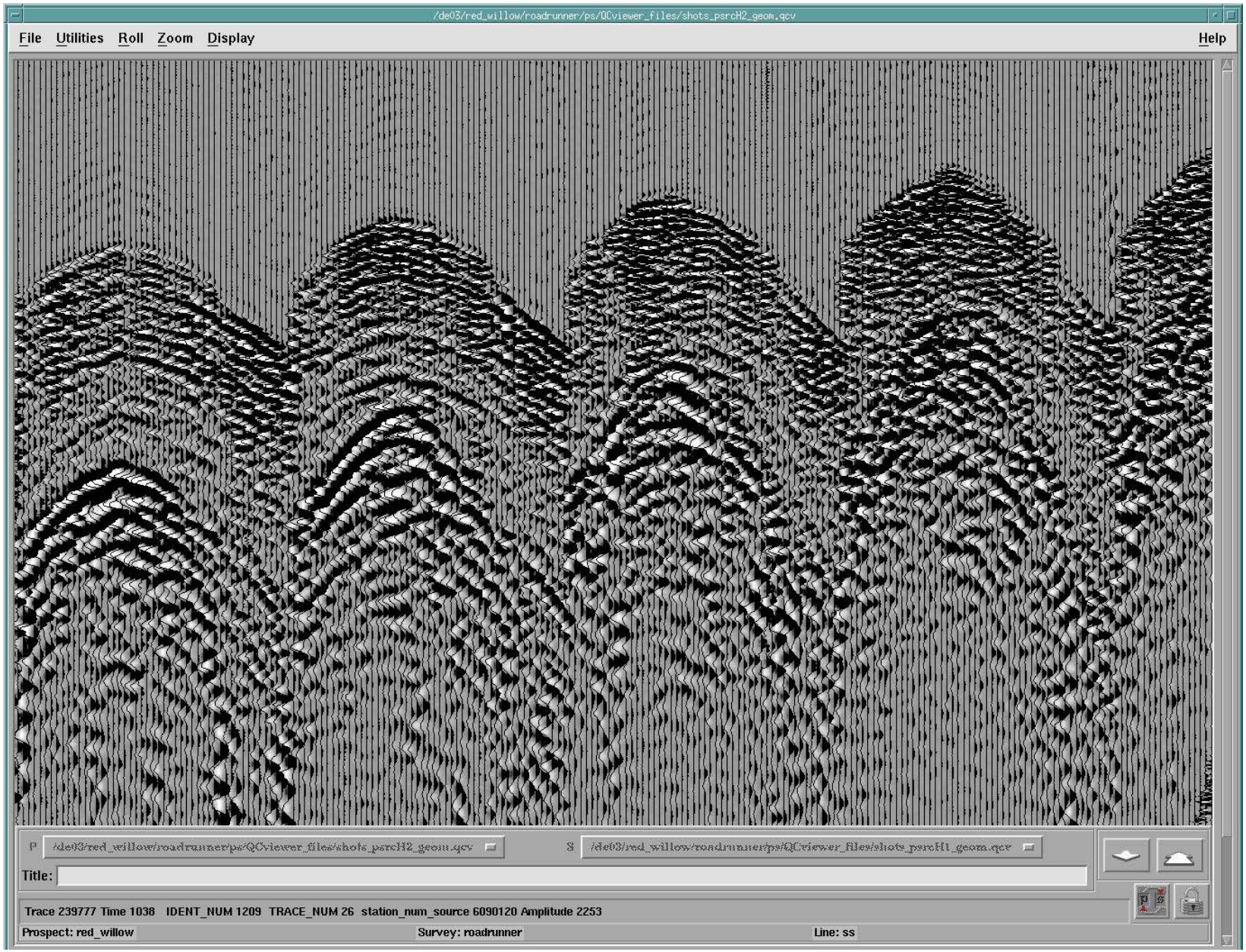

Figure 4-3. Typical Shot Record: P source – Y detector.

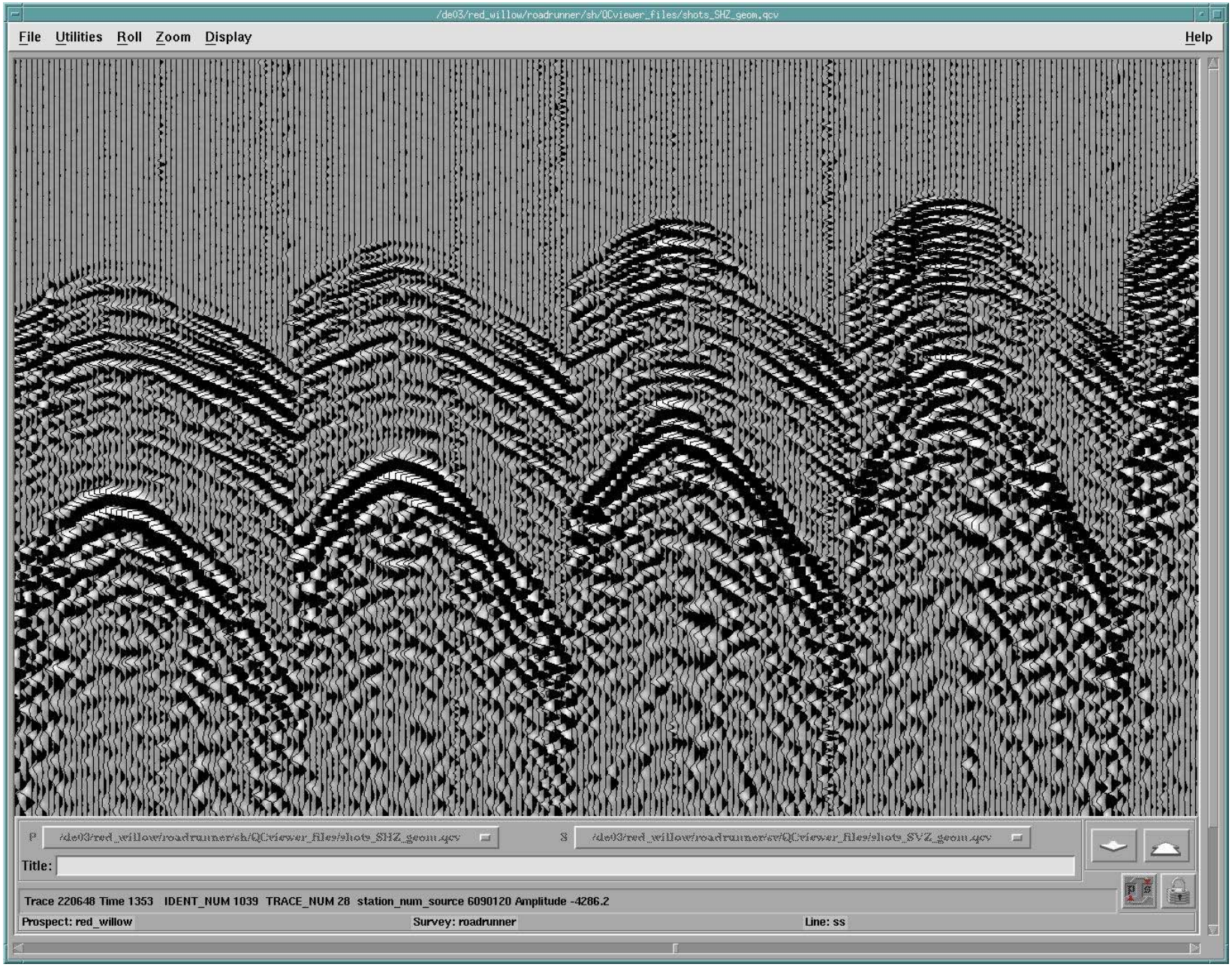

Figure 4-4. Typical Shot Record: S1 source – Z detector.

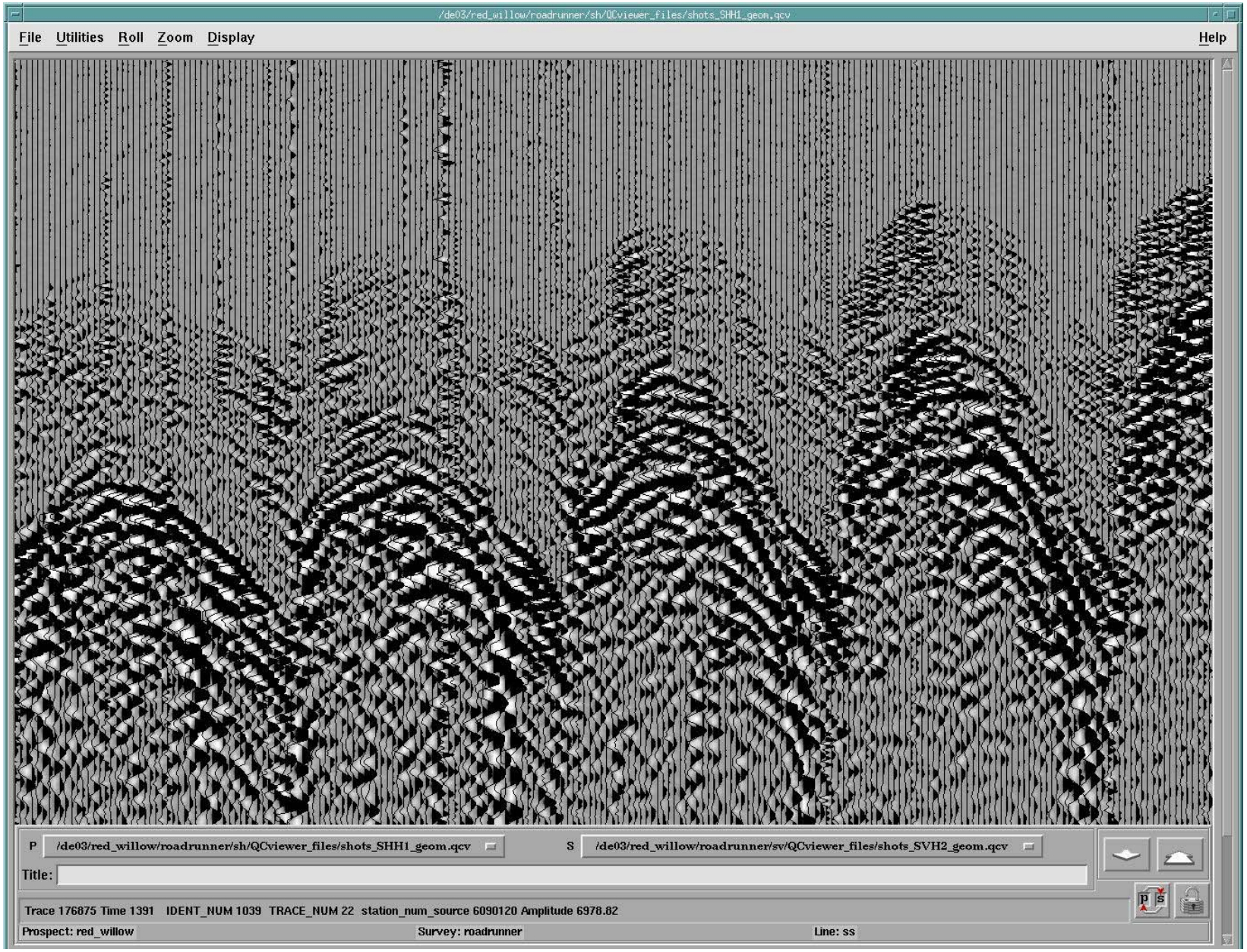

Figure 4-5. Typical Shot Record: S1 source – X detector.

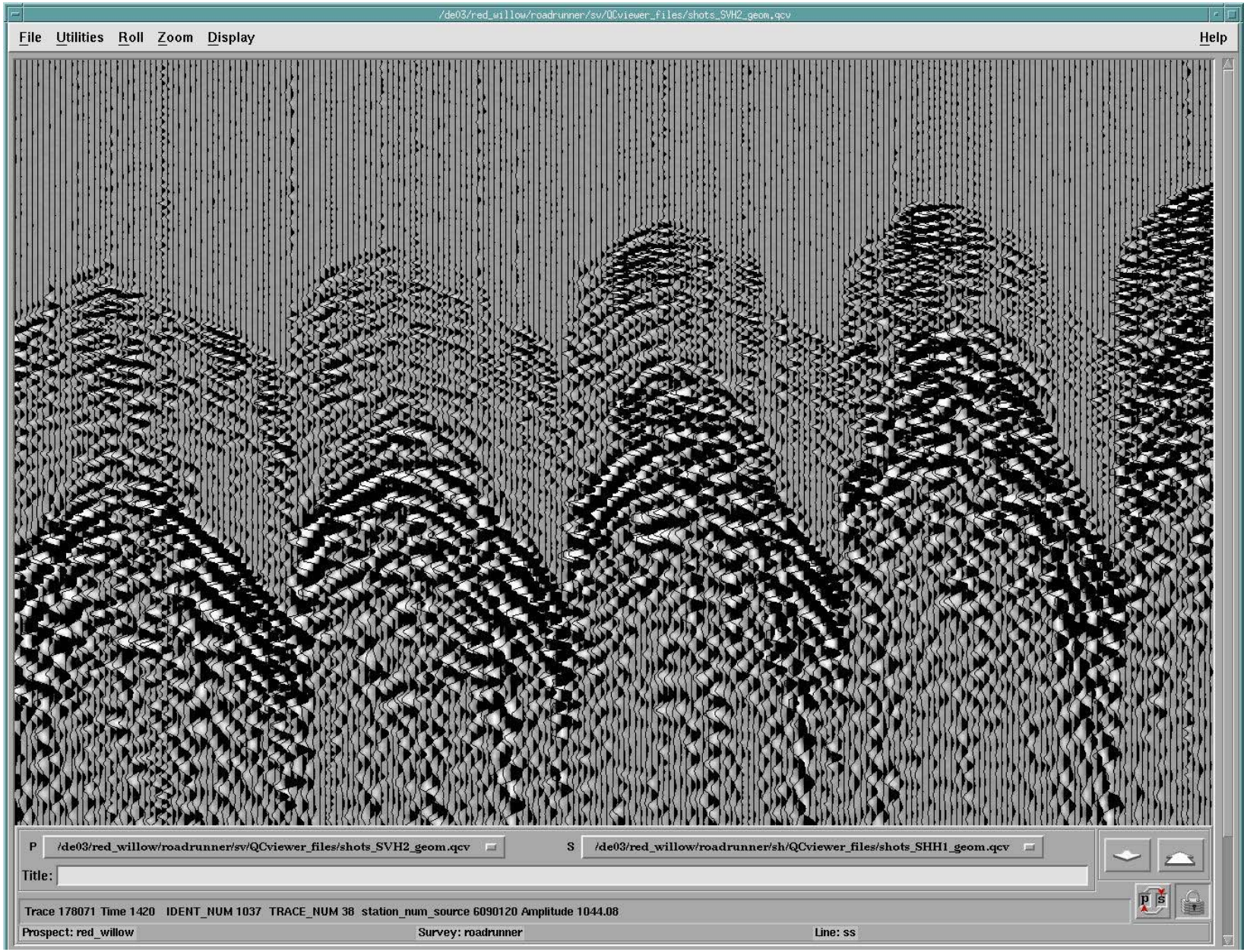

Figure 4-6. Typical Shot Record: S1 source – Y detector.

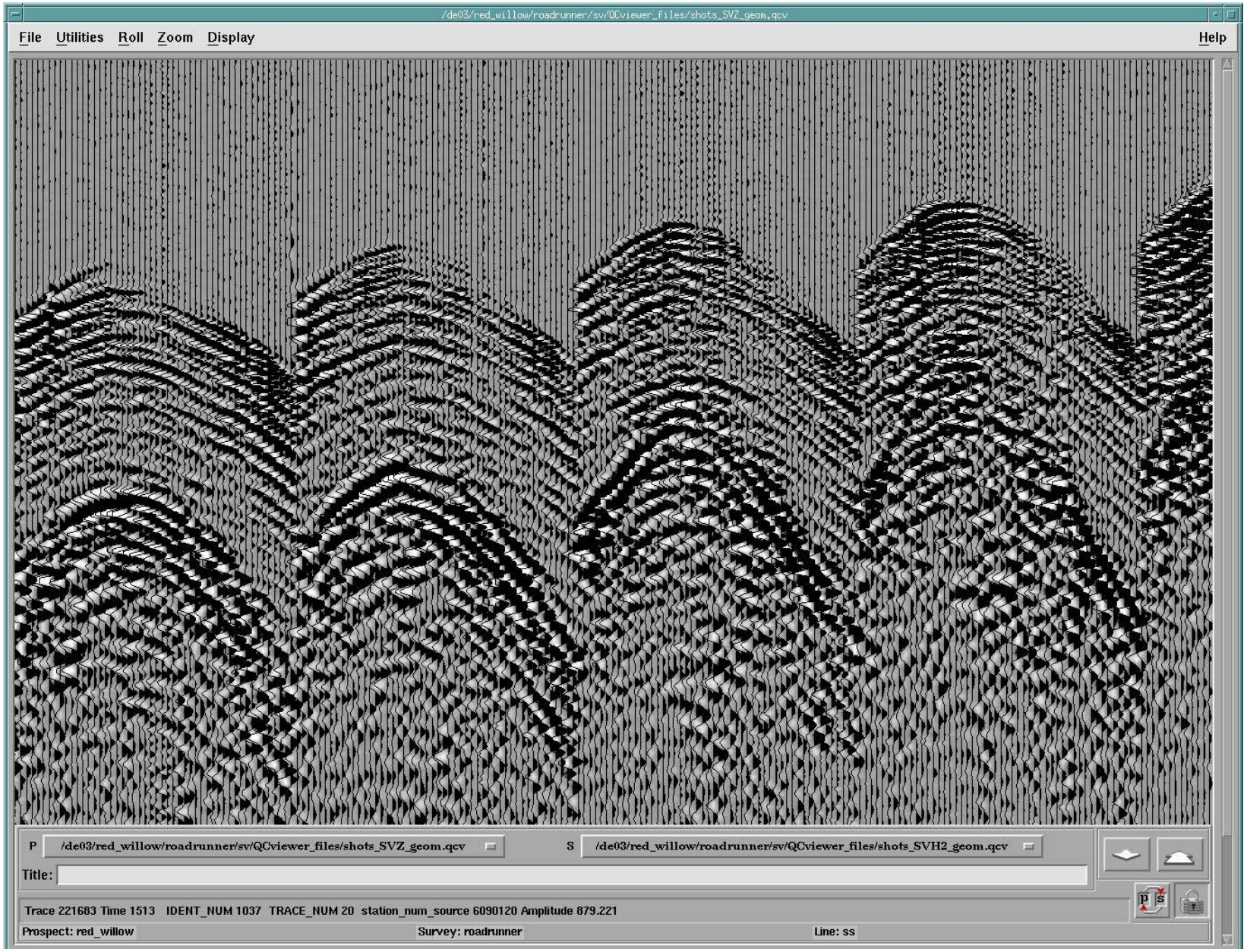

Figure 4-7. Typical Shot Record: S2 source – Z detector.

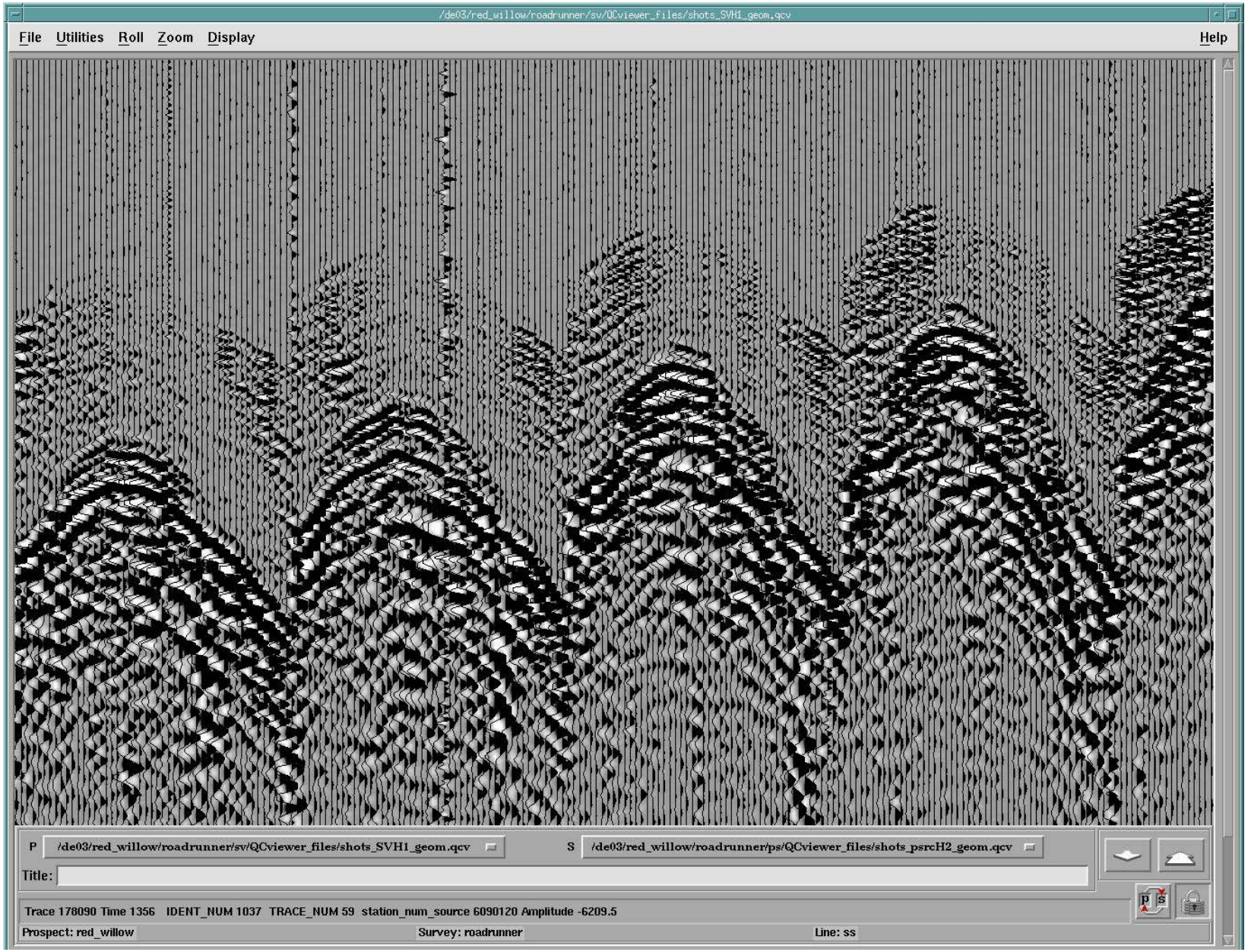

Figure 4-8. Typical Shot Record: S2 source – X detector.

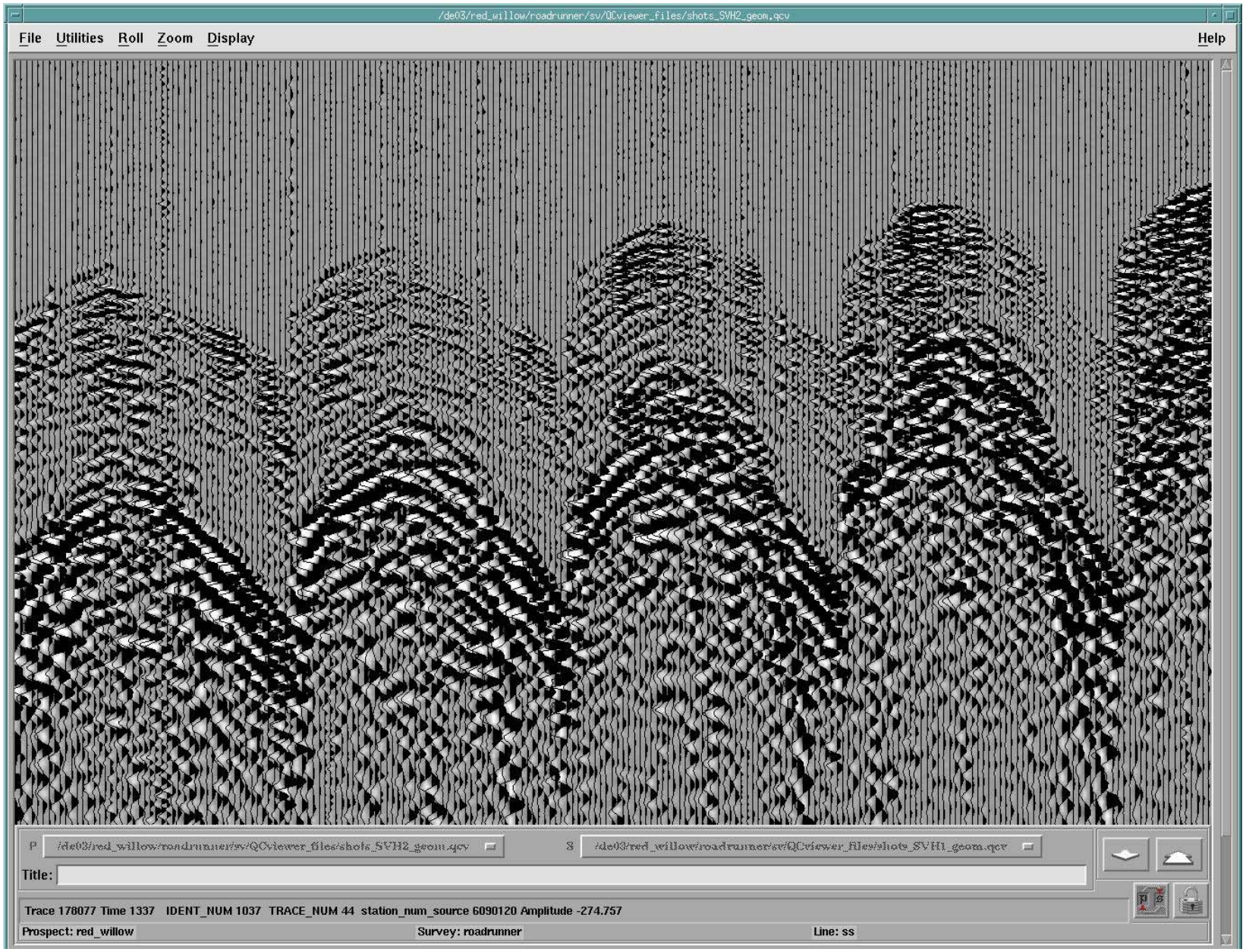

Figure 4-9 Typical Shot Record: S2 source – Y detector.

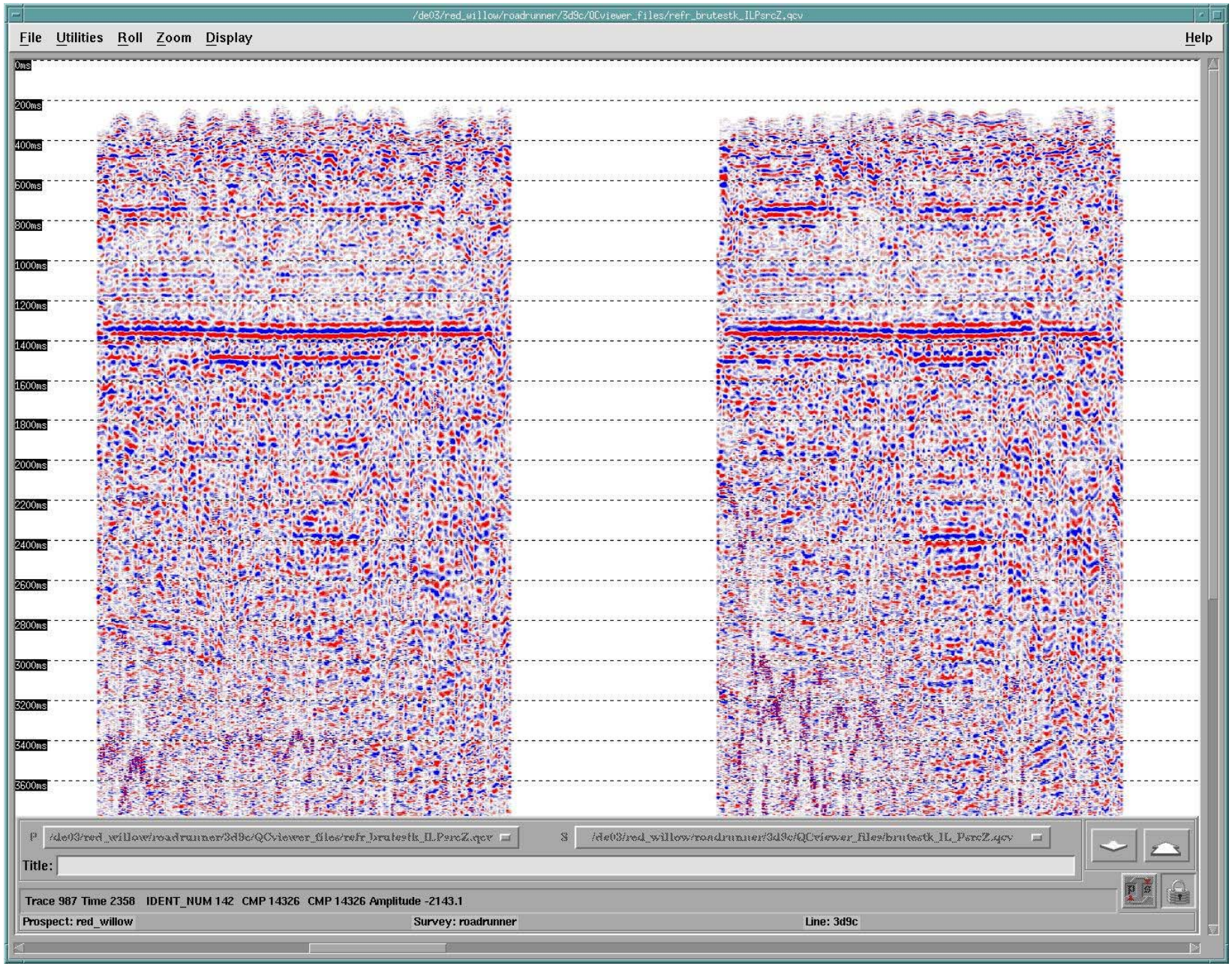

Figure 4-10. Brute Stack: P source – Vertical component.

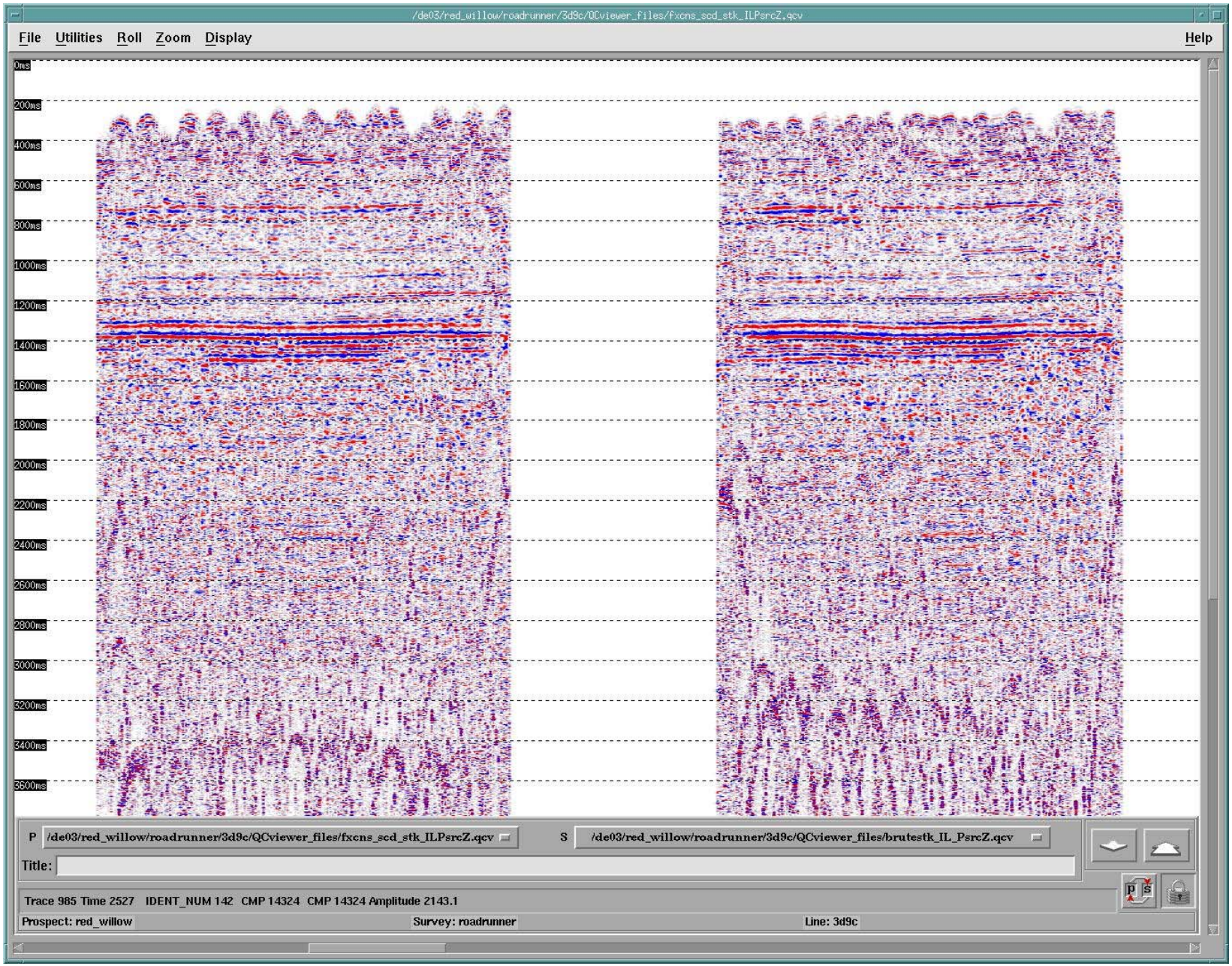

Figure 4-11. Refraction Stack: P source – Vertical component.

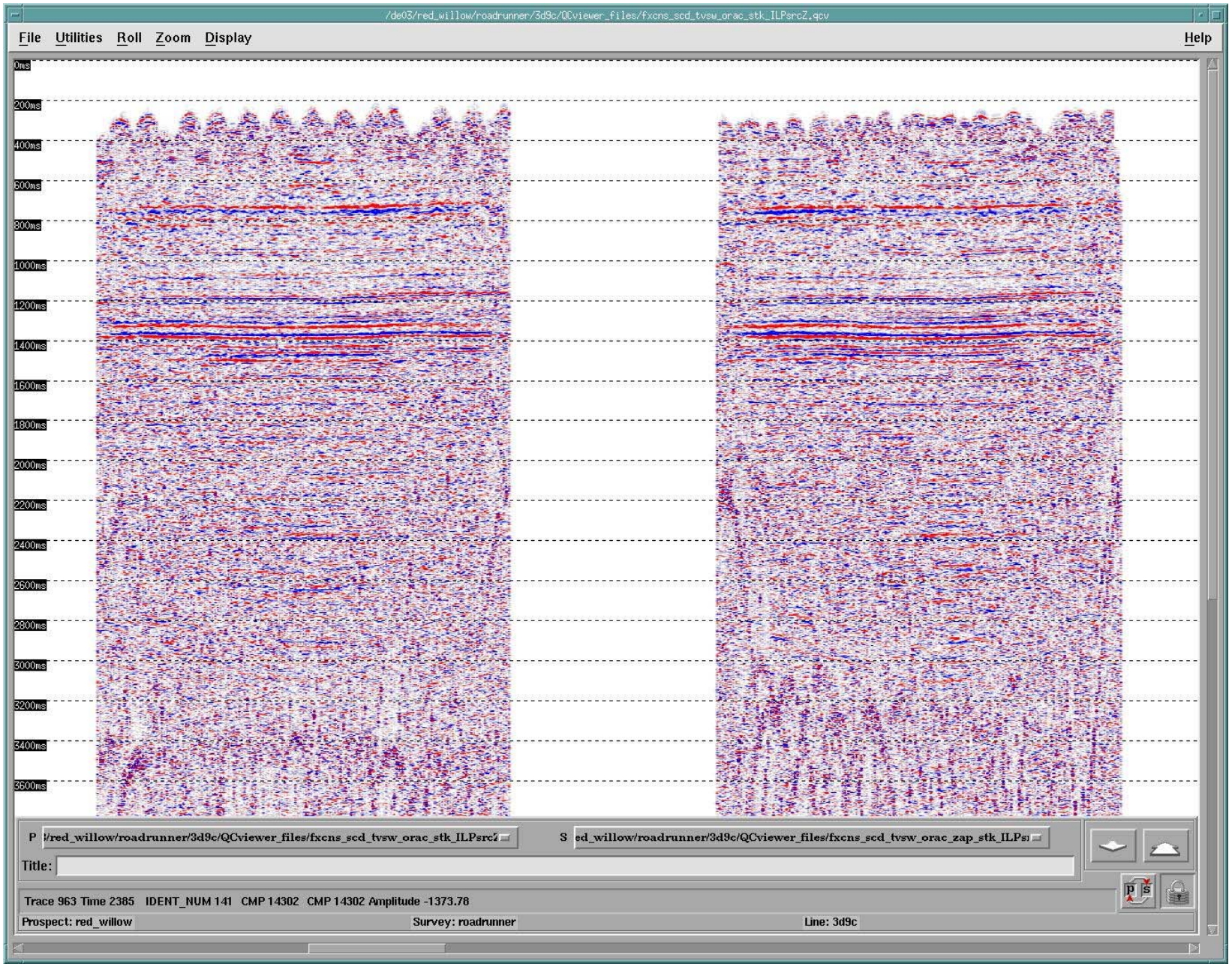

Figure 4-12. SCD Stack: P source – Vertical component.

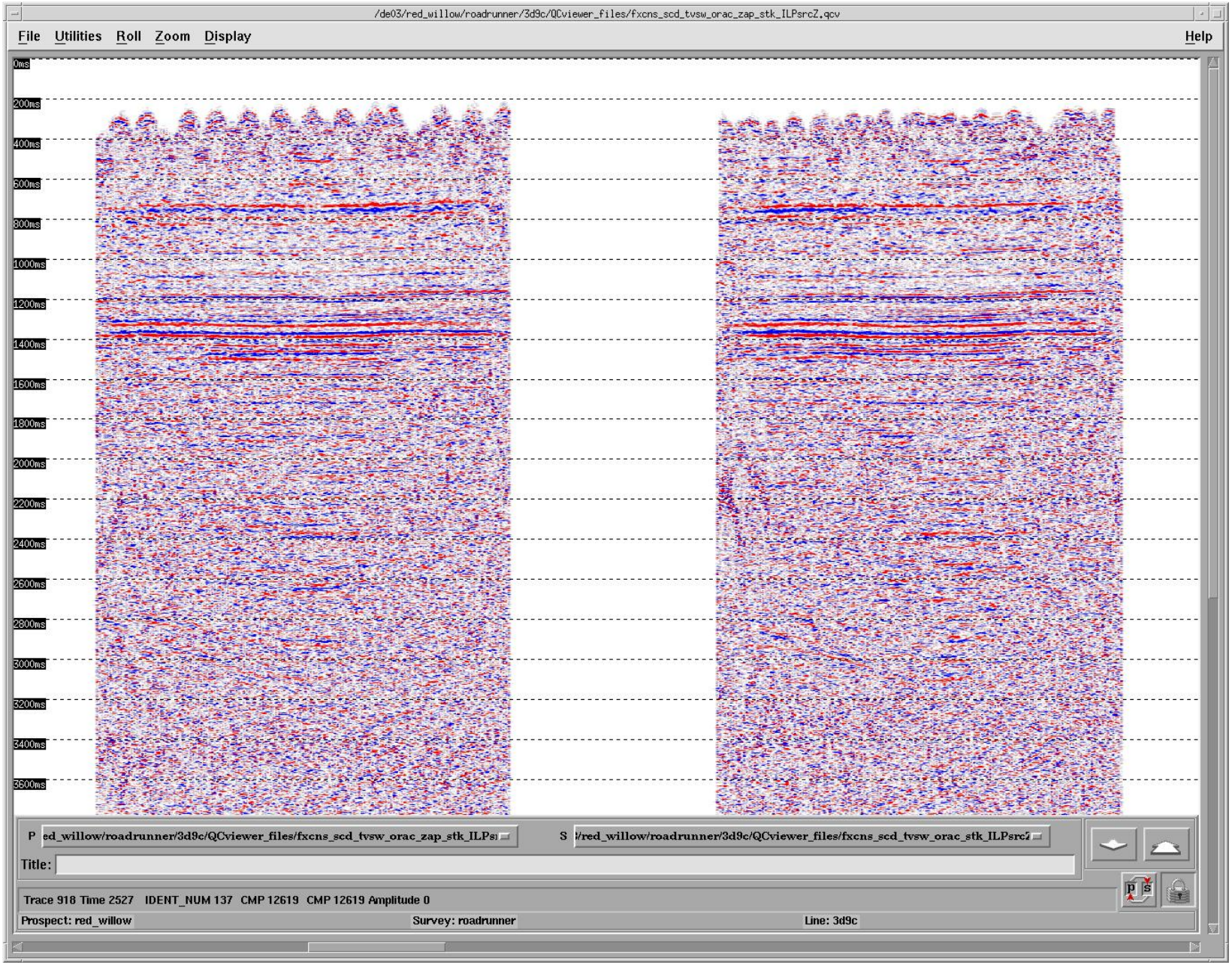

Figure 4-13. SCD/TVSW Stack: P source – Vertical component.

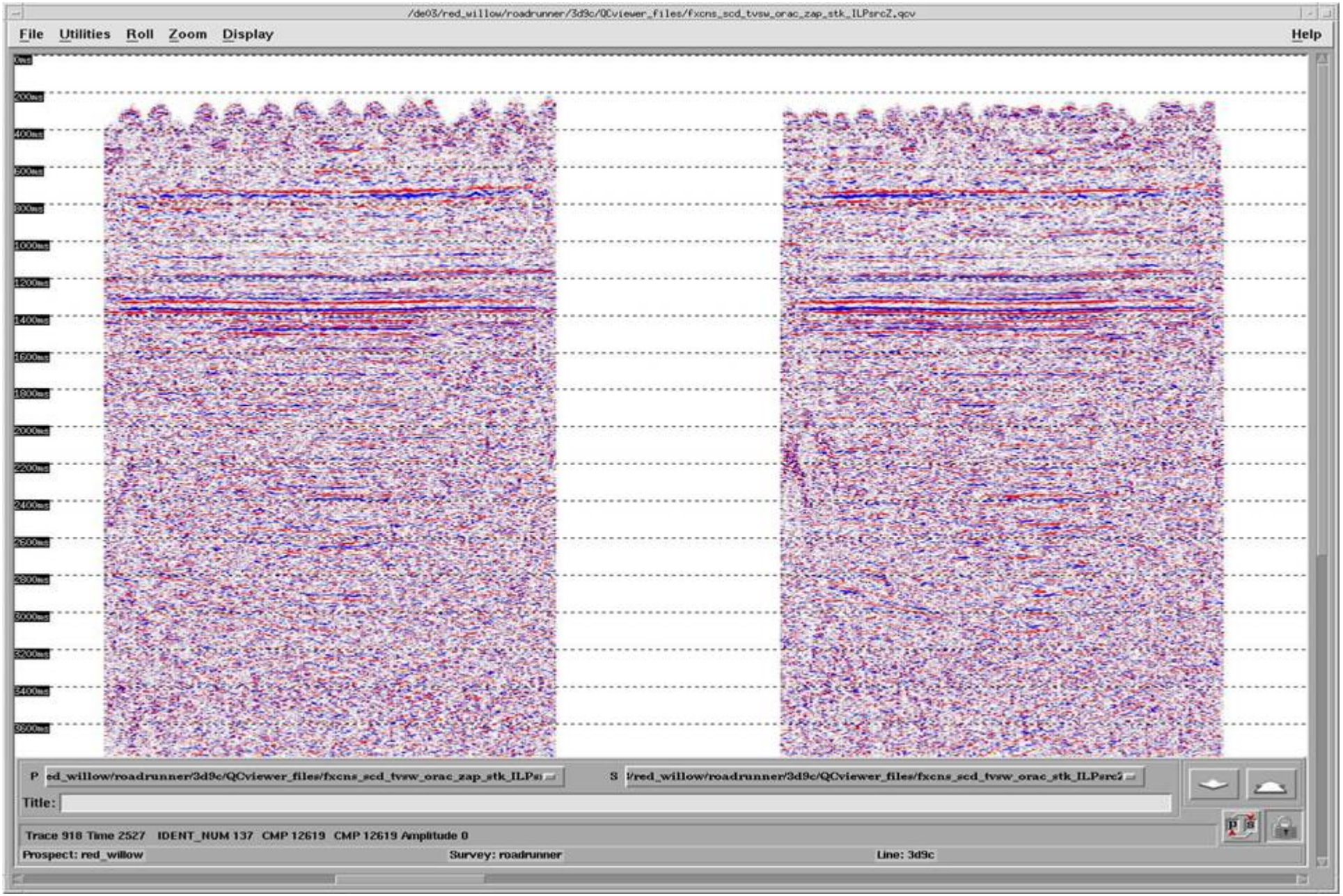

Figure 4-14. SCD/TVSW/ZAP Stack: P source – Vertical component.

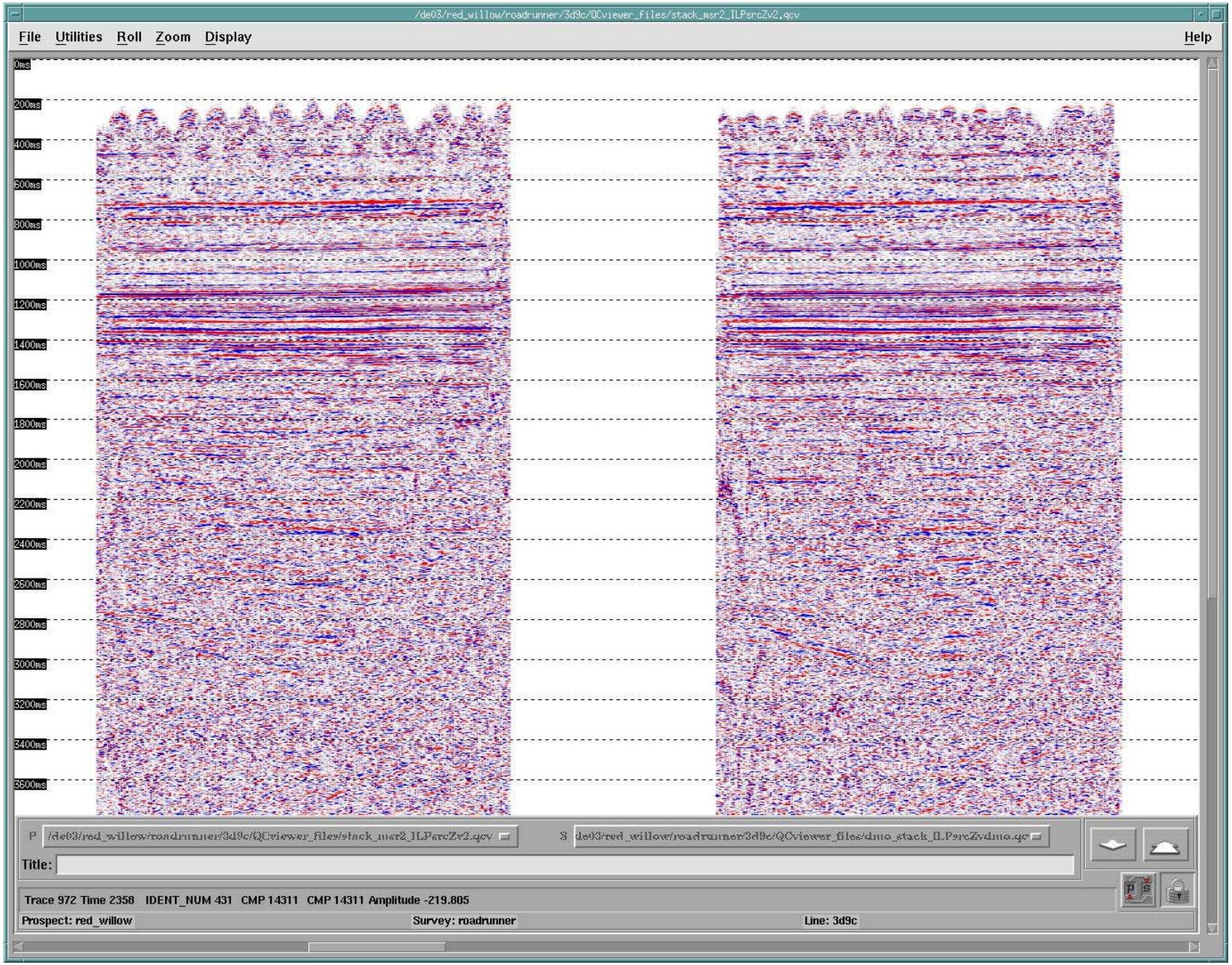

Figure 4-15. Reflection Statics Stack: P source – Vertical component

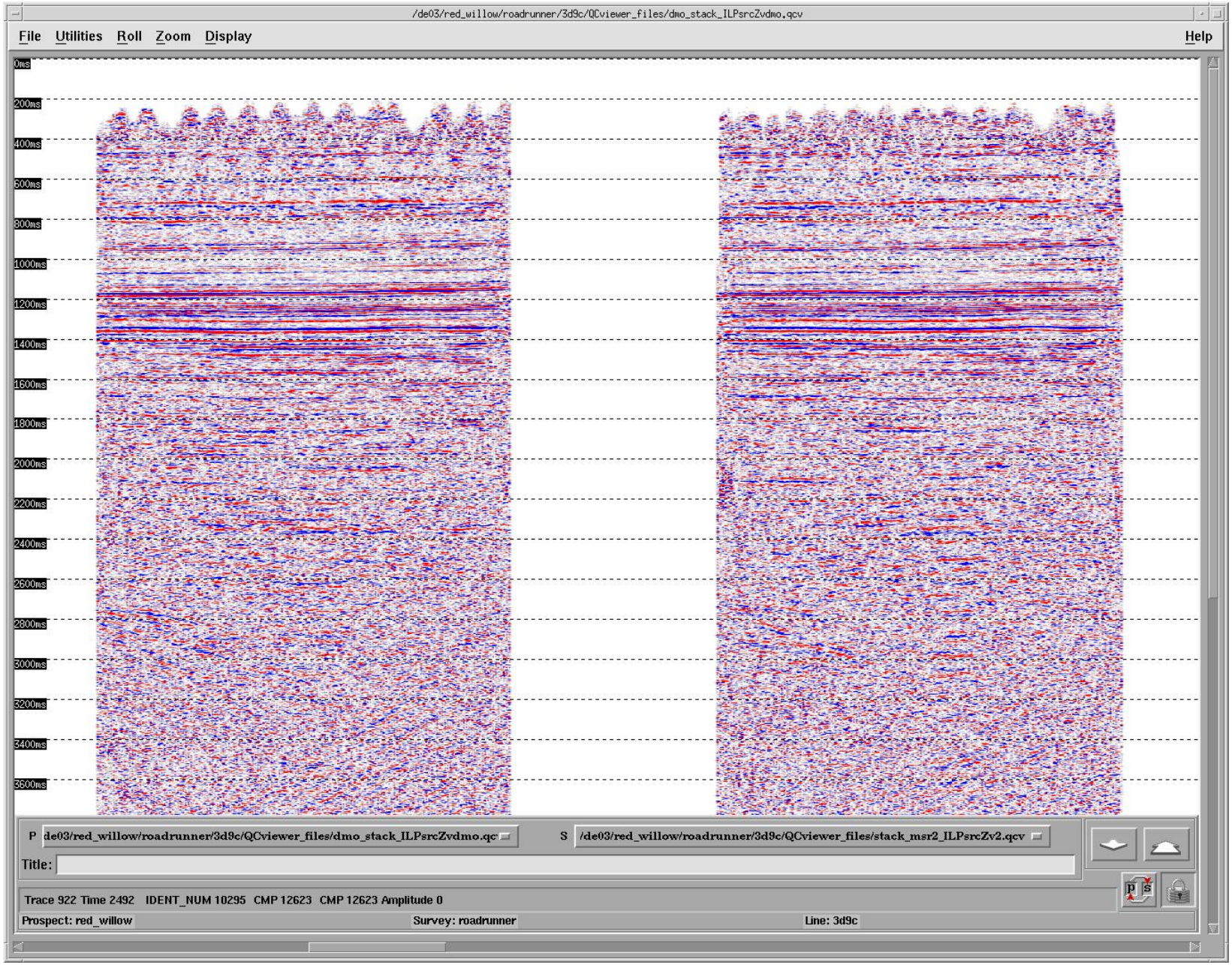

Figure 4-16. DMO Stack: P source – Vertical component.

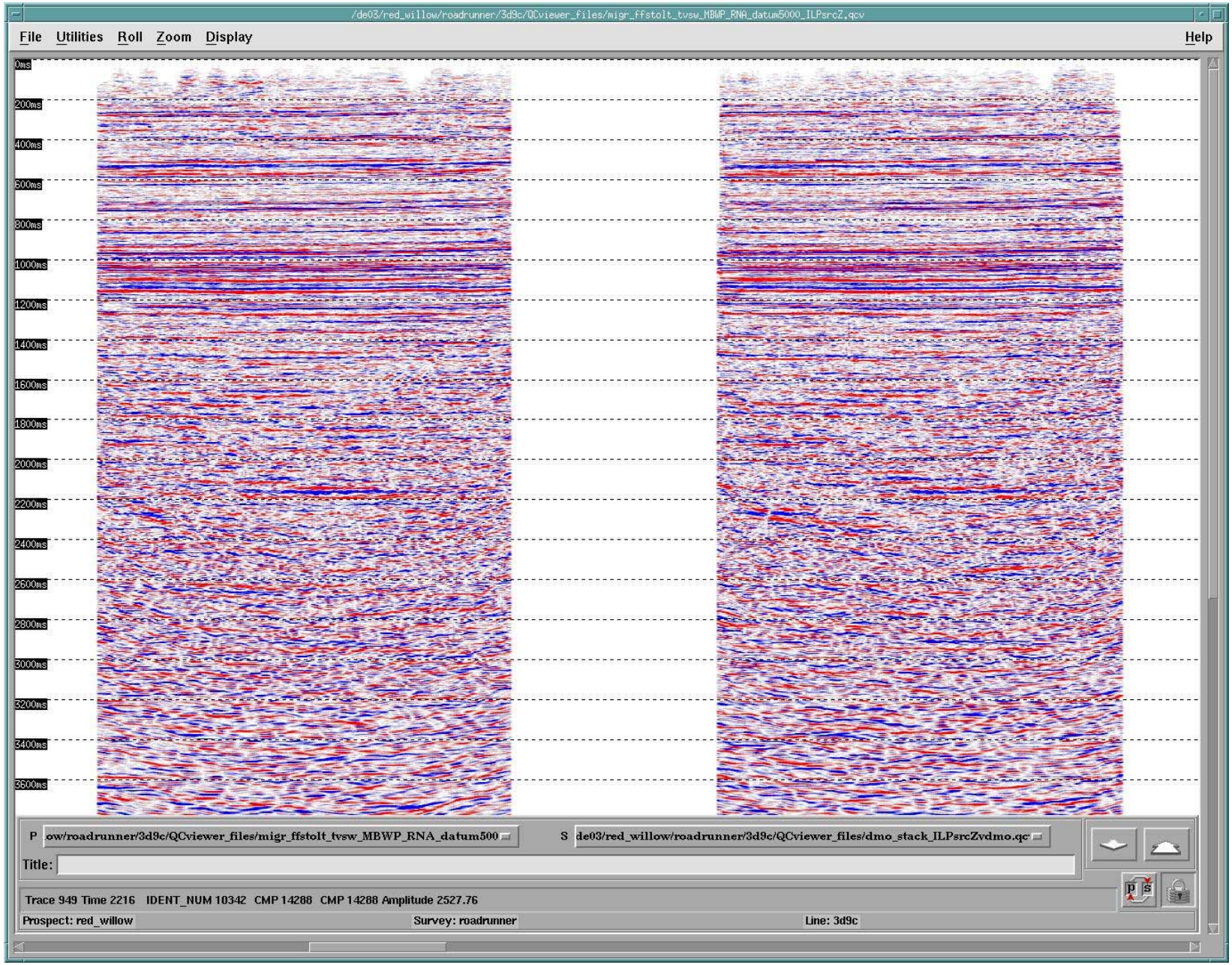

Figure 4-17. Final Migration: P source – Vertical component.

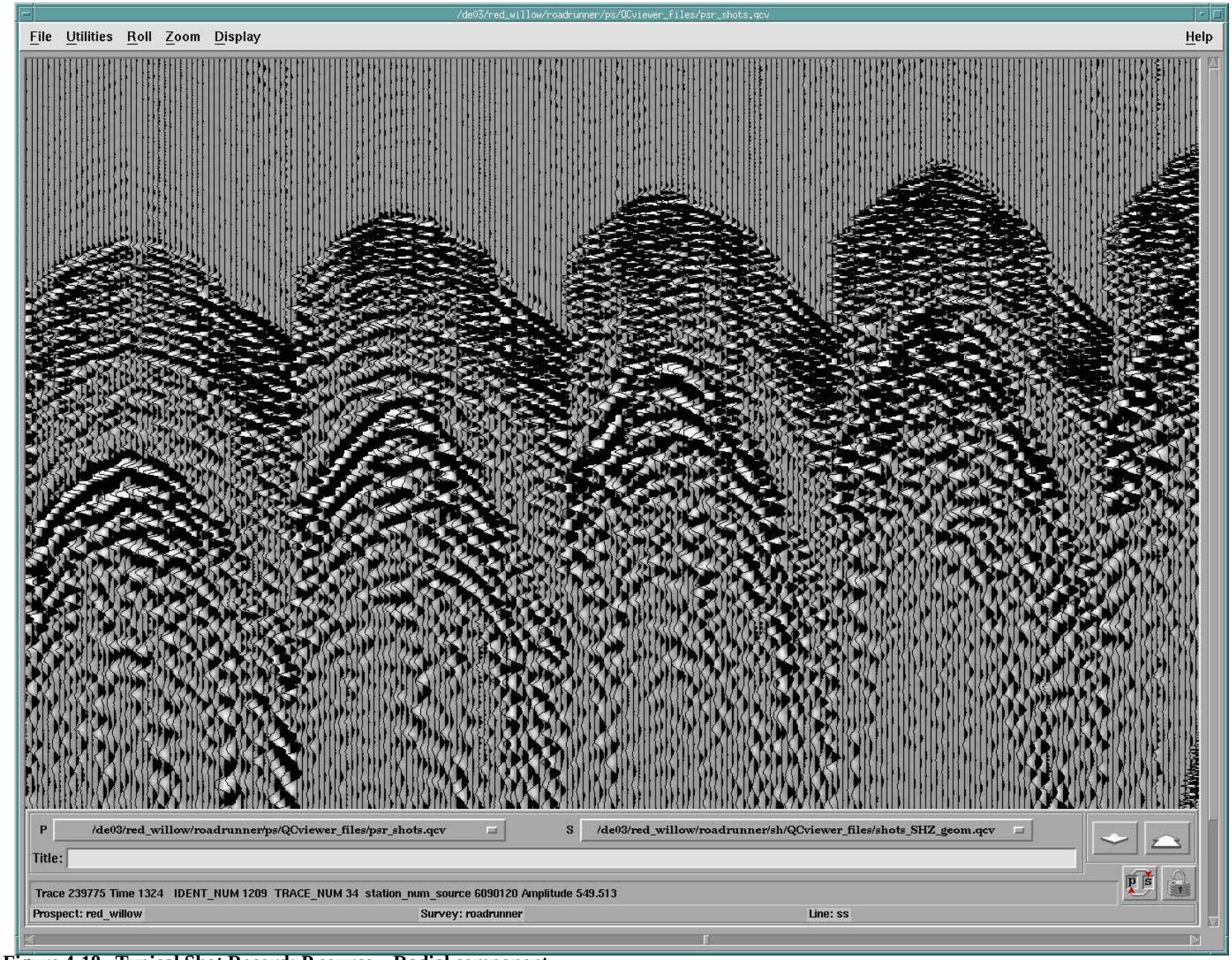

Figure 4-18. Typical Shot Record: P source – Radial component.

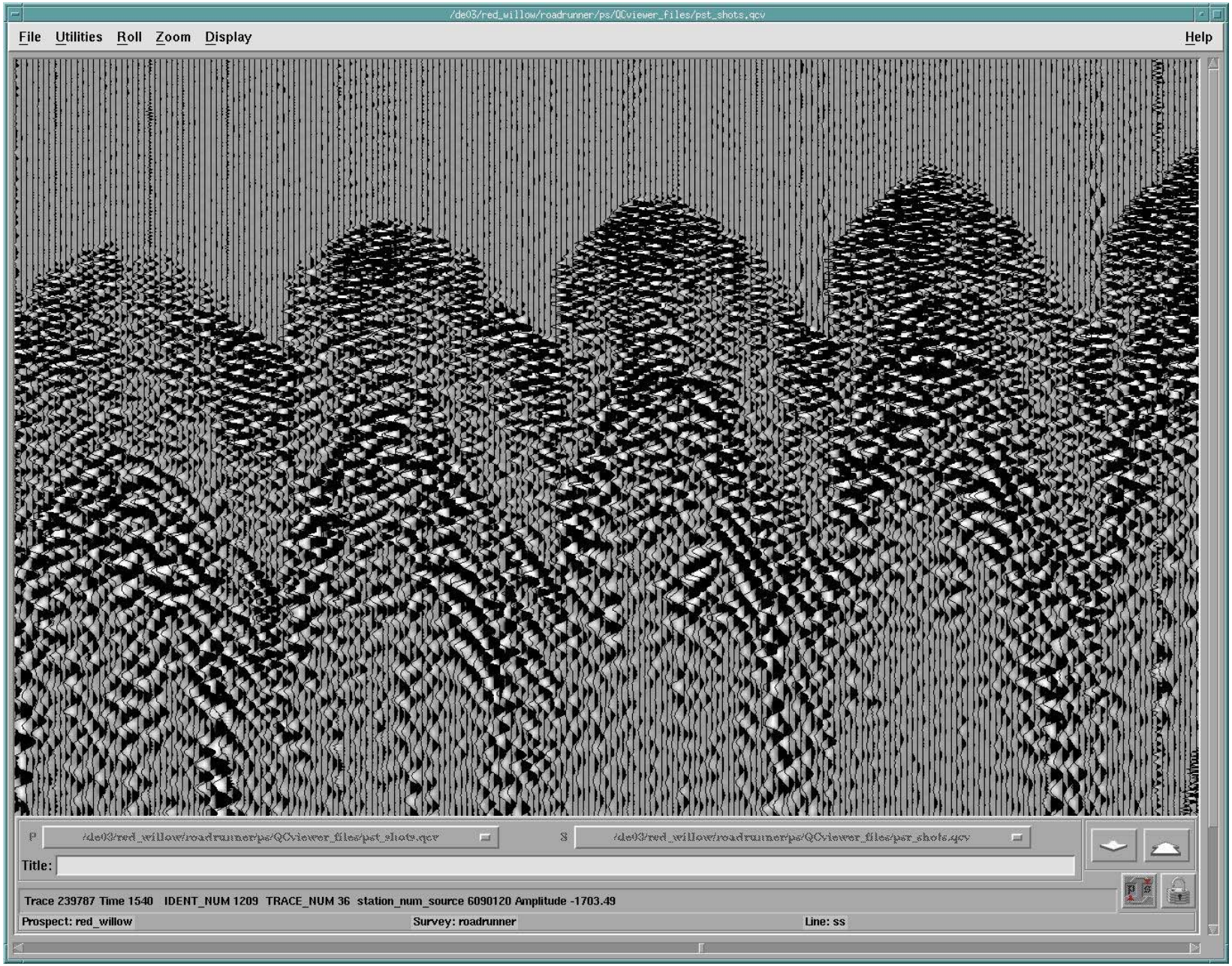

Figure 4-19. Typical Shot Record: P source – Transverse component.

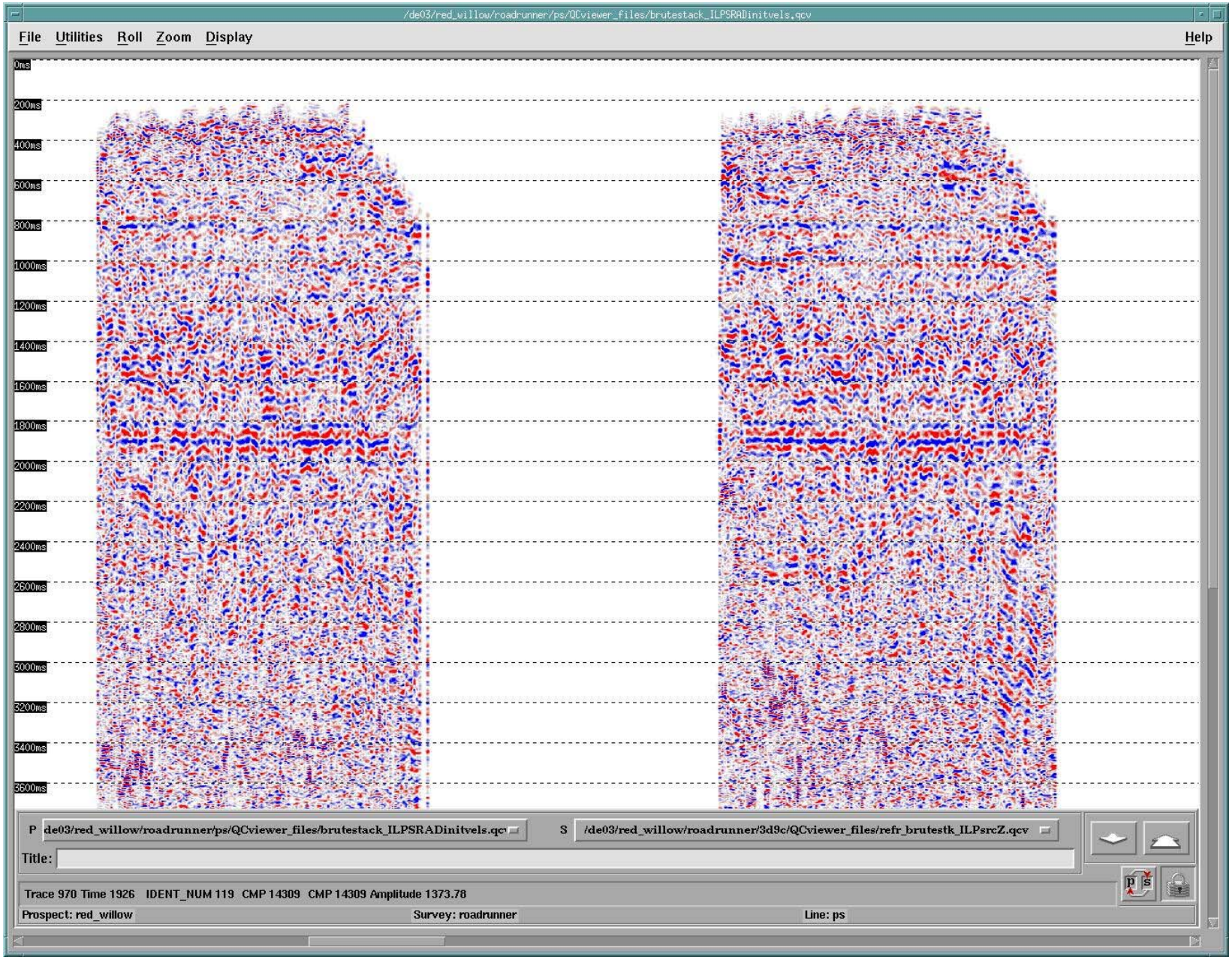

Figure 4-20. Brute Stack: P source – Radial component.

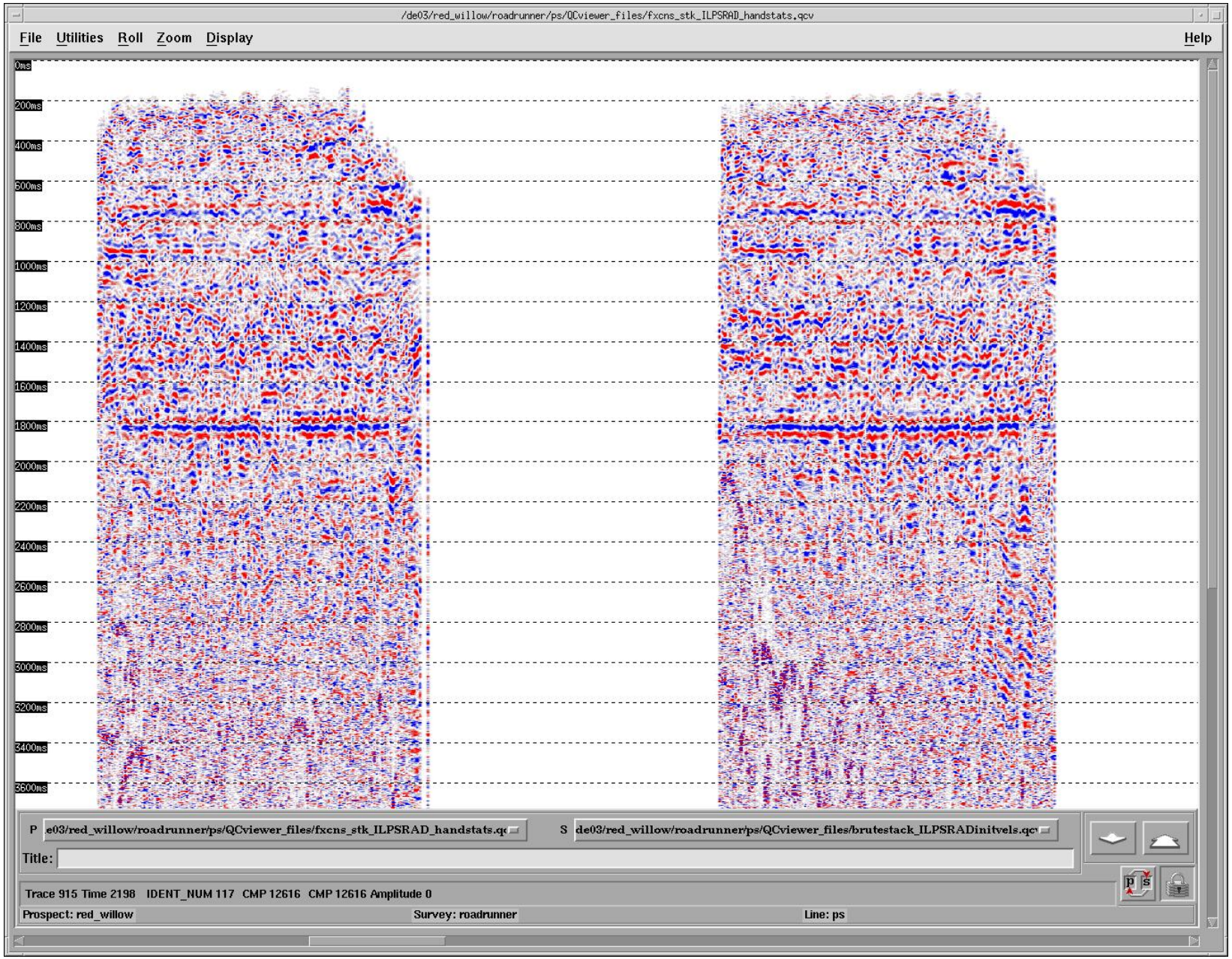

Figure 4-21. Preliminary Statics Stack: P source – Radial component.

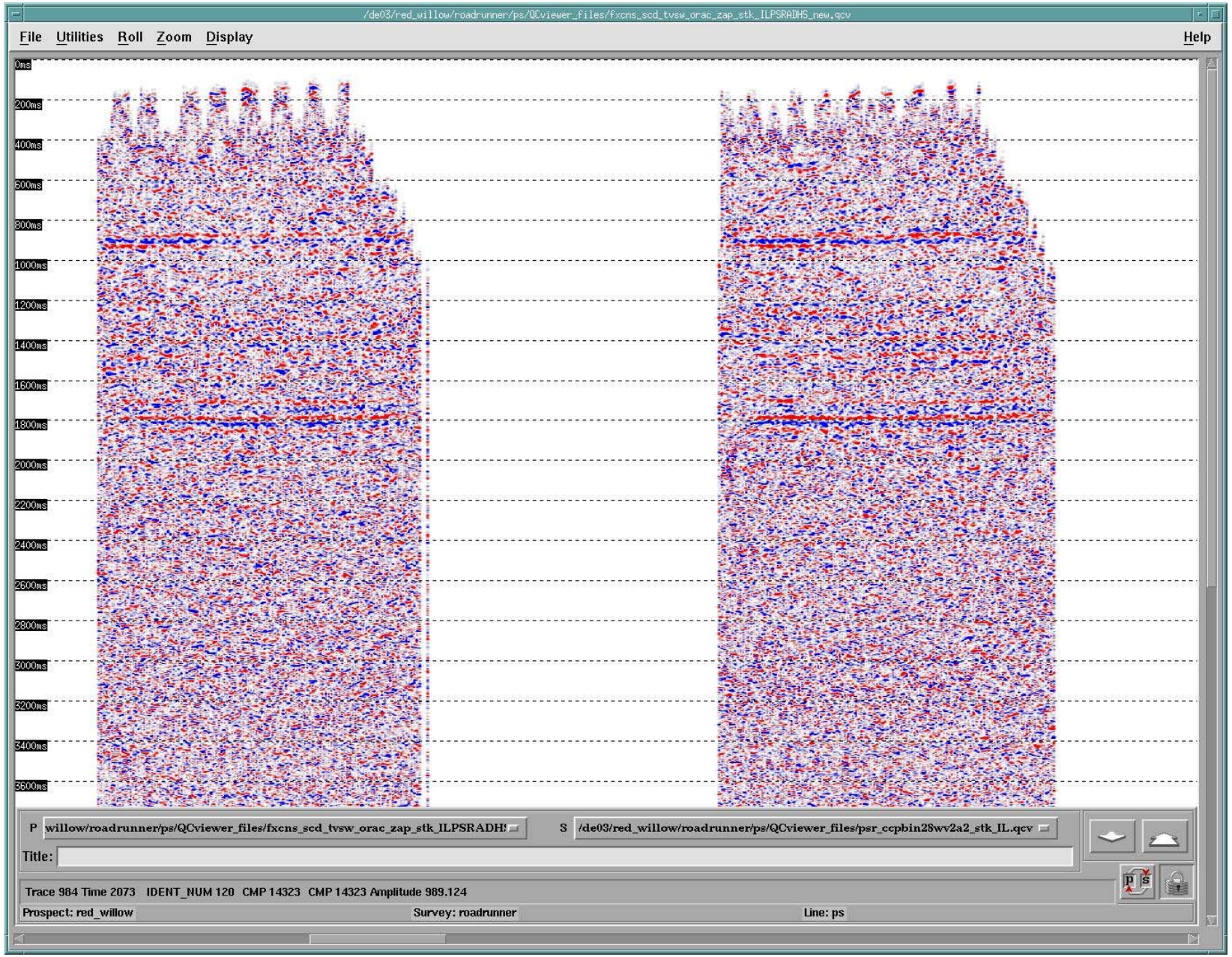

Figure 4-22. SCD/TVSW/ZAP Stack: P source – Radial component.

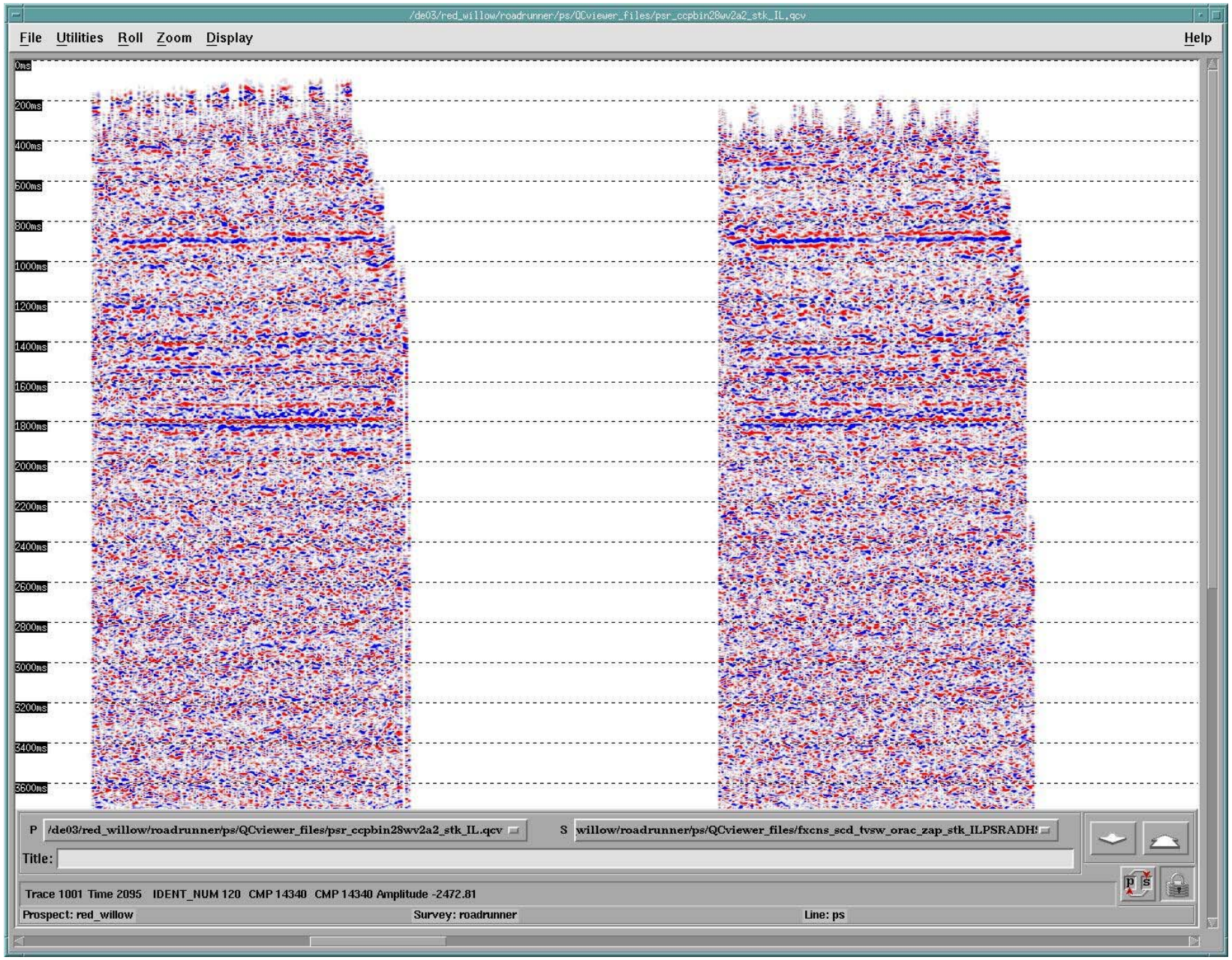

Figure 4-23. Final CCP Stack: P source – Radial component.

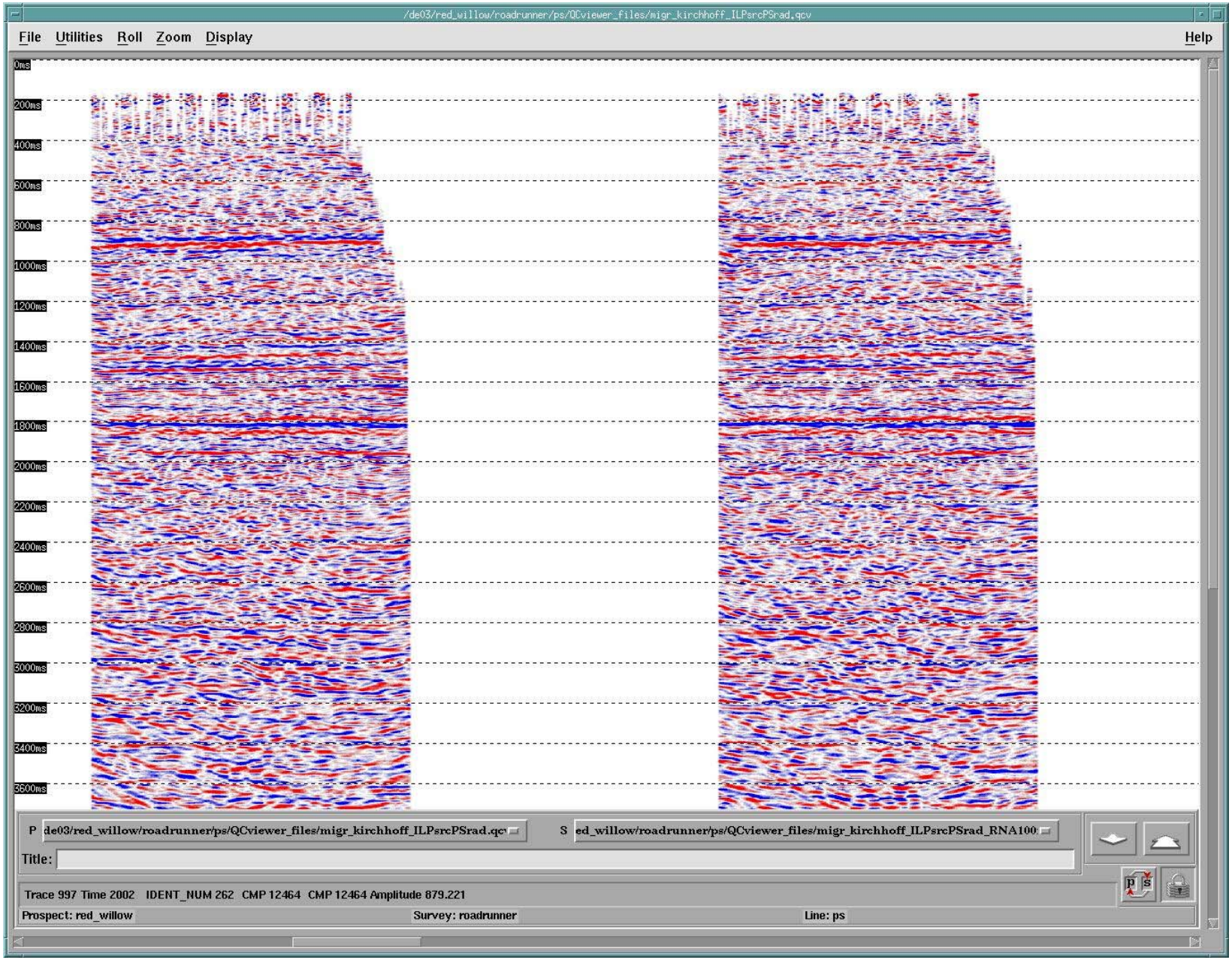

Figure 4-24. Final Migration: P source – Radial component.

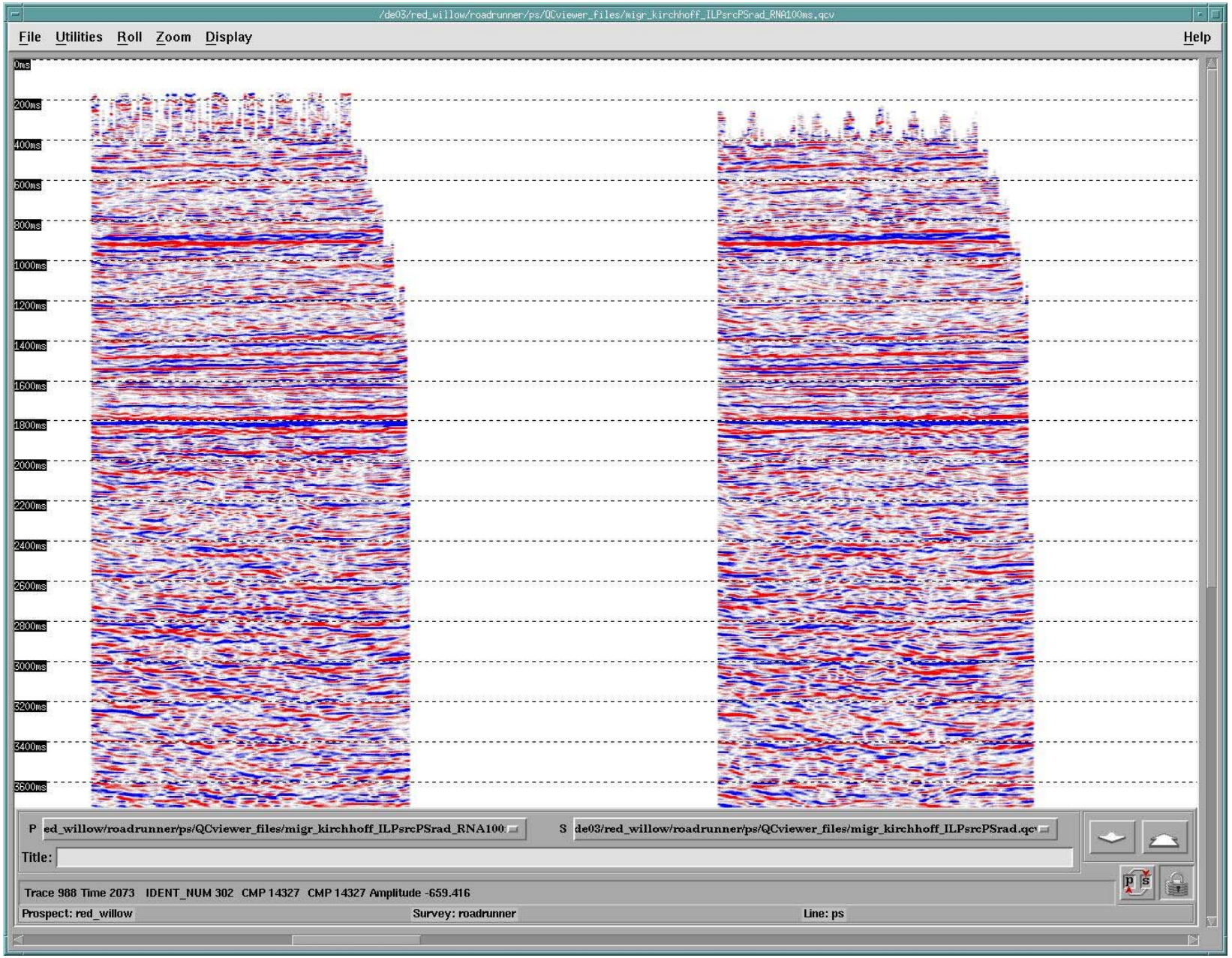

Figure 4-25. Final Migration/FXY Dcn: P source – Radial component.

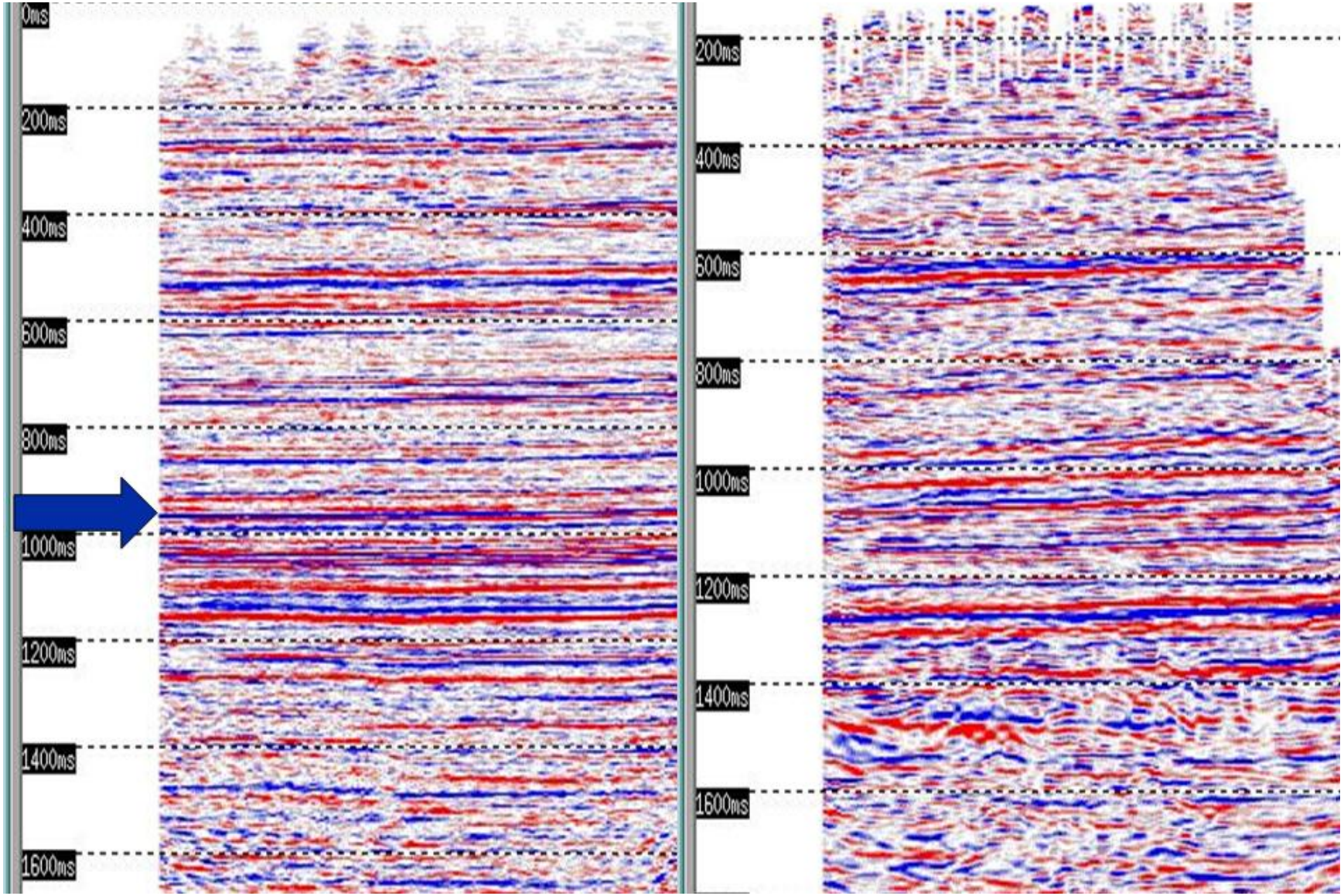

Figure 4-26. Final Migration Comparison: PP to PS.

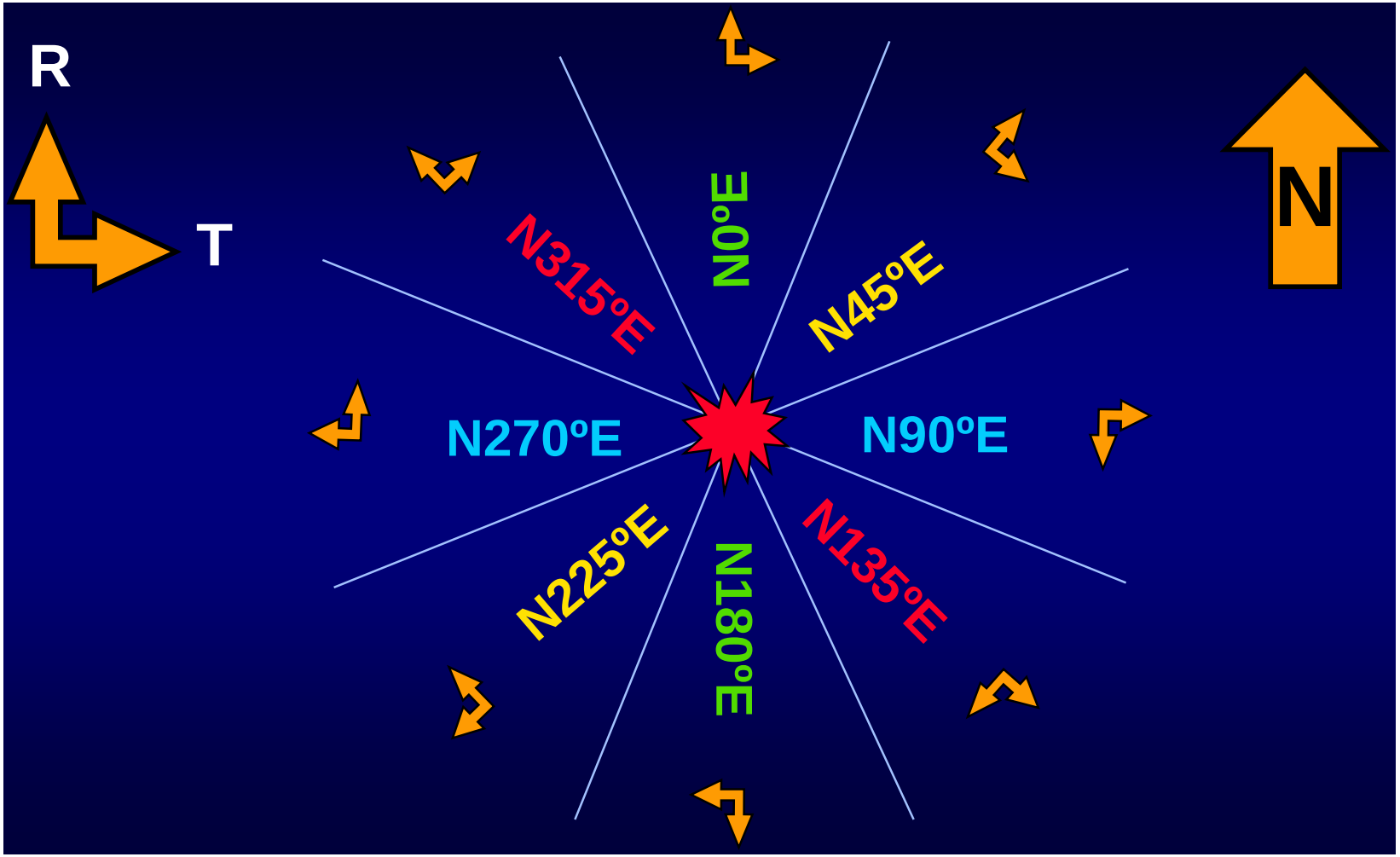

Figure 4-27. Source to Receiver Azimuth Limitation.

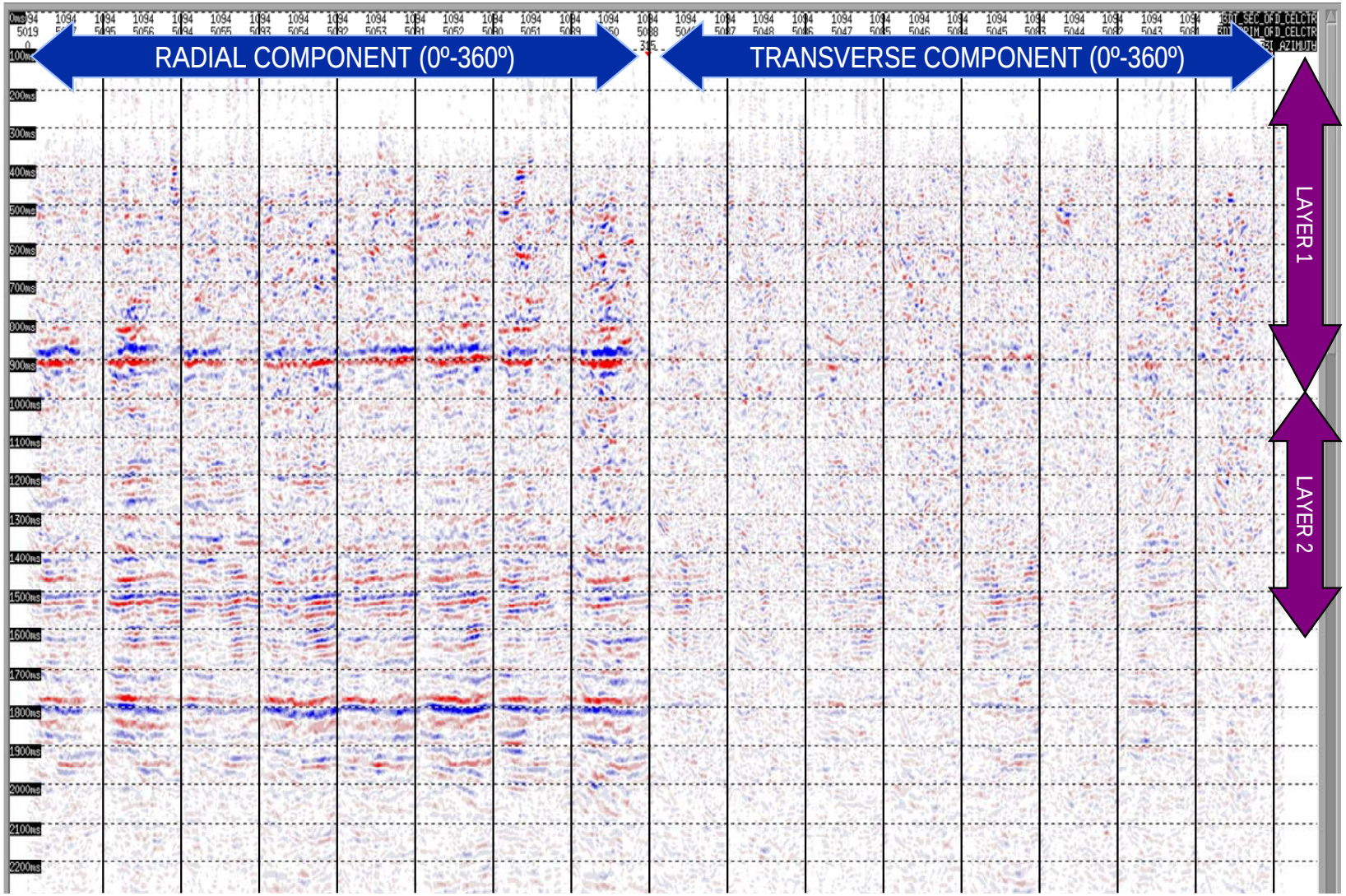

Figure 4-28. PS Input to 2Cx2C Layer Stripping.

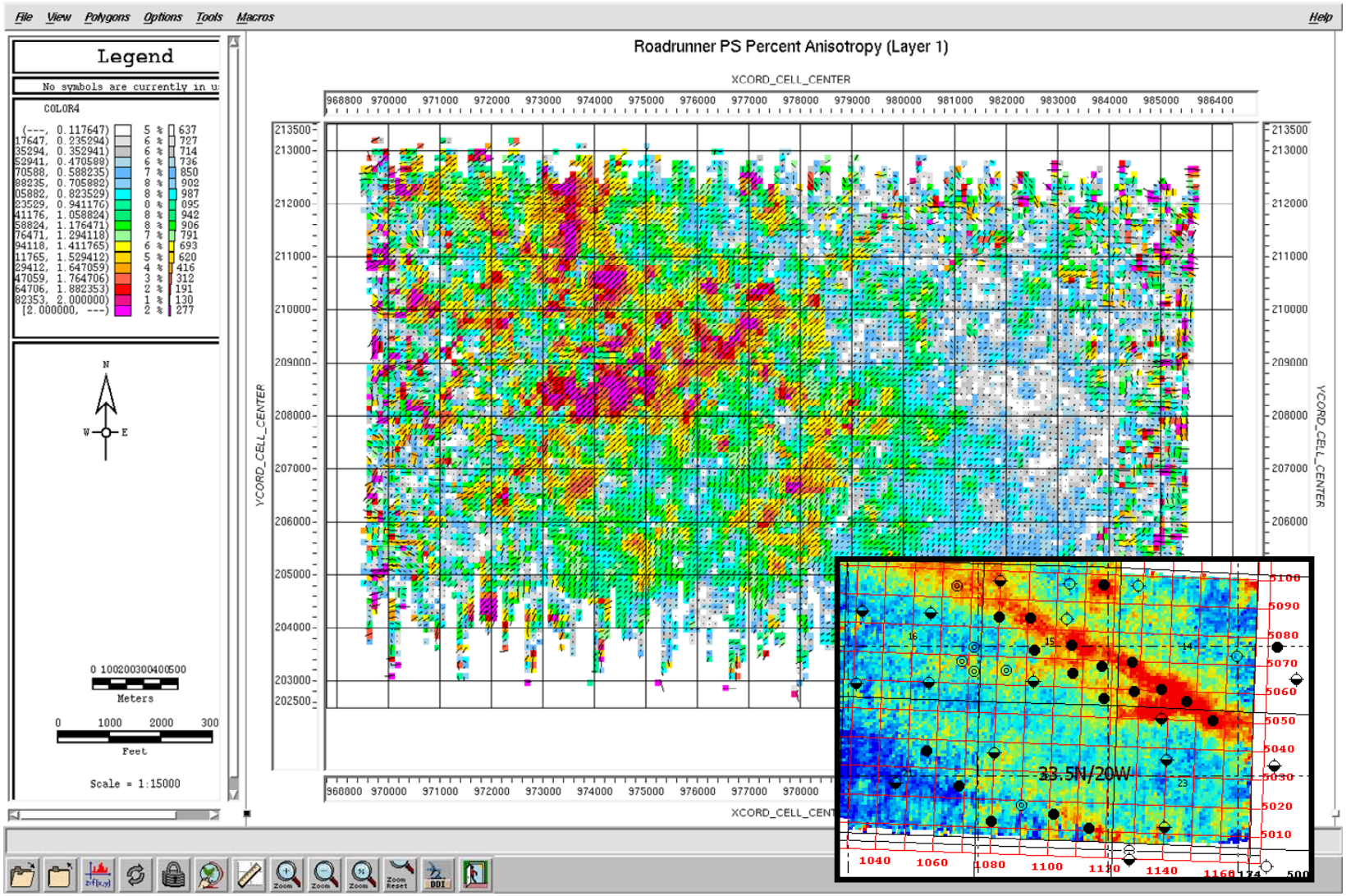

Figure 4-29. S-wave Birefringence: Layer 1.

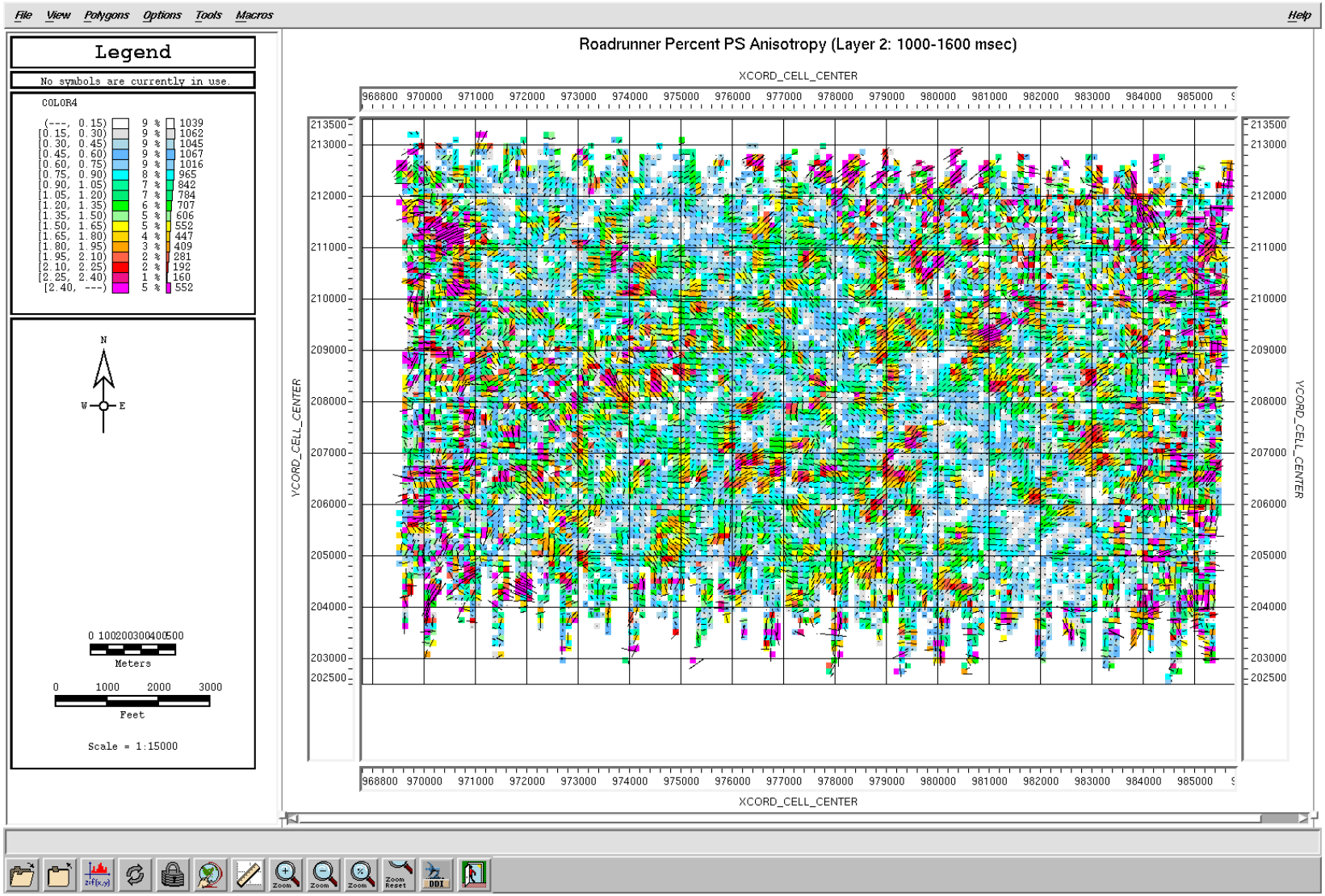

Figure 4-30. S-wave Birefringence: Layer 2.

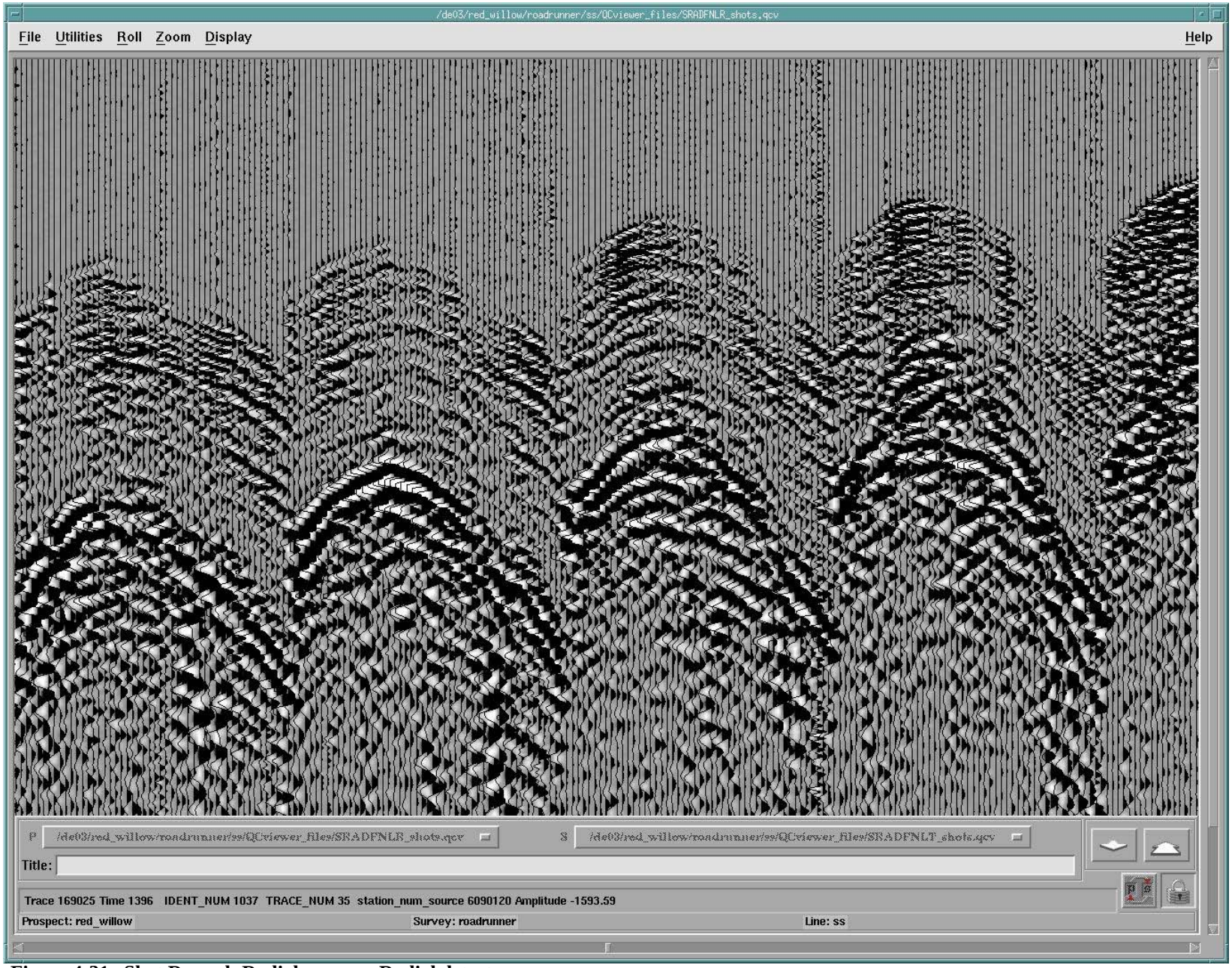

Figure 4-31. Shot Record: Radial source – Radial detector.

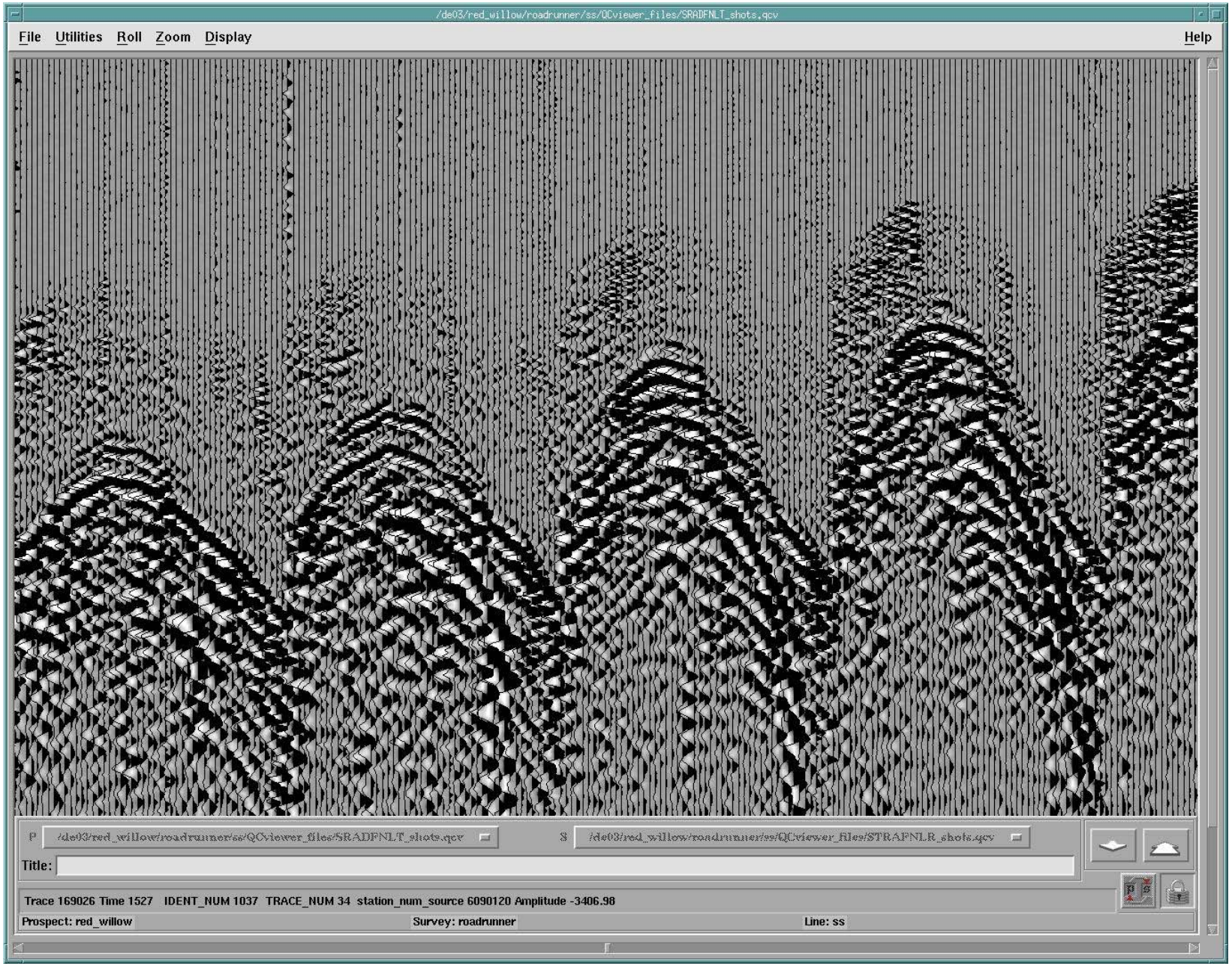

Figure 4-32. Shot Record: Radial source – Trans detector.

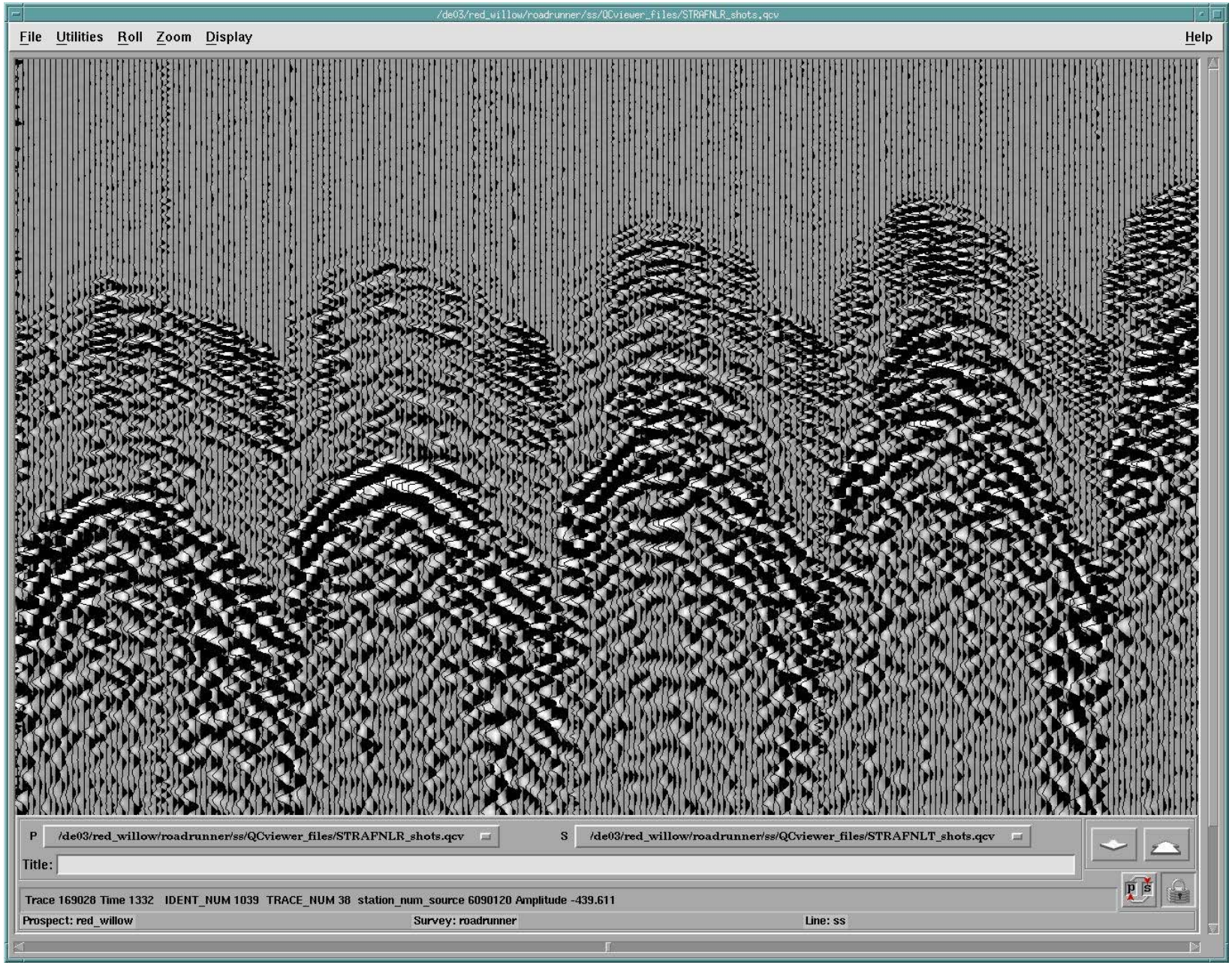

Figure 4-33. Shot Record: Trans source – Radial detector.

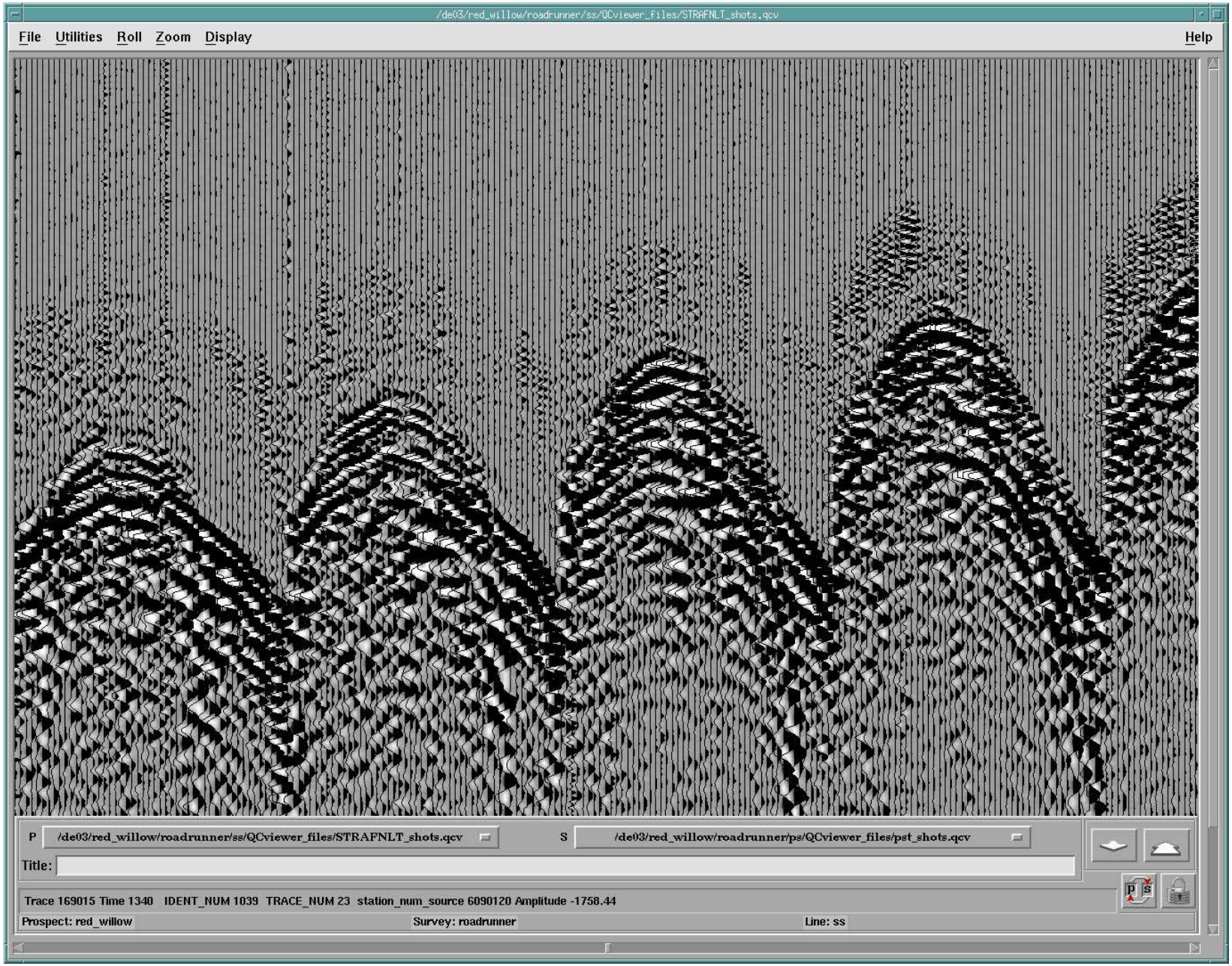

Figure 4-34. Shot Record: Trans source – Trans detector.

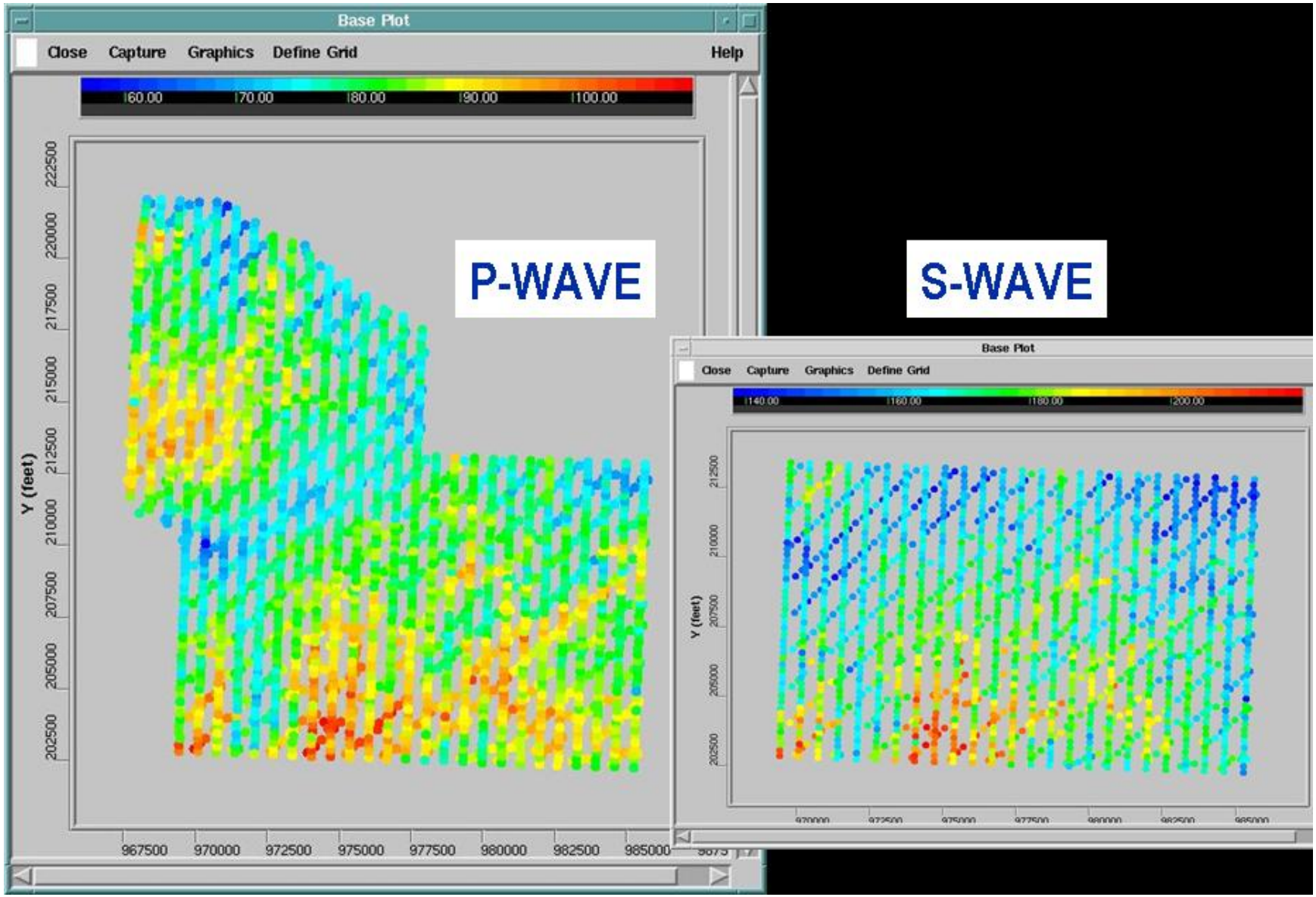

Figure 4-35. Source and receiver statics corrections.

4.2 Interpretation

4.2.1 MAP GENERATION

The Spearman and Kendall correlation coefficients are presented in Table 4-1 and Table 4-2, respectively. The strength of the correlation varies from -1.0 (perfect negative correlation) to +1.0 (perfect positive correlation). The statistical significance, which is the probability of obtaining the observed correlation given the fact that the two variables are uncorrelated, is also shown, along with the number of sample pairs. Correlation coefficients that have a high significance are additionally denoted by a single asterisk (probability < 0.05) or a double asterisk (probability < 0.01). These two tables show that there are many strong correlations among the variables, and also that results for the Spearman and Kendall tests are very similar to one another. More detailed explanations of these two tests can be found in Press and others (1992) and in many introductory statistics texts.

The isopachs between the top of the Ismay and the Top of the Upper Ismay Carbonate (variable IS_UIC) shows the strongest correlation with the Ismay Amplitude (IsAMP) for any of the seismic variables. One would expect that the stepwise regression would include this variable, and that its relation would be both significant and positive. Looking next at the row corresponding to the Ismay Amplitude, the only significant correlation between the amplitude and other seismic variables is for the Mississippian. The other seismic variables do not have significant correlation with Ismay Amplitude.

The multivariate regression results are shown in Figure 4-36 through Figure 4-41. Figure 4-36 shows the results for the isopachs between the Top of the Ismay and the Top of the Upper Ismay Carbonate. As expected, the most significant predictive variable is the Ismay Amplitude. The significance of each coefficient can be determined from the p-value associated with it; the lower the p-value the more significant the variable. The impact is also positive, as inferred from the correlation coefficient. The overall regression, as measured by the F-test, is also statistically significant, as the associated p-value for the F-test is well below 0.05. Visual inspection of the residuals indicates no bias, correlation or obvious departure from a Gaussian distribution. As a consequence, the regression is statistically valid.

Figure 4-37 and Figure 4-38 represent two statistically equal regression models for the isopachs between the top of the Ismay and the top of the Desert Creek. The difference is that one of the variables differs among the two models. These two variables are highly correlated, and thus do not materially effect the regression, but both were analyzed. Both regressions are statistically significant and valid.

Figure 4-39 shows the results for the isopachs between the Top of the Upper Ismay to the Top of the Lower Ismay. This regression is statistically valid as well. The variables that were retained in the stepwise regression consist of the Ismay Peak to Desert Creek isochron, and two variables that have a negative relation to the depth to the top of the

Mississippian (note that the Ismay Amplitude has a negative correlation with the depth to the top of the Mississippian). This might be an indication that the thicker sections of the Upper Ismay may occur where (1) the overall Ismay section is thick; and (2) where the depth to the Mississippian is shallower, perhaps indicating that the mounds preferentially develop along Mississippian highs.

The isopach for the Lower Ismay section (Figure 4-40 and Figure 4-41) are the weakest among all of the regressions, but are still statistically significant. In model 1, only two variables are used. The positive loading with the Ismay Peak to Desert Creek peak isochron includes the Lower Ismay section, and so it is natural that these two should have a positive correlation. The negative loading with the Ismay Amplitude may reflect a Mississippian high, and so the regression is in many ways similar to the one for the Upper Ismay isopach. Regression model 2 contains five variables. The regression may not be valid, as there is substantial colinearity between the seismic variables, and it is not used, even though the F-test has greater significance.

The time-structure maps are shown in Figure 4-42 through Figure 4-46. The isopachs produced through the multivariate regressions are shown in Figure 4-47 through Figure 4-49. Figure 4-50 through Figure 4-53 show depth (structural contour) maps for selected horizons. Each map also contains symbols showing whether the well was a producing well or a dry hole.

4.2.2 TIME STRUCTURE MAPS

Time structure maps for the key seismic horizons were generated. Time structure highs are in red. Time structure lows are in green to blue. Time structure mapping indicates that Ismay regional dip, as indicated by the Ismay Zero Crossing map (Figure 4-42) is to the southwest. Very subtle four-way time structural closures and noses are noted in Ismay producing areas. Time structure maps for the Ismay Peak, Hovenweep Trough, and Desert Creek Peak are shown in Figures 4-43 through 4-45, respectively. In general, all these time structure maps exhibit very similar characteristics.

The Mississippian Time Structure map (Figure 4-46) shows that the Mississippian structure is more variable than Pennsylvanian Ismay structure. Multiple time structural closures and noses are noted within the Roadrunner survey. These Mississippian time structure highs may be prospective for oil and gas drilling. In most cases the structurally favorable Mississippian features do not correspond to Ismay mound areas. Ismay mound production does not seem to be associated with Mississippian structural highs in any direct manner.

Correlations

			AblS	IS0	ISPeak	DCPeak	Miss	Ipeak_DC	ISO_DC	ISPEAK_DC	IsAMP	IS_UIC	IS_DC	TUI_TLI	TLI_TDC
Spearman's rho	AblS	Correlation Coefficient	1.000	.962**	.951**	.950**	.277	-.537**	-.613**	-.541**	-.209	-.168	-.568**	-.332*	-.070
		Sig. (2-tailed)	.	.000	.000	.000	.069	.000	.000	.000	.173	.277	.002	.031	.730
		N	44	44	44	44	44	44	44	44	44	44	27	42	27
	IS0	Correlation Coefficient	.962**	1.000	.993**	.965**	.235	-.574**	-.635**	-.578**	-.217	-.140	-.552**	-.292	-.097
		Sig. (2-tailed)	.000	.	.000	.000	.124	.000	.000	.000	.158	.365	.003	.061	.631
		N	44	44	44	44	44	44	44	44	44	44	27	42	27
	ISPeak	Correlation Coefficient	.951**	.993**	1.000	.948**	.214	-.622**	-.663**	-.624**	-.168	-.113	-.589**	-.342*	-.134
		Sig. (2-tailed)	.000	.000	.	.000	.164	.000	.000	.000	.275	.466	.001	.026	.506
		N	44	44	44	44	44	44	44	44	44	44	27	42	27
	DCPeak	Correlation Coefficient	.950**	.965**	.948**	1.000	.194	-.426**	-.481**	-.428**	-.277	-.215	-.425*	-.153	-.017
		Sig. (2-tailed)	.000	.000	.000	.	.208	.004	.001	.004	.069	.160	.027	.334	.935
		N	44	44	44	44	44	44	44	44	44	44	27	42	27
	Miss	Correlation Coefficient	.277	.235	.214	.194	1.000	-.214	-.315*	-.205	-.413**	-.097	-.341	-.131	-.285
		Sig. (2-tailed)	.069	.124	.164	.208	.	.163	.037	.181	.005	.532	.082	.408	.149
		N	44	44	44	44	44	44	44	44	44	44	27	42	27
	Ipeak_DC	Correlation Coefficient	-.537**	-.574**	-.622**	-.426**	-.214	1.000	.928**	.995**	-.040	-.016	.898**	.622**	.468*
		Sig. (2-tailed)	.000	.000	.000	.004	.163	.	.000	.000	.797	.918	.000	.000	.014
		N	44	44	44	44	44	44	44	44	44	44	27	42	27
	ISO_DC	Correlation Coefficient	-.613**	-.635**	-.663**	-.481**	-.315*	.928**	1.000	.928**	.133	.091	.868**	.532**	.470*
		Sig. (2-tailed)	.000	.000	.000	.001	.037	.000	.	.000	.391	.557	.000	.000	.013
		N	44	44	44	44	44	44	44	44	44	44	27	42	27
	ISPEAK_DC	Correlation Coefficient	-.541**	-.578**	-.624**	-.428**	-.205	.995**	.928**	1.000	-.049	-.008	.910**	.619**	.486*
		Sig. (2-tailed)	.000	.000	.000	.004	.181	.000	.000	.	.751	.957	.000	.000	.010
		N	44	44	44	44	44	44	44	46	44	44	27	42	27
	IsAMP	Correlation Coefficient	-.209	-.217	-.168	-.277	-.413**	-.040	.133	-.049	1.000	.476**	.008	-.431**	-.159
		Sig. (2-tailed)	.173	.158	.275	.069	.005	.797	.391	.751	.	.001	.967	.004	.427
		N	44	44	44	44	44	44	44	44	44	44	27	42	27
	IS_UIC	Correlation Coefficient	-.168	-.140	-.113	-.215	-.097	-.016	.091	-.008	.476**	1.000	.050	-.646**	-.566**
		Sig. (2-tailed)	.277	.365	.466	.160	.532	.918	.557	.957	.001	.	.805	.000	.002
		N	44	44	44	44	44	44	44	44	44	44	27	42	27
	IS_DC	Correlation Coefficient	-.568**	-.552**	-.589**	-.425*	-.341	.898**	.868**	.910**	.008	.050	1.000	.759**	.518**
		Sig. (2-tailed)	.002	.003	.001	.027	.082	.000	.000	.000	.967	.805	.	.000	.006
		N	27	27	27	27	27	27	27	27	27	27	27	27	27
	TUI_TLI	Correlation Coefficient	-.332*	-.292	-.342*	-.153	-.131	.622**	.532**	.619**	-.431**	-.646**	.759**	1.000	.663**
		Sig. (2-tailed)	.031	.061	.026	.334	.408	.000	.000	.000	.004	.000	.000	.	.000
		N	42	42	42	42	42	42	42	42	42	42	27	42	27
	TLI_TDC	Correlation Coefficient	-.070	-.097	-.134	-.017	-.285	.468*	.470*	.486*	-.159	-.566**	.518**	.663**	1.000
		Sig. (2-tailed)	.730	.631	.506	.935	.149	.014	.013	.010	.427	.002	.006	.000	.
		N	27	27	27	27	27	27	27	27	27	27	27	27	27

**. Correlation is significant at the 0.01 level (2-tailed).

*. Correlation is significant at the 0.05 level (2-tailed).

Table 4-1. Spearman correlation coefficients for Western #1 seismic variables.

Correlations

			AblS	IS0	ISPeak	DCPeak	Miss	Ipeak_DC	ISO_DC	ISPEAK_DC	IsAMP	IS_UIC	IS_DC	TUI_TLI	TLI_TDC
Kendall's tau_b	AblS	Correlation Coefficient	1.000	.884**	.847**	.833**	.217*	-.387**	-.433**	-.386**	-.145	-.125	-.423**	-.241*	-.038
		Sig. (2-tailed)	.	.000	.000	.000	.040	.000	.000	.000	.169	.236	.002	.026	.786
		N	44	44	44	44	44	44	44	44	44	44	27	42	27
	IS0	Correlation Coefficient	.884**	1.000	.948**	.867**	.183	-.420**	-.459**	-.419**	-.158	-.109	-.409**	-.214*	-.052
		Sig. (2-tailed)	.000	.	.000	.000	.082	.000	.000	.000	.132	.302	.003	.048	.707
		N	44	44	44	44	44	44	44	44	44	44	27	42	27
	ISPeak	Correlation Coefficient	.847**	.948**	1.000	.837**	.166	-.458**	-.485**	-.464**	-.122	-.085	-.430**	-.249*	-.084
		Sig. (2-tailed)	.000	.000	.	.000	.114	.000	.000	.000	.245	.418	.002	.021	.544
		N	44	44	44	44	44	44	44	44	44	44	27	42	27
	DCPeak	Correlation Coefficient	.833**	.867**	.837**	1.000	.169	-.290**	-.319**	-.294**	-.203	-.165	-.285*	-.123	.000
		Sig. (2-tailed)	.000	.000	.000	.	.108	.006	.002	.005	.052	.117	.039	.255	1.000
		N	44	44	44	44	44	44	44	44	44	44	27	42	27
	Miss	Correlation Coefficient	.217*	.183	.166	.169	1.000	-.144	-.218*	-.145	-.295**	-.071	-.237	-.089	-.217
		Sig. (2-tailed)	.040	.082	.114	.108	.	.172	.040	.171	.005	.504	.087	.410	.117
		N	44	44	44	44	44	44	44	44	44	44	27	42	27
	Ipeak_DC	Correlation Coefficient	-.387**	-.420**	-.458**	-.290**	-.144	1.000	.817**	.965**	-.032	-.009	.749**	.430**	.299*
		Sig. (2-tailed)	.000	.000	.000	.006	.172	.	.000	.000	.761	.935	.000	.000	.031
		N	44	44	44	44	44	44	44	44	44	44	27	42	27
	ISO_DC	Correlation Coefficient	-.433**	-.459**	-.485**	-.319**	-.218*	.817**	1.000	.814**	.088	.068	.701**	.355**	.303*
		Sig. (2-tailed)	.000	.000	.000	.002	.040	.000	.	.000	.406	.523	.000	.001	.030
		N	44	44	44	44	44	44	44	44	44	44	27	42	27
	ISPEAK_DC	Correlation Coefficient	-.386**	-.419**	-.464**	-.294**	-.145	.965**	.814**	1.000	-.039	-.009	.773**	.433**	.320*
		Sig. (2-tailed)	.000	.000	.000	.005	.171	.000	.000	.	.715	.935	.000	.000	.022
		N	44	44	44	44	44	44	44	46	44	44	27	42	27
	IsAMP	Correlation Coefficient	-.145	-.158	-.122	-.203	-.295**	-.032	.088	-.039	1.000	.331**	.017	-.312**	-.113
		Sig. (2-tailed)	.169	.132	.245	.052	.005	.761	.406	.715	.	.002	.900	.004	.415
		N	44	44	44	44	44	44	44	44	44	44	27	42	27
	IS_UIC	Correlation Coefficient	-.125	-.109	-.085	-.165	-.071	-.009	.068	-.009	.331**	1.000	.041	-.495**	-.423**
		Sig. (2-tailed)	.236	.302	.418	.117	.504	.935	.523	.935	.002	.	.770	.000	.002
		N	44	44	44	44	44	44	44	44	44	44	27	42	27
	IS_DC	Correlation Coefficient	-.423**	-.409**	-.430**	-.285*	-.237	.749**	.701**	.773**	.017	.041	1.000	.561**	.380**
		Sig. (2-tailed)	.002	.003	.002	.039	.087	.000	.000	.000	.900	.770	.	.000	.007
		N	27	27	27	27	27	27	27	27	27	27	27	27	27
	TUI_TLI	Correlation Coefficient	-.241*	-.214*	-.249*	-.123	-.089	.430**	.355**	.433**	-.312**	-.495**	.561**	1.000	.515**
		Sig. (2-tailed)	.026	.048	.021	.255	.410	.000	.001	.000	.004	.000	.000	.	.000
		N	42	42	42	42	42	42	42	42	42	42	27	42	27
	TLI_TDC	Correlation Coefficient	-.038	-.052	-.084	.000	-.217	.299*	.303*	.320*	-.113	-.423**	.380**	.515**	1.000
		Sig. (2-tailed)	.786	.707	.544	1.000	.117	.031	.030	.022	.415	.002	.007	.000	.
		N	27	27	27	27	27	27	27	27	27	27	27	27	27

**. Correlation is significant at the 0.01 level (2-tailed).

*. Correlation is significant at the 0.05 level (2-tailed).

Table 4-2. Kendall correlation coefficients for Western #1 seismic variables.

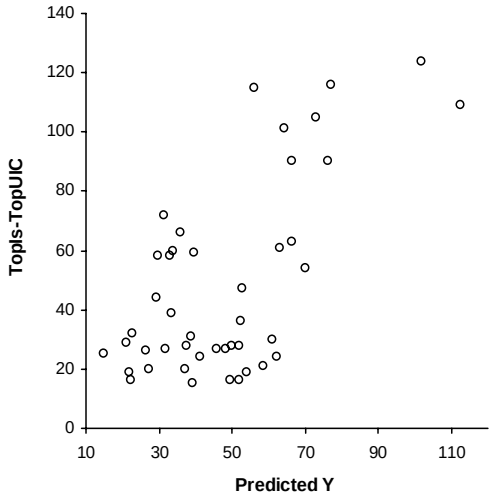

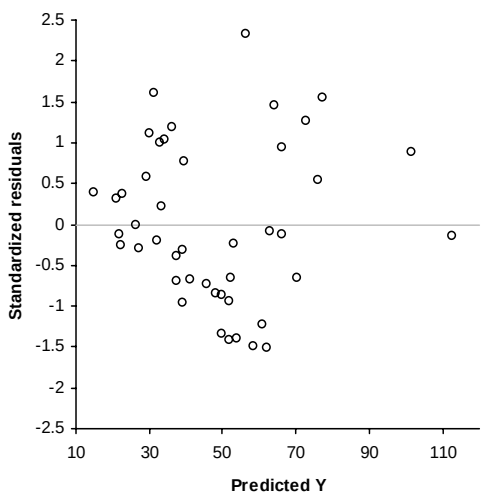

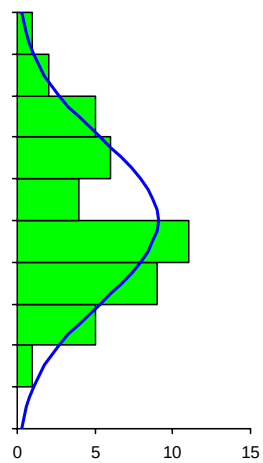

n	44

R^2	0.42
Adjusted R^2	0.38
SE	25.2389

Term	Coefficient	SE	p	95% CI of Coefficient
Intercept	545.0627	868.3481	0.5338	-1209.9340 to 2300.0594
Western 1 Above Ismay	-0.5309	0.8854	0.5522	-2.3203 to 1.2586
Western 1 Ismay Amp	0.0284	0.0063	<0.0001	0.0157 to 0.0411
Western 1 Ismay Peak-DC	-3.6444	3.2006	0.2616	-10.1132 to 2.8243

Source of variation	SSq	DF	MSq	F	p
Due to regression	18810.707	3	6270.236	9.84	<0.0001
About regression	25480.089	40	637.002		
Total	44290.795	43			

Figure 4-36. Regression for the Isoapch Top Ismay to Top Upper Ismay Carbonate.

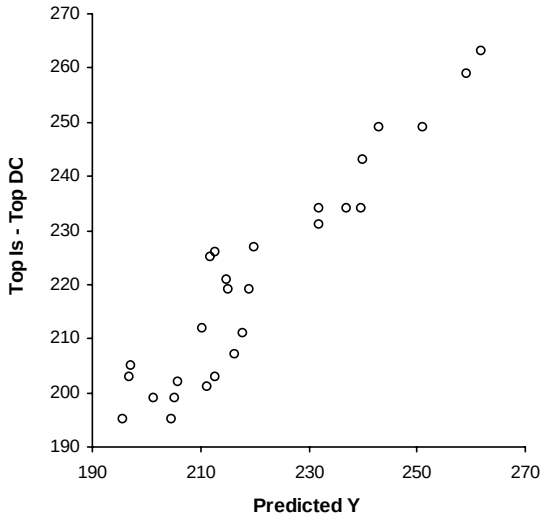

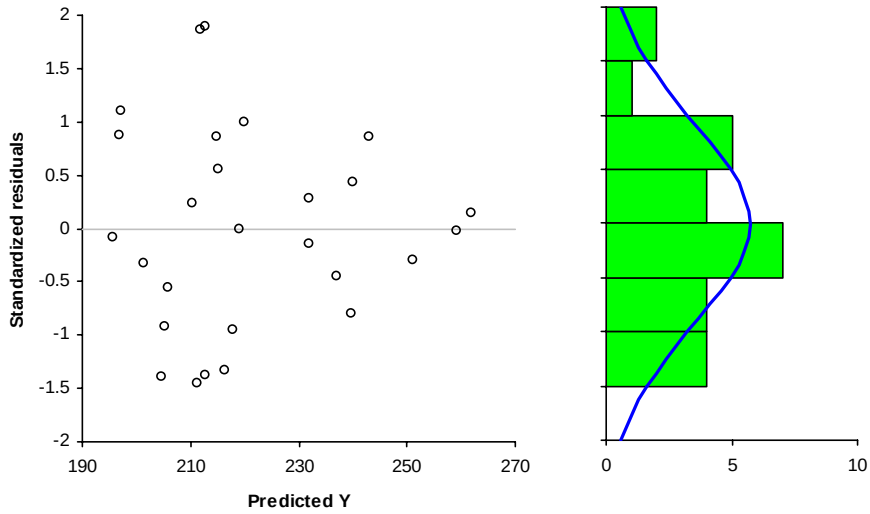

n	27 (cases excluded: 17 due to missing values)

R^2	0.89
Adjusted R^2	0.88
SE	7.0132

Term	Coefficient	SE	p	95% CI of Coefficient
Intercept	23.1340	322.0309	0.9434	-643.0376 to 689.3055
Western 1 I Peak(E) -DC (E)	8.8485	1.5161	<0.0001	5.7121 to 11.9849
Western 1 Above Ismay	-3.2802	1.5389	0.0440	-6.4638 to -0.0967
Western 1 DC Peak	3.1412	1.5359	0.0524	-0.0361 to 6.3184

Source of variation	SSq	DF	MSq	F	p
Due to regression	9182.589	3	3060.863	62.23	<0.0001
About regression	1131.263	23	49.185		
Total	10313.852	26			

Figure 4-37. Regression for the Isoapch Top Ismay to Top Desert Creek, version 1.

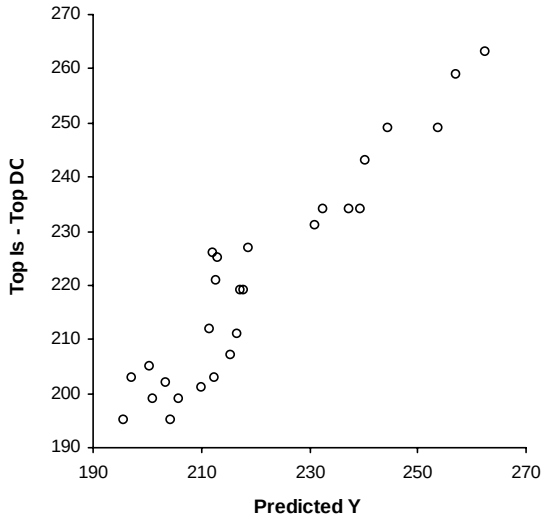

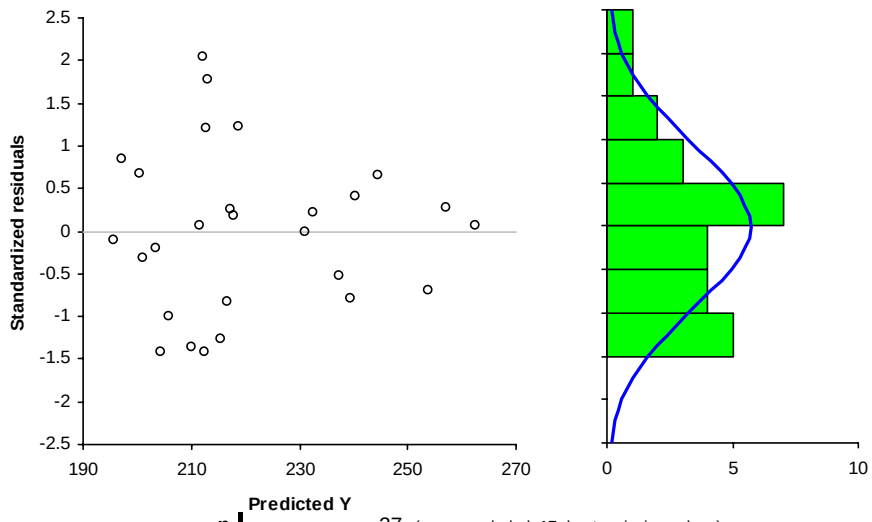

n	27 (cases excluded: 17 due to missing values)

R^2	0.90
Adjusted R^2	0.89
SE	6.7207

Term	Coefficient	SE	p	95% CI of Coefficient
Intercept	-90.7656	314.0162	0.7751	-740.3575 to 558.8262
Western 1 Ismay Peak-DC	9.3886	1.5008	<0.0001	6.2840 to 12.4932
Western 1 DC Peak	3.0108	1.4673	0.0517	-0.0246 to 6.0462
Western 1 Above Ismay	-3.0345	1.4817	0.0521	-6.0996 to 0.0306

Source of variation	SSq	DF	MSq	F	p
Due to regression	9274.984	3	3091.661	68.45	<0.0001
About regression	1038.868	23	45.168		
Total	10313.852	26			

Figure 4-38. Regression for the Isoapch Top Ismay to Top Desert Creek, version 2.

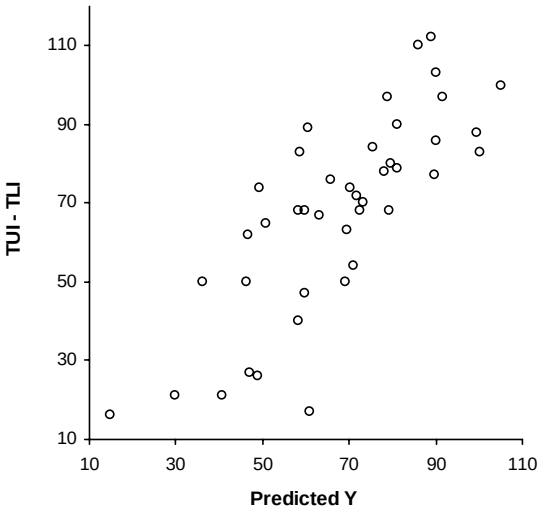

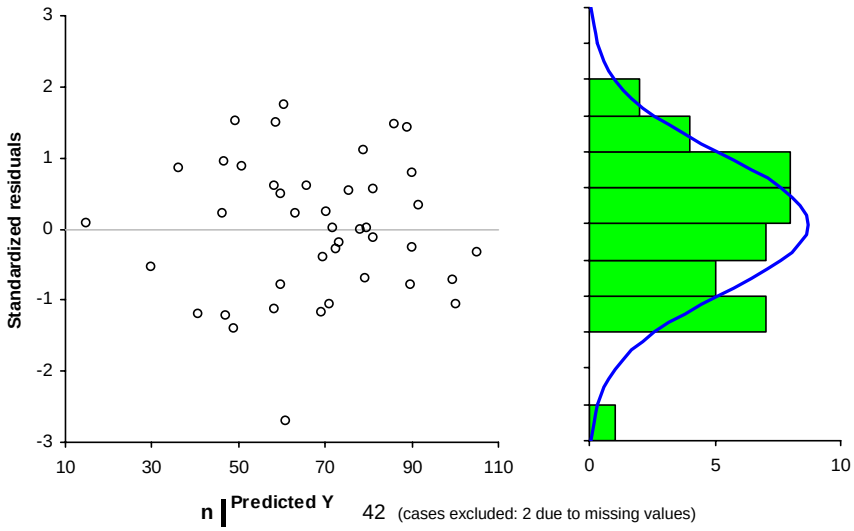

n 42 (cases excluded: 2 due to missing values)

R^2	0.62
Adjusted R^2	0.59
SE	16.2678

Term	Coefficient	SE	p	95% CI of Coefficient
Intercept	823.4024	794.3348	0.3065	-784.6441 to 2431.4489
Western 1 Ismay Peak-DC	8.4230	1.7687	<0.0001	4.8424 to 12.0036
Western 1 Miss	-0.7903	0.6829	0.2544	-2.1727 to 0.5921
Western 1 Ismay Amp	-0.0198	0.0040	<0.0001	-0.0279 to -0.0116

Source of variation	SSq	DF	MSq	F	p
Due to regression	16162.769	3	5387.590	20.36	<0.0001
About regression	10056.374	38	264.641		
Total	26219.143	41			

Figure 4-39. Regression for the Isoapch Top Upper Ismay to Top Lower Ismay.

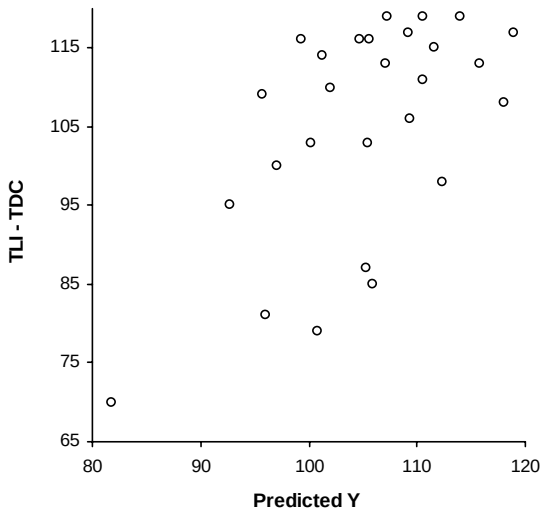

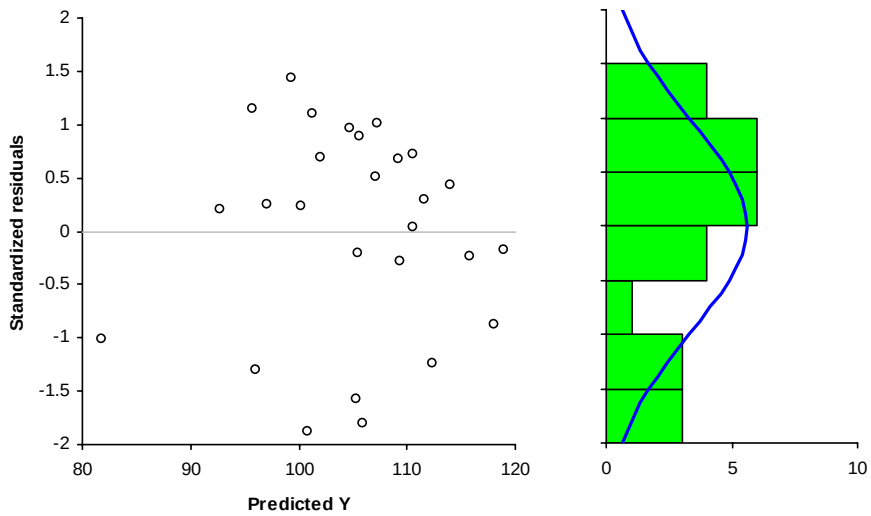

n	27 (cases excluded: 17 due to missing values)

R^2	0.36
Adjusted R^2	0.30
SE	11.5973

Term	Coefficient	SE	p	95% CI of Coefficient
Intercept	38.0264	33.0545	0.2613	-30.1947 to 106.2475
Western 1 Ismay Amp	-0.0084	0.0033	0.0179	-0.0153 to -0.0016
Western 1 I Peak(E) -DC (E)	3.8804	1.4046	0.0108	0.9815 to 6.7794

Source of variation	SSq	DF	MSq	F	p
Due to regression	1789.467	2	894.734	6.65	0.0050
About regression	3227.940	24	134.498		
Total	5017.407	26			

Figure 4-40. Regression for the Isoapch Top Lower Ismay to Top Desert Creek, version 1.

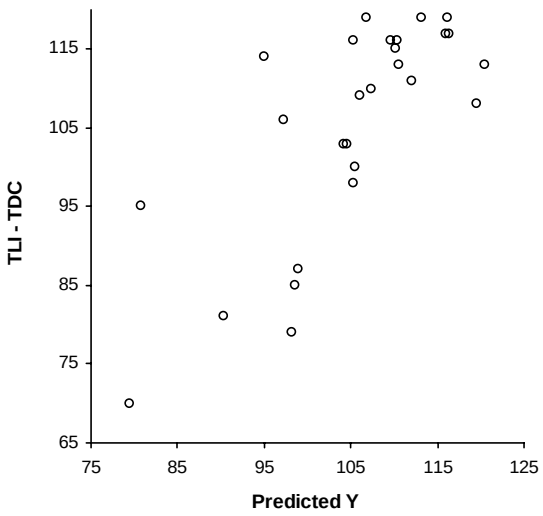

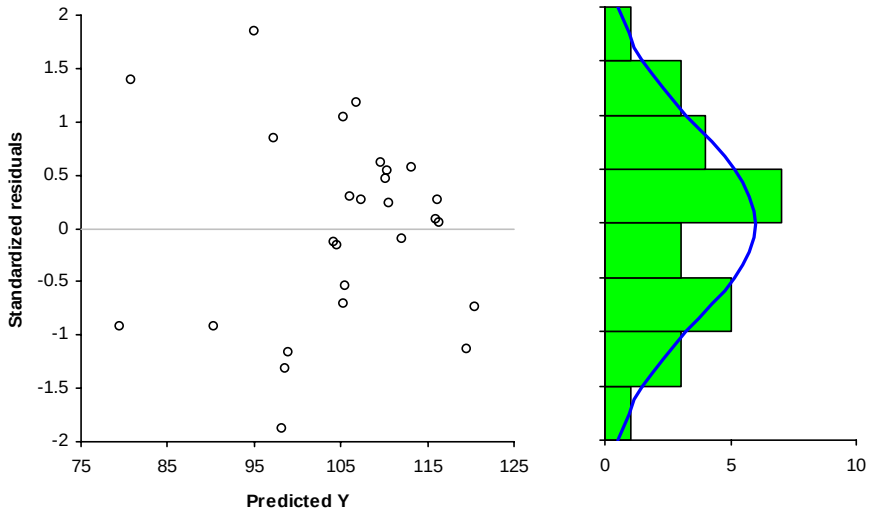

n	27 (cases excluded: 17 due to missing values)

R^2	0.56
Adjusted R^2	0.46
SE	10.2527

Term	Coefficient	SE	p	95% CI of Coefficient
Intercept	-395.6754	498.2033	0.4360	-1431.7458 to 640.3950
Western 1 Above Ismay	7.2644	2.9143	0.0211	1.2038 to 13.3251
Western 1 DC Peak	-6.8326	2.8604	0.0264	-12.7810 to -0.8841
Western 1 I Peak(E) -DC (E)	-10.8921	6.0752	0.0874	-23.5261 to 1.7420
Western 1 Ismay Zero-DC	23.6705	8.0114	0.0076	7.0098 to 40.3312
Western 1 Ismay Amp	-0.0135	0.0038	0.0017	-0.0213 to -0.0057

Source of variation	SSq	DF	MSq	F	p
Due to regression	2809.919	5	561.984	5.35	0.0025
About regression	2207.489	21	105.119		
Total	5017.407	26			

Figure 4-41. Regression for the Isoapch Top Lower Ismay to Top Desert Creek, version 2.

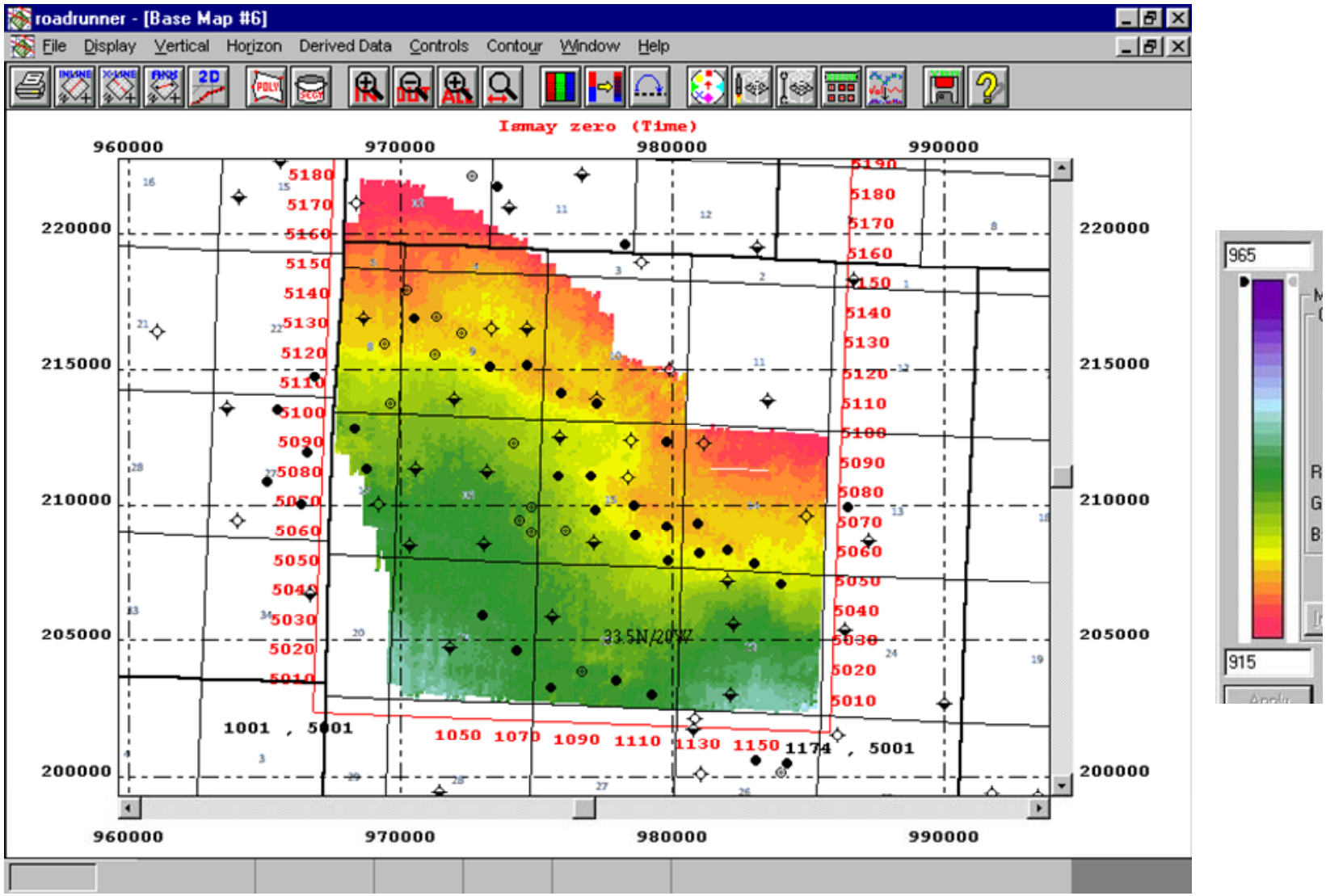

Figure 4-42. Ismay Zero Crossing Time Structure Map.

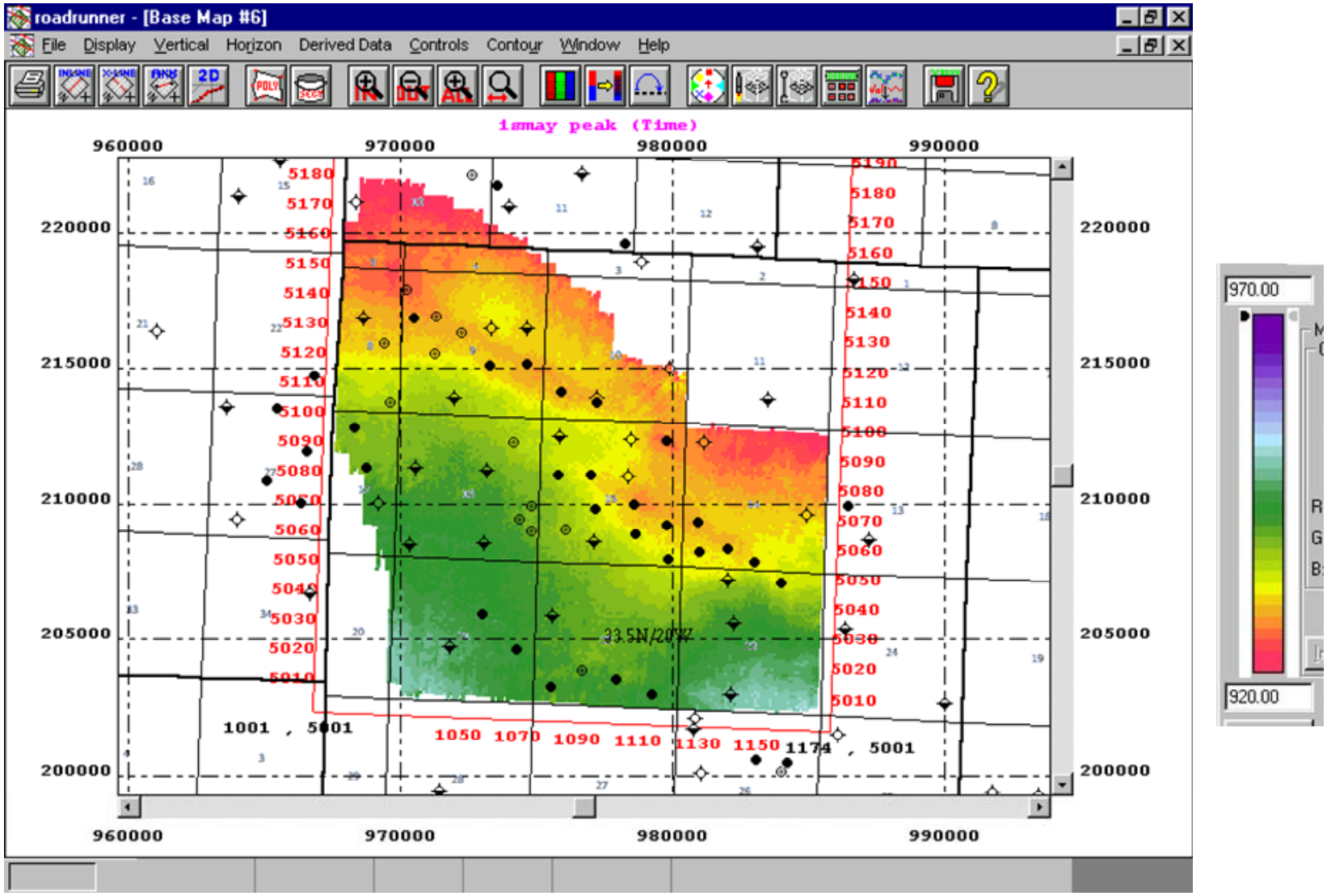

Figure 4-43 Ismay Peak Time Structure Map.

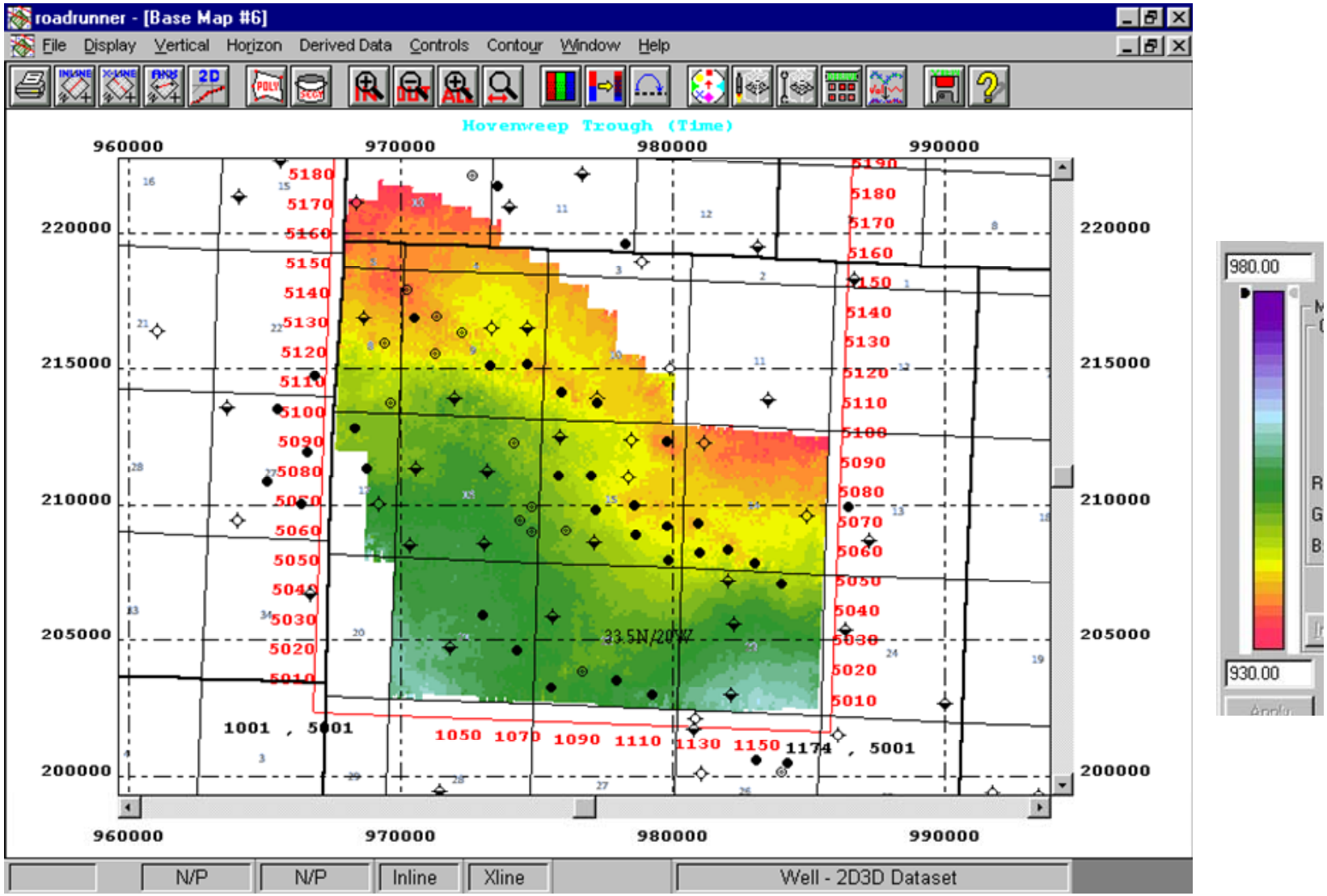

Figure 4-44. Hovenweep Trough Time Structure Map.

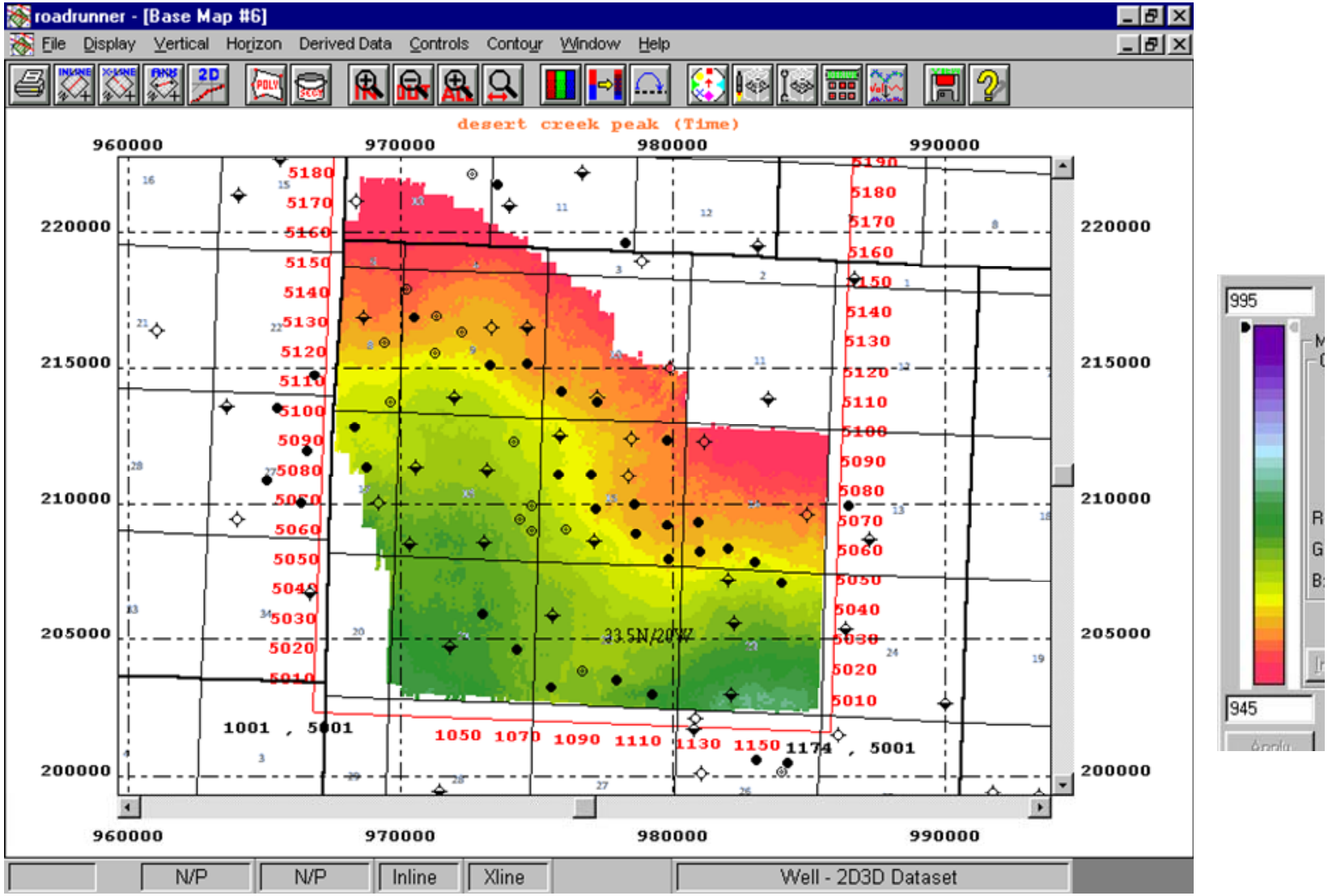

Figure 4-45. Desert Creek Peak Time Structure Map.

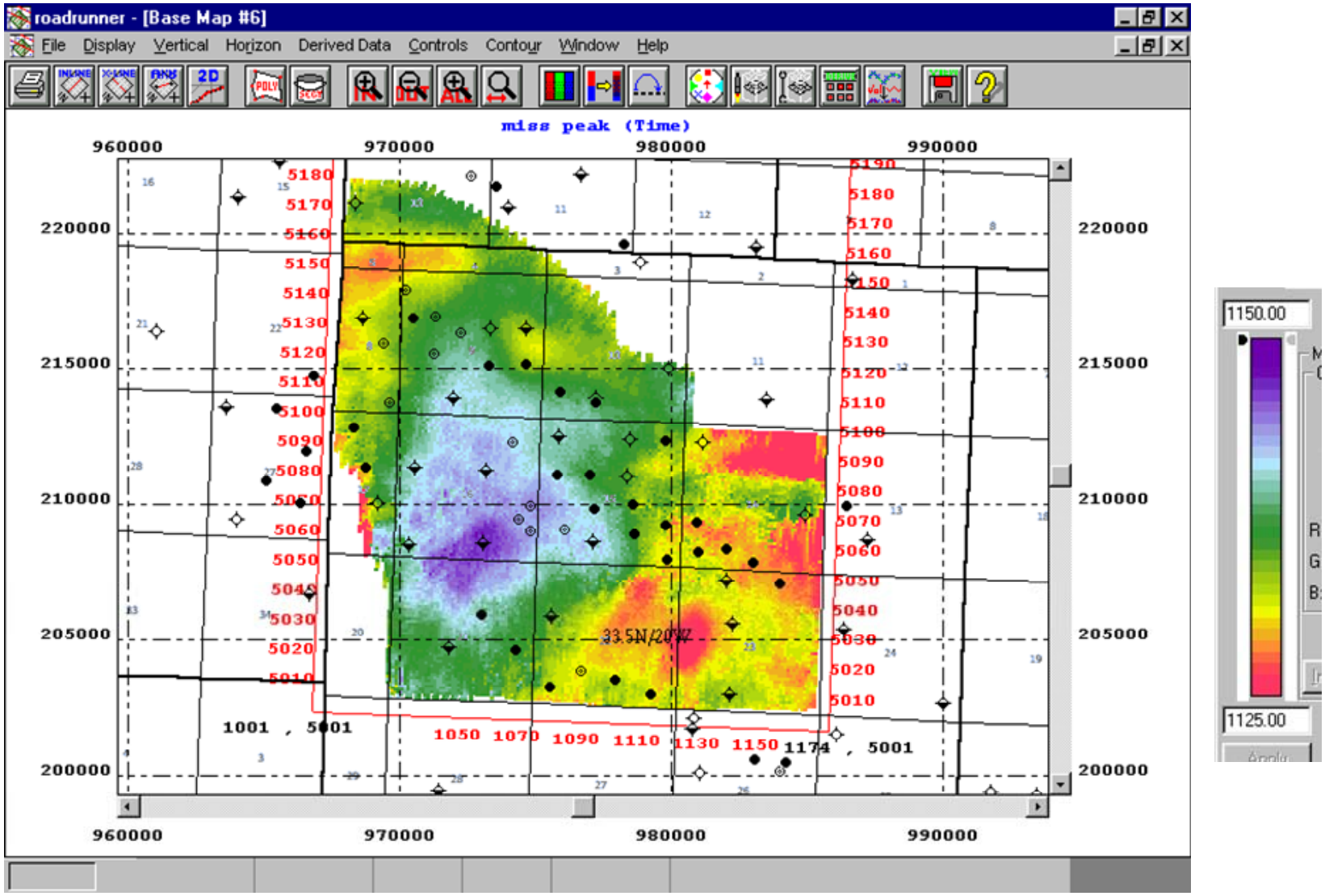

Figure 4-46. Mississippian Peak Time Structure Map.

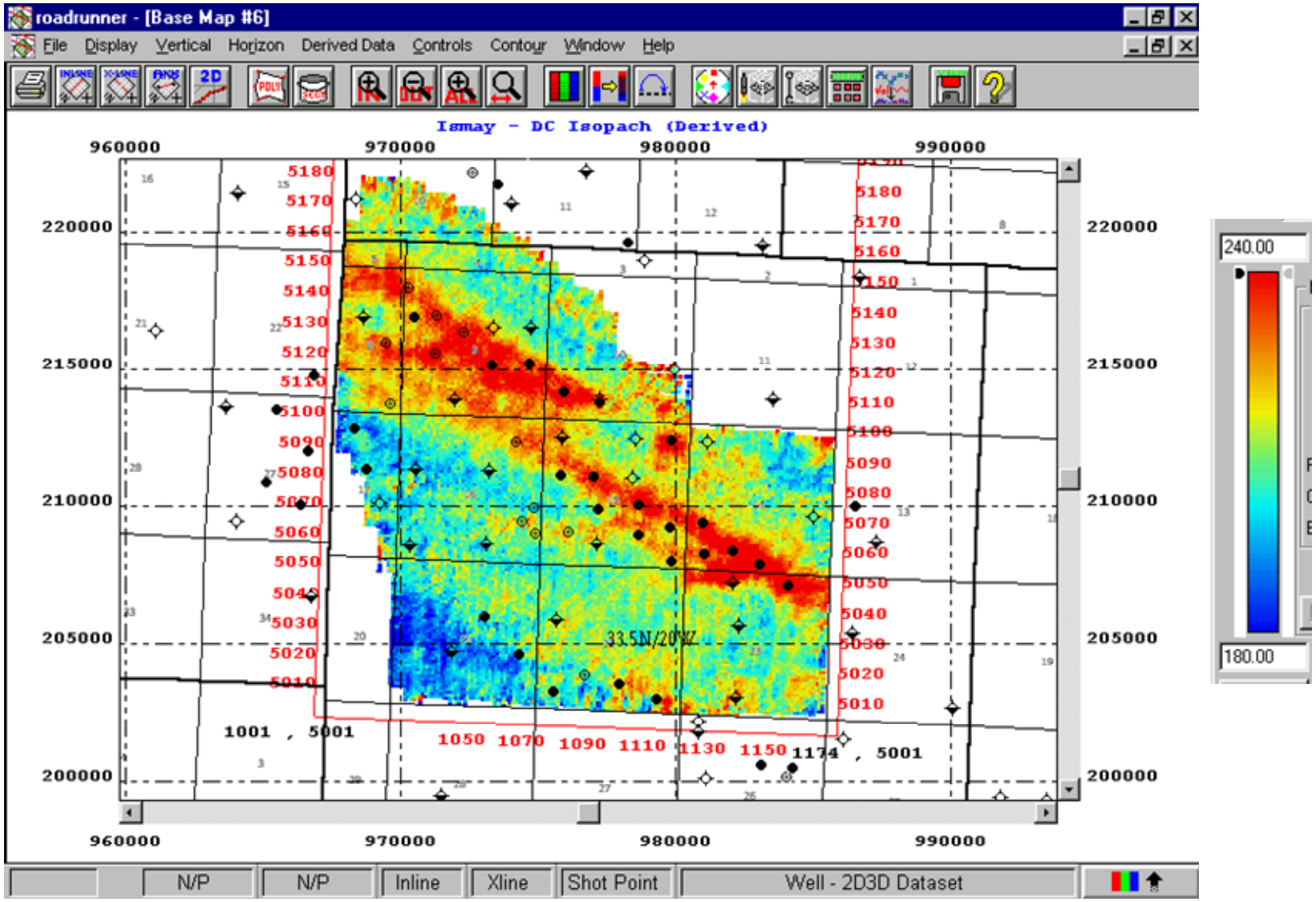

Figure 4-47. Top Ismay to Top Desert Creek Isopach Map.

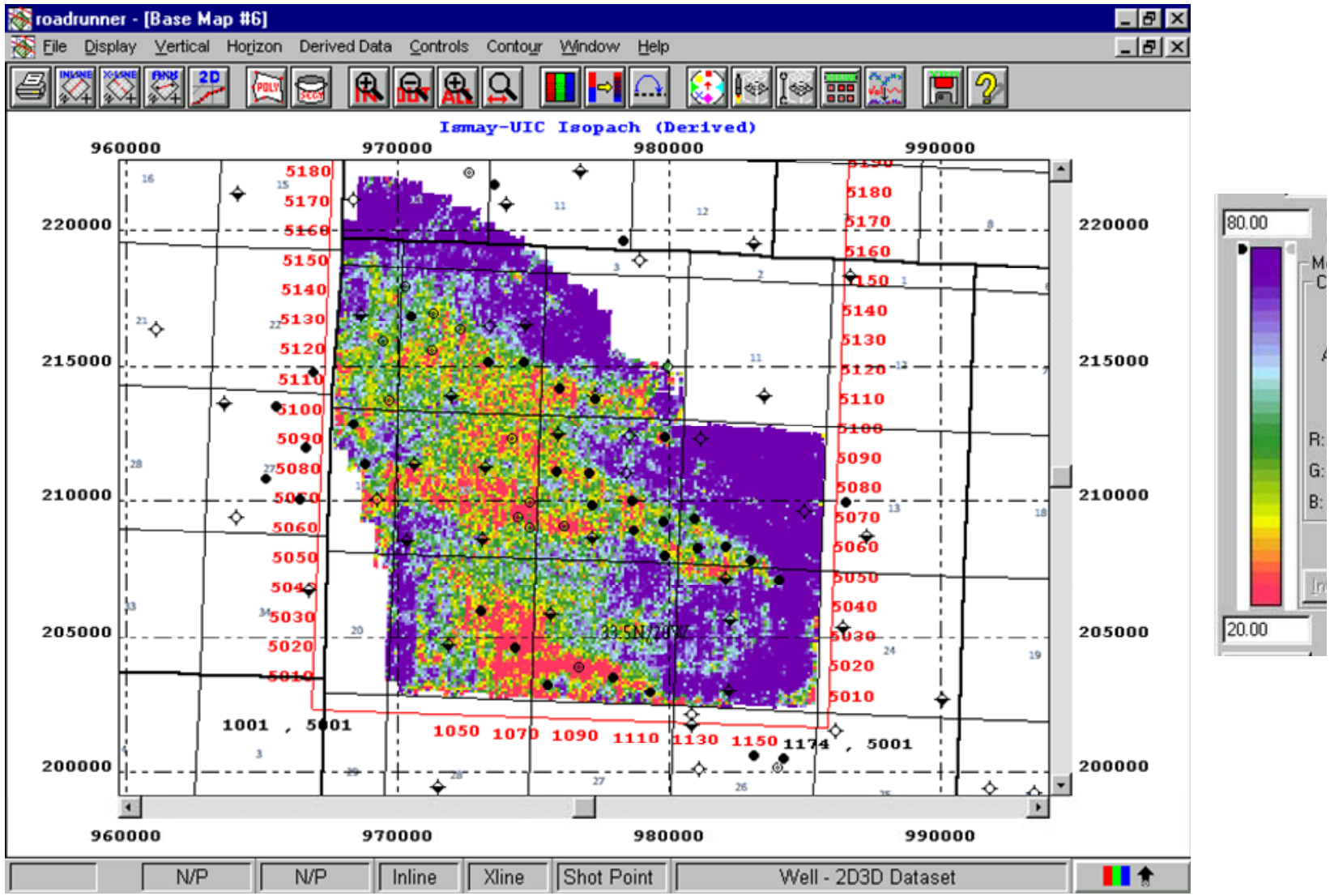

Figure 4-48. Top Ismay to Top Upper Ismay Carbonate Isopach Map.

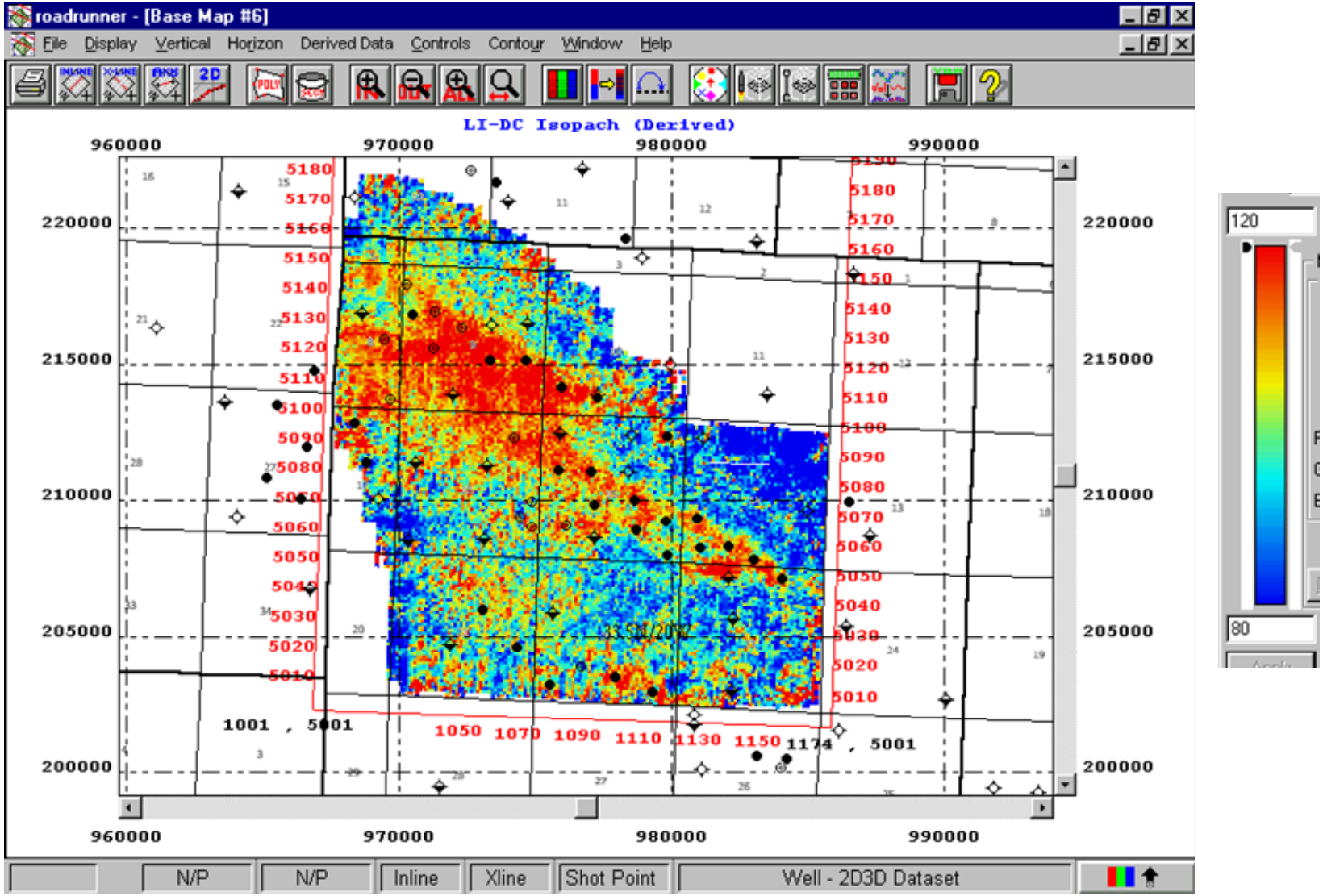

Figure 4-49. Top Lower Ismay to Top Desert Creek Isopach Map.

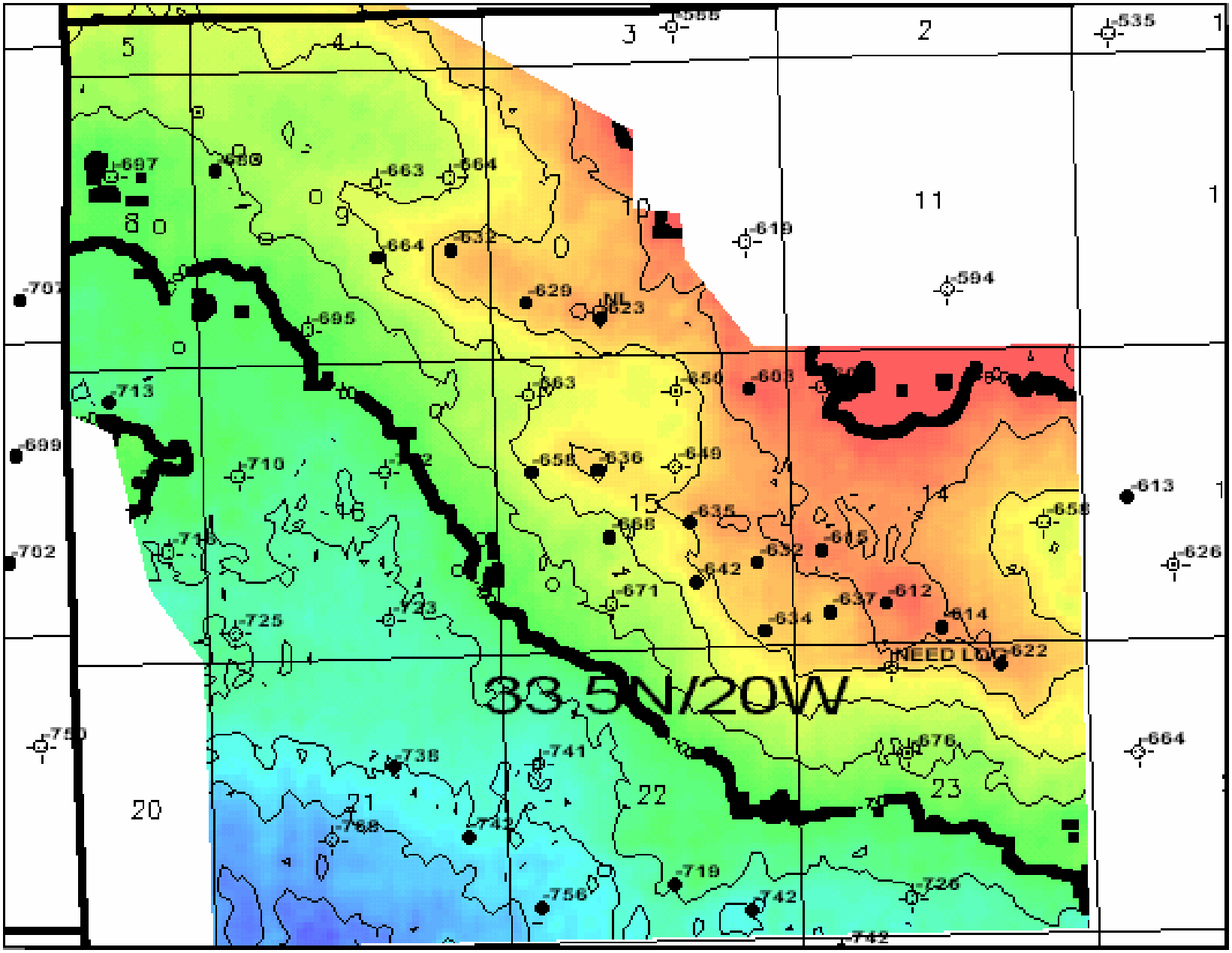

Figure 4-50. Top Ismay Depth Map CI = 20 ft

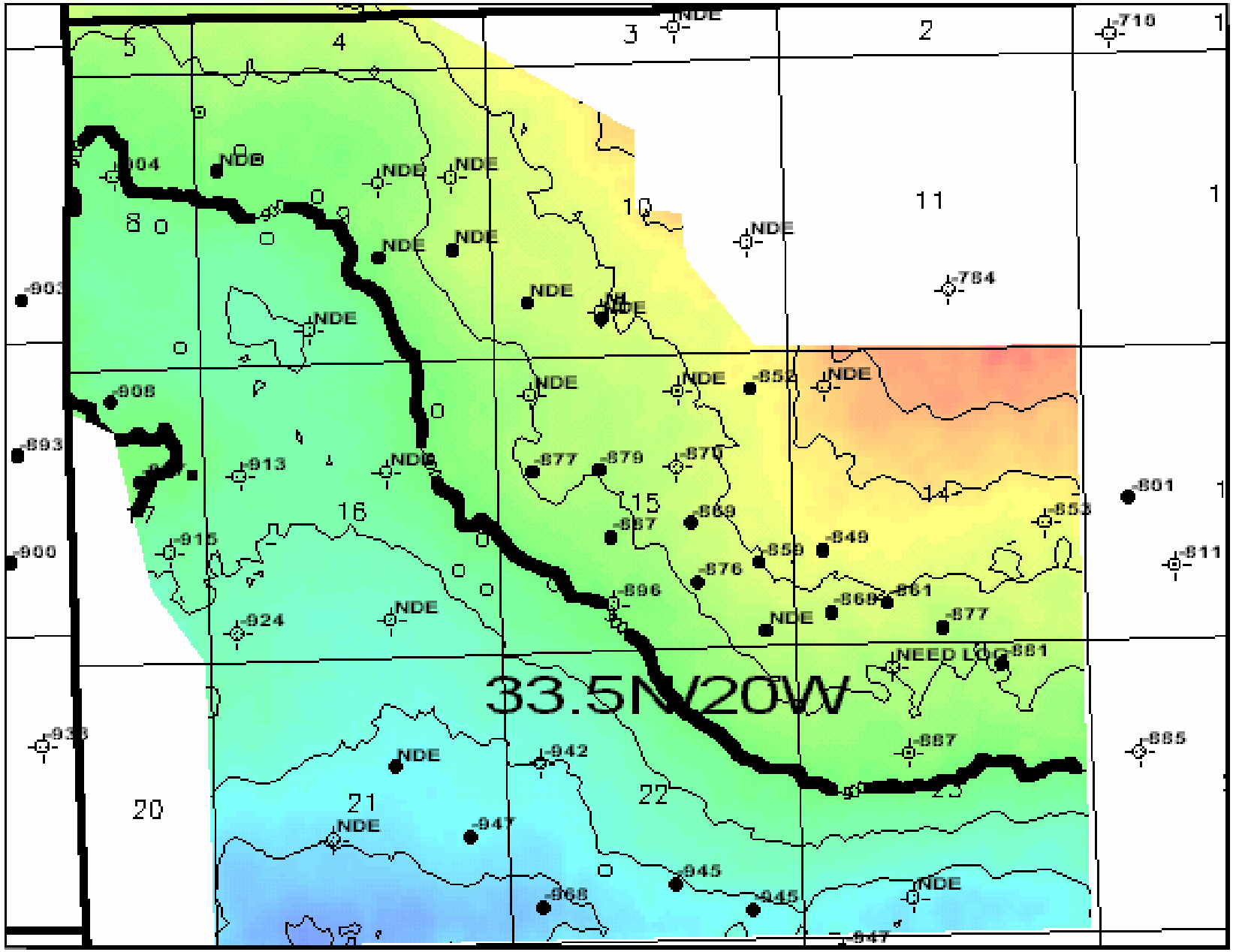

Figure 4-51. Top Desert Creek Depth Map, CI = 20 ft.

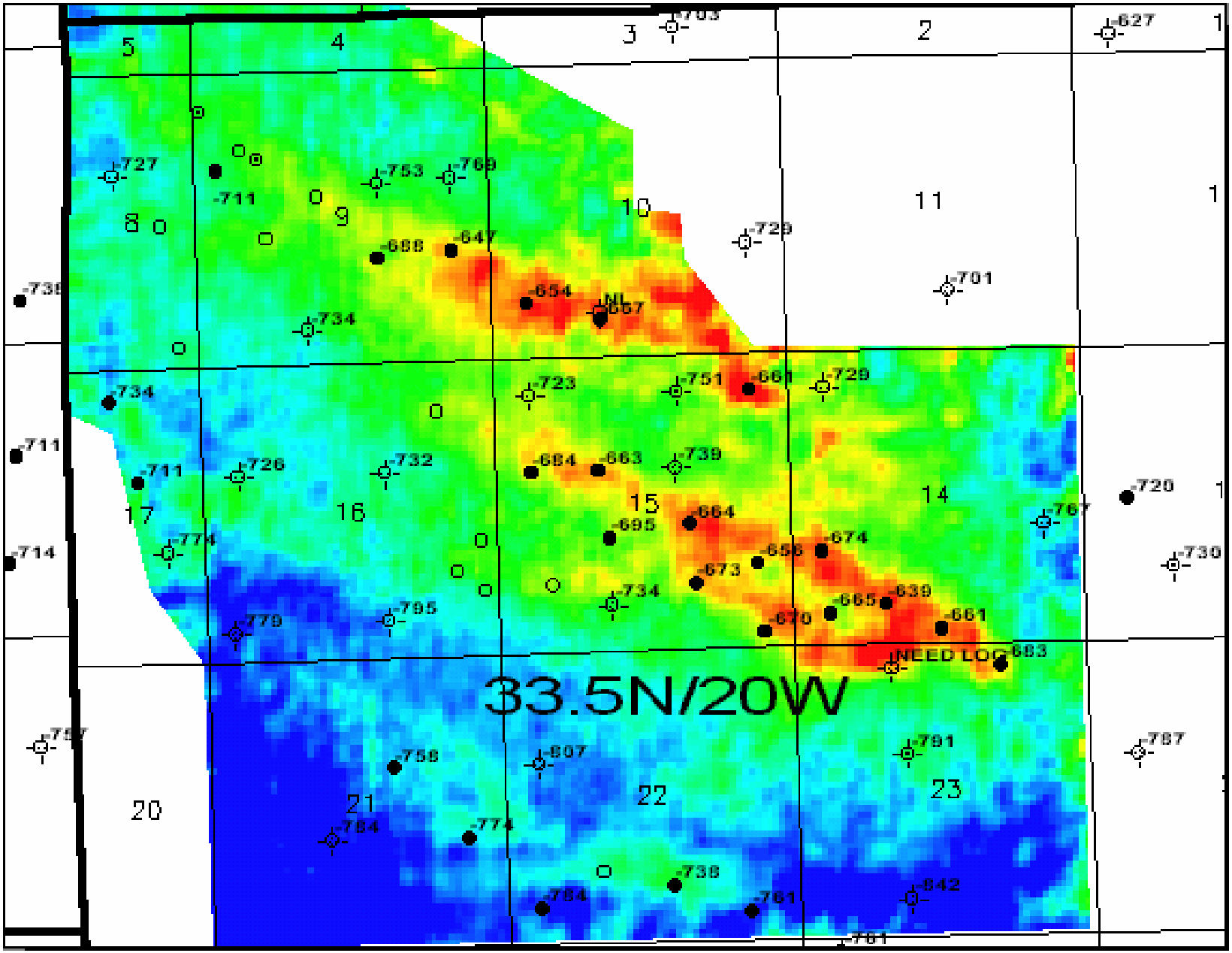

Figure 4-52. Upper Ismay Carbonate Depth Map.

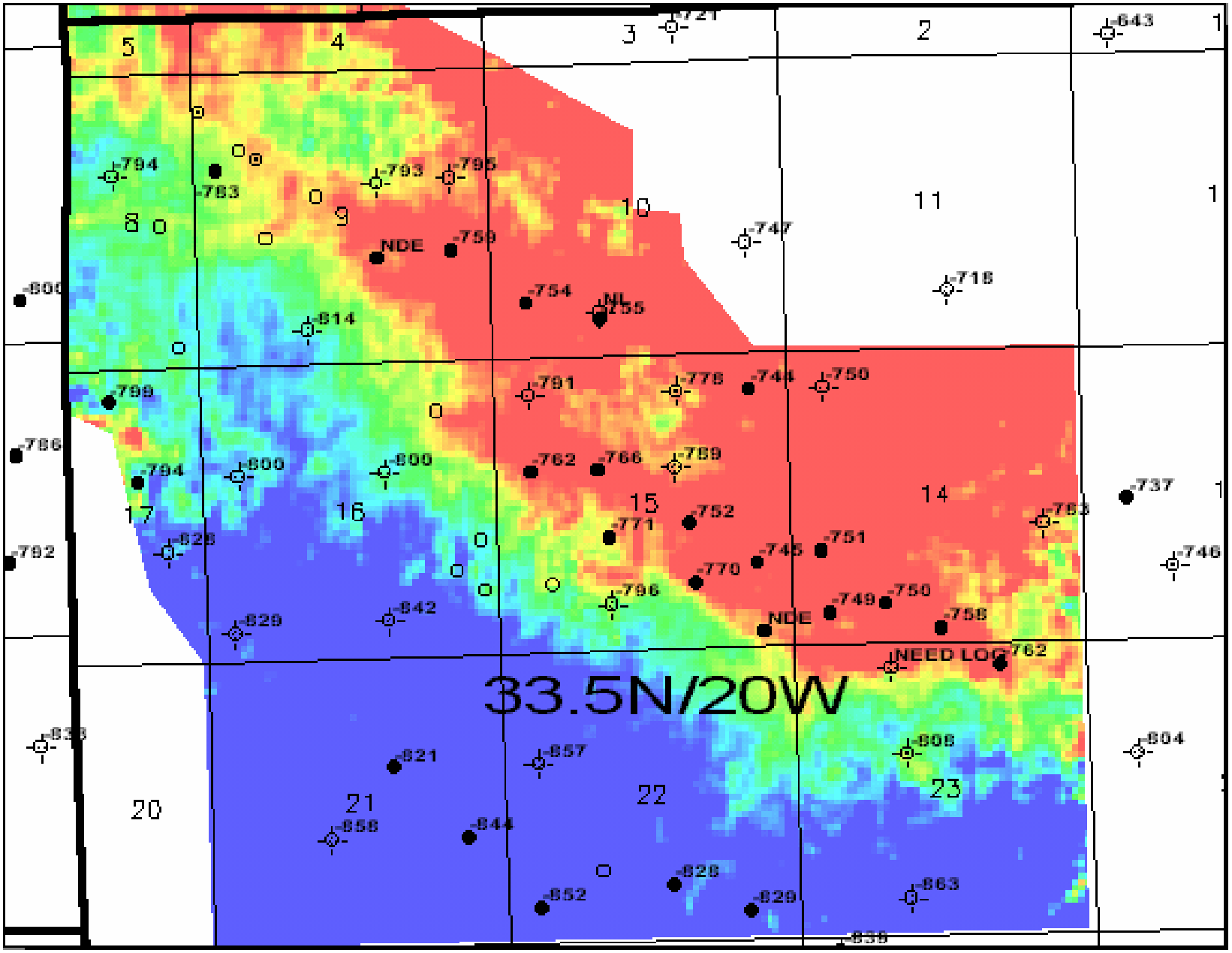

Figure 4-53. Lower Ismay Depth Map.

4.2.3 ISOPACH MAPS

Multivariate regression analysis using various seismic attributes from the WesternGeco Version 1 data were used to calculate isopach maps, as previously described. Red colors indicate isopach thicks, while blue colors illustrate isopach thins.

Figure 4-47 shows the resulting Ismay to Desert Creek Isopach Map. Note that Ismay productive mound areas are associated with Ismay-Desert Creek isopach thicks. Note that there are prospective isopach thick areas located primarily in the northwest portion of the survey. As a consequence, proposed drilling locations in those areas are currently being permitted with the Ute Mountain Ute Tribe.

The Top Ismay to Top Upper Ismay Carbonate Isopach (Figure 4-48) includes the Ismay Massive Anhydrite which is known to be thin in mound areas and thick in off-mound regions. Red colors are associated with isopach thins, whereas blue colors represent isopach thicks. As expected, this isopach interval is anomalously thin in Ismay producing areas. The isopach thins are most dramatic in the Towaoc field area which is located in the southern portion of the survey. It is possible that there may be at least one more new drilling location in the southern portion of the 3D based on this isopach..

The Top Lower Ismay to Top Desert Creek Isopach is shown in Figure 4-49. Isopach thicks are noted in red, while thins are illustrated with blue colors. This interval is anomalously thick in producing areas, especially in the Marble Wash and Roadrunner fields which trend through the northwest and center of the 3D survey. This isopach map indicates undrilled Lower Ismay mound areas may exist in the northwest portion of the survey.

In summary, the new isopach maps derived from seismic regression analysis helped to identify prospective Upper Ismay and Lower Ismay mound areas, and have led to the selection of potential drilling locations that are currently being negotiated with the Ute Mountain Ute Tribe. In addition, the isopach maps were used to help in constructing various depth structure maps.

4.2.4 DEPTH STRUCTURE MAPS

Depth maps were also constructed from seismic data. In constructing depth maps, velocity maps must first be generated. Horizon seismic times and actual horizon depth values at wells are used to calculate velocity. The velocity and seismic time grids are then used to create a depth structure map.

The Top Ismay Depth Map (Figure 4-50) was generated by using Ismay Zero Crossing Time and Top Ismay Velocity grids. For all depth maps, structurally high areas are noted in red and structurally low areas are indicated in blue. Subtle southwest plunging noses

are noted, however, no large structural closures on the Top Ismay Depth Map are observed.

The Top Desert Creek Depth Map is shown in Figure 4-51. The Desert Creek Peak Time Map was used along with the associated velocity grid to generate the Desert Creek Depth Map.

In order to construct a depth map on the top of the Upper Ismay Carbonate reservoir, it was necessary to combine the Top Ismay Depth Map with the Top Ismay to Top Upper Ismay Carbonate Isopach Map. In other words, the isopach map was subtracted from the Top Ismay Depth Map to give the resulting Upper Ismay Carbonate Depth Map (Figure 4-52).

A Lower Ismay Depth Map (Figure 4-53) was generated by combining the Desert Creek Depth Map with the Top Lower Ismay to Top Desert Creek Isopach Map. The isopach grid was added to the Desert Creek Depth grid to create the resulting Lower Ismay Depth Map.

4.3 P-Wave Seismic Interpretation – New Oil and Gas Drilling Proposed

Seismic attribute mapping, multivariate regressions analysis and resulting depth structure maps help in identifying current Ismay mound producing areas. Furthermore, based on the P-wave seismic interpretation, it appears that there are prospective undrilled Ismay mound areas within the 3D survey. The northwest portion of the 3D area contains the greatest undrilled potential. Red Mountain Energy, LLC, a company of the Southern Ute Indian Tribe, is currently permitting five drilling locations within the Roadrunner survey. Red Mountain is working closely with the Ute Mountain Ute Tribe to develop these potential resources. Red Mountain hopes to drill one or two of these proposed wells in the summer of 2005.

4.4 Predicting Productive Properties of Wells from P-wave Data

Although the intent is to resolve internal mound properties like porosity through the PS- and SS-wave data, it is interesting to see how the P-wave data might correlate with well productivity variables, in order to further refine the geological exploration model for the algal mounds.

Principal Component Analysis (PCA) is a method, previously described in La Pointe and others (2004), which among other purposes, can be used to explore for underlying uncorrelated factors in data that is correlated. If the seismic factors can be interpreted geologically, then they may clarify the geological factors related to productivity. Figure 4-54 is a PCA plot for only the seismic variables; Figure 4-55 also includes the lithologic isopachs.

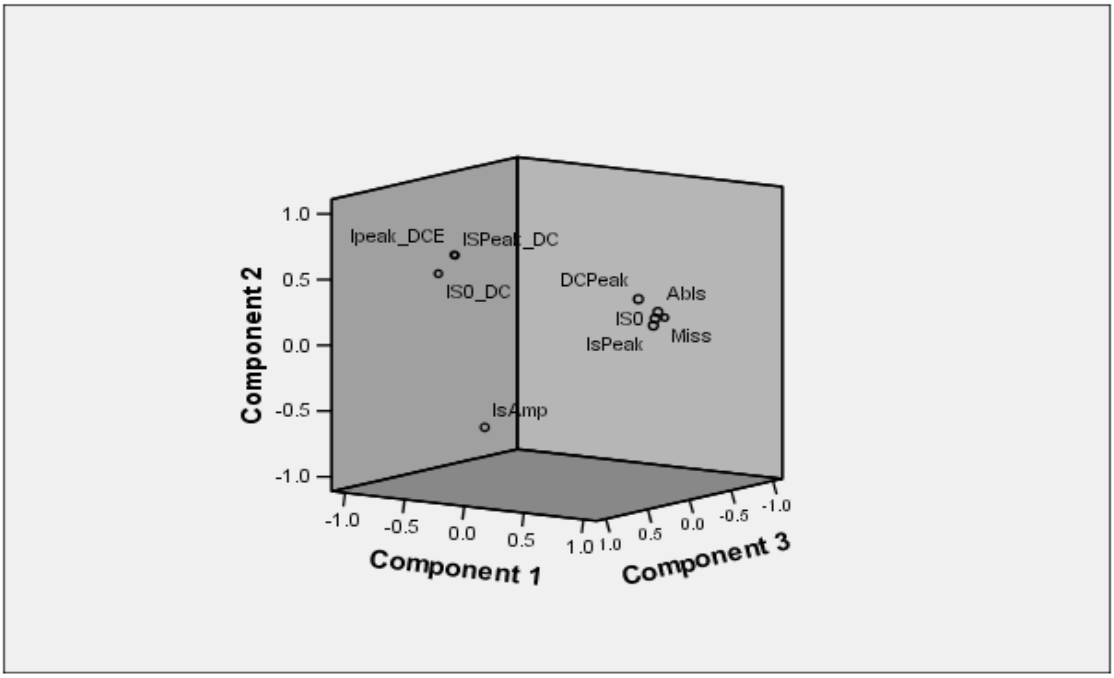

Figure 4-54. Principal component plot, showing groupings of underlying seismic variables into three components.

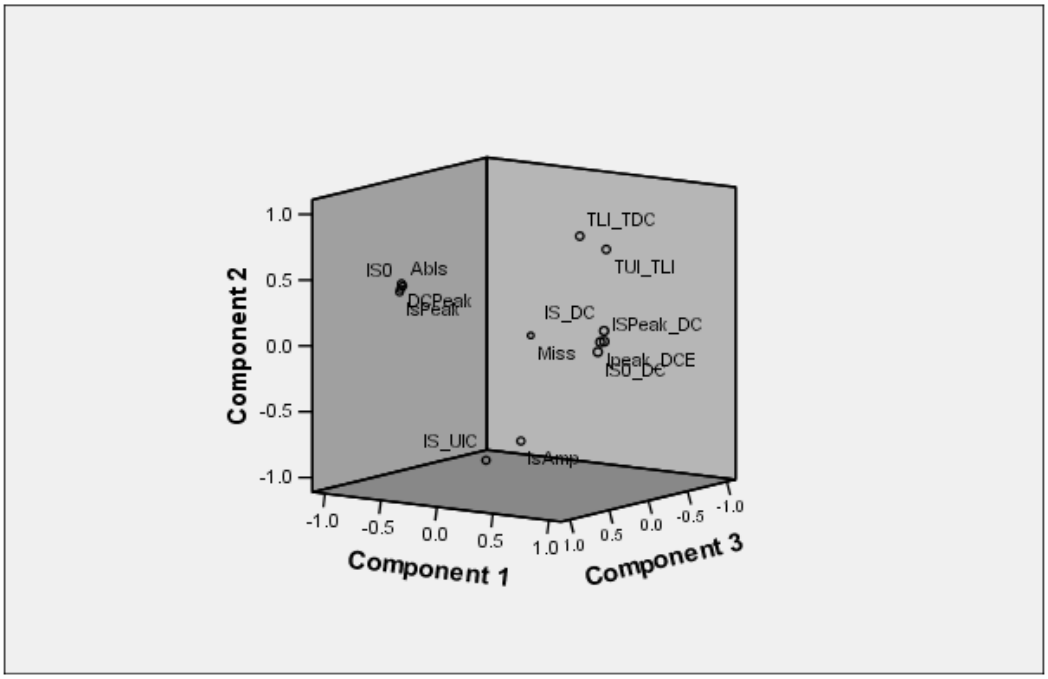

Figure 4-55. Principal component plot showing groupings of underlying seismic and lithological isopach variables.

The component plot for the seismic variables (Figure 4-54) show which seismic variables are closely correlated and which are not. One component consists of only the Ismay Amplitude. Another component with the isochron between some marker in the upper Ismay and the top of the Desert Creek. The third component consists primarily of all of the time structure variables.

When the lithologic thickness variables are included with the seismic (Figure 4-55), two of the component are slightly different. The first component, consisting of the Ismay Amplitude, still constitutes a single component. Note, however, the close association with the Ismay to Upper Ismay Carbonate isopach. This indicates that these two variables are very much correlated, such that as the amplitude changes, the thickness in this interval changes. Note that the association in the component plot does not indicate whether the association is positive or negative, so it is not possible to state whether the correlation is positive or negative. The previous third component is now similar to the second component. This new second component consists of various time structure variables, such as the Ismay Zero crossing, the Above Ismay marker, The Desert Creek Peak and the Ismay Peak. The new third component consists of the isopach thickness and the isochron thicknesses, plus the time structure variable to the top of the Mississippian. This association between the isopachs and the time (depth) to the Mississippian suggests that there is in fact a relation between the present-day Mississippian highs and lows and mound development.

Note that the TLI_TDC and TUI_TLI isopachs are not close to any of the three most tightly clustered groups. This indicates that these thickness require at least the interplay of *two* geological factors to explain their thickness variations.

The Spearman correlation coefficients between the production variables and some of the seismic and isopach variables (Table 4-3), together with the coefficients in

Table 4-1, clarify the possible controls on productivity. Note that there is a high negative correlation between Ismay Amplitude and production and recovery in Table 4-3.

Table 4-1 shows that there are only two statistically significant correlations between Ismay amplitude and the other variables: a positive correlation with the isopach thickness from the Ismay to the Upper Ismay Carbonate; and a negative correlation with the thickness between Upper Ismay to the Lower Ismay. Since the correlation between well productivity is negatively correlated with amplitude, this means that productivity is negatively correlated with thick isopachs from the Ismay to Upper Ismay Carbonate, and positively correlated with thick isopachs from the Upper Ismay to the Lower Ismay. As previously discussed, the existence of a thinner anhydrite layer in the Upper Ismay section has been qualitatively thought to be correlated with mound development, as is a thicker Upper Ismay to Lower Ismay section.

Table 4-3 also shows that there is a negative correlation with all of the time structure variables to markers in the Ismay and Desert Creek, a negative correlation with time (depth) to the Mississippian, and positive correlations with the three Ismay markers to

Desert Creek isopachs. What this appears to imply, not surprisingly, is that when productive mounds develop, there is a buildup that increase the section between the Desert Creek and the Upper Ismay markers, and that these horizons themselves, including the Desert Creek, are relatively higher. Interestingly, there is the positive correlation with the Mississippian, as if the interval between the top of the Desert Creek and the top of the Mississippian is thicker where the mounds develop, and that the actual Mississippian horizon is slightly lower than the surrounding non-algal mound area. This could easily be explained by a stacked mound development in the Desert Creek and Ismay that either occurs where there are slight depressions in the top of the Mississippian or causes them in some way. However, as the Mississippian time structure map shows (Figure 4-46), there is no clear relation of production to the larger scale highs and lows in the Mississippian. If positive correlation with the Mississippian time structure is more than a statistical artifact, then it is only of a local nature and is not a factor that can be used in regional exploration.

		AbIs	IS0	IsPeak	DCPeak	Miss	Ipeak_DCE	IS0_DC	ISPeak_DC	IsAmp	IS_UIC	IS_DC	TUI_TLI	TLI_TDC
Cum_Oil	Correlation Coefficient	-0.31	-0.289	-0.336	-0.201	0.406	0.244	0.251	0.287	-.562(*)	0.092	0.254	0.28	-0.258
	Sig. (2-tailed)	0.211	0.245	0.173	0.423	0.095	0.33	0.315	0.248	0.015	0.717	0.427	0.294	0.419
	N	18	18	18	18	18	18	18	18	18	18	12	16	12
Cum_Gas	Correlation Coefficient	-0.293	-0.306	-0.355	-0.195	0.263	0.365	0.392	0.402	-0.317	-0.027	0.401	0.419	-0.113
	Sig. (2-tailed)	0.238	0.217	0.149	0.438	0.291	0.137	0.108	0.098	0.2	0.916	0.196	0.106	0.727
	N	18	18	18	18	18	18	18	18	18	18	12	16	12
EUR_Oil	Correlation Coefficient	-0.147	-0.127	-0.136	-0.073	0.308	0.121	0.134	0.158	-0.296	-0.132	0.053	0.316	-0.026
	Sig. (2-tailed)	0.492	0.554	0.527	0.734	0.144	0.575	0.534	0.461	0.16	0.539	0.835	0.152	0.919
	N	24	24	24	24	24	24	24	24	24	24	18	22	18
EUR_Gas	Correlation Coefficient	-0.221	-0.187	-0.191	-0.122	0.142	0.264	0.285	0.295	-0.109	-0.088	0.229	.424*	0.25
	Sig. (2-tailed)	0.299	0.383	0.37	0.571	0.507	0.212	0.178	0.161	0.613	0.684	0.361	0.049	0.317
	N	24	24	24	24	24	24	24	24	24	24	18	22	18
EUR_Tot	Correlation Coefficient	-0.177	-0.182	-0.197	-0.116	0.287	0.239	0.231	0.277	-0.222	-0.176	0.202	0.325	0.156
	Sig. (2-tailed)	0.396	0.385	0.345	0.58	0.164	0.25	0.266	0.18	0.287	0.4	0.422	0.13	0.538
	N	25	25	25	25	25	25	25	25	25	25	18	23	18
Net_Pay	Correlation Coefficient	-0.209	-0.103	-0.106	-0.108	0.036	0.158	0.214	0.155	-0.268	0.019	0.195	0.38	0.091
	Sig. (2-tailed)	0.296	0.608	0.598	0.592	0.858	0.432	0.284	0.441	0.177	0.925	0.423	0.061	0.712
	N	27	27	27	27	27	27	27	27	27	27	19	25	19

Table 4-3. Spearman correlation coefficients between production variables and seismic & lithologic variables.

4.5 Technology Transfer

Technology transfer occurred through publications, presentations and additions to the project website.

4.5.1 PUBLICATIONS & PRESENTATIONS

- Two presentations were made at the Reservoir Characterization Conference at the Colorado School of Mines in conjunction with CSM's Reservoir Characterization Project (RCP) consortium meeting. The talks presented were:

  P-wave interpretation (presented by P. La Pointe)

  Processing Update (present by R. Van Dok, WesternGeco)

- In addition, a paper was submitted and accepted for presentation by R. Van Dok, J. Gaiser, P. La Pointe and R. Benson at the EAGE/SEG Summer Research Workshop on Multicomponent Seismic (Pau, France, Sept. 5-7, 2005). This paper is entitled: "Multicomponent processing and analysis of a 3D/9C survey over an algal mound carbonate reservoir in the Paradox Basin: Roadrunner Field, Colorado."

The Power Point™ files for the RCP talks can be viewed and downloaded from the project web page (Figure 4-56). The text of the SEG paper can also be accessed on the project website, and is included in an appendix in this report.

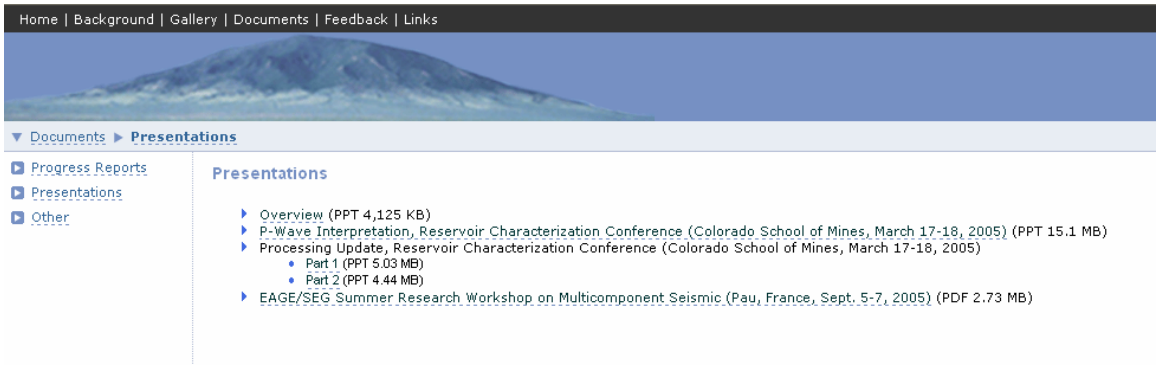

Figure 4-56. Screen shot of project web page with links to recent publications and presentations.

4.5.2 PROJECT WEBSITE

The project website has been moved to a new address to make it more accessible and maintainable. The new address is: http://utemountain.golder.com.

Several additions have been made to this website over the project period. These include:

- Update contacts
- Update of progress reports and presentations
- Slide shows of seismic and 3D VSP acquisition
- Update of project news

4.6 Decision Points

One remaining Decision Point (DP3) was successfully passed during this project period. DP3 was established to assess whether, after the S-wave processing had taken place, there was sufficient data quality at the reservoir level to proceed with the interpretation of this data volume. Based upon the processing results presented in this report, the interpretation was not dropped and is currently in progress.

There are no remaining Decision Points for the Project.

5 CONCLUSIONS

The following conclusions were made during the fifth SemiAnnual project period:

1. The multivariate approach to the interpretation of the P-wave data provided robust regressions between the seismic parameters and the lithostratigraphic horizons and their thicknesses;

2. Thins and thicks in these derived isopachs correlate both with drilling success and to a lesser extent with production characteristics;

3. The geological exploration model for algal mounds has been refined based on these quantitative substantiations of the previous qualitative understandings. In addition, although mounds do not appear to be related to highs in the Mississippian, they do have some correlation with local depressions in the Mississippian time structure data;

4. The processing results from the PS- and SS-wave data are of sufficient quality that interpretation of these data volumes was initiated;

REFERENCES

La Pointe, P. R., C. Rebne and S. Dobbs, 2004. Multicomponent seismic analysis and calibration to improve recovery from algal mounds, FourthTechnical Report, DOE Award DE-FG26-02NT15451, 138 p.

Press, W. H., S. A. Teukolsky, W. T. Vetterling and B. P. Flannery, 1992. Numerical Recipes in FORTRAN: The Art of Scientific Computing. 2nd Edition. Cambridge University Press, Cambridge.963p.

6 LIST OF ACRONYMS AND ABBREVIATIONS

3D3C – three dimensional, three component

3D9C – three dimensional, nine component

AVO - amplitude variation with offset

BIA – U. S. Bureau of Indian Affairs

DOE – U. S. Department of Energy

RW – Red Willow Production

SU – Southern Ute Tribe

UM – Ute Mountain Ute Tribe

VSP – Vertical Seismic Profiling

7 APPENDICES

Z-99

Multicomponent processing and analysis of a 3D/9C survey over an algal mound carbonate reservoir in the Paradox Basin: Roadrunner Field, Colorado

R. VAN DOK[1], J. GAISER[1], P. LA POINTE[2] AND R. BENSON[3]

7.1 [1] *WesternGeco, 1625 Broadway, Suite 1300, Denver, Colorado, 80202, USA*

[2] *Golder Associates, Inc.*

[3] *Colorado School of Mines, Department of Geophysics*

Summary

The Paradox Basin in southwestern Colorado contains several isolated carbonate reservoirs created by algal limestone buildups. These algal mounds are relatively straightforward to locate on conventional P-wave seismic data. The reservoirs, however, are generally not internally homogeneous and ultimate recovery depends on locating zones of increased porosity and permeability. In 2003, a nine-component (9-C) 3-D survey was acquired over the Roadrunner Field in the Paradox Basin northwest of the town of Towaoc (Figure 1) in order to investigate a porous carbonate oil reservoir of Pennsylvanian age. This survey was part of a U.S. Department of Energy study (DE-FG26-02NT15451) on the Ute Mountain Ute Tribal Lands. In addition to the surface seismic, a 9-C, zero offset and P-wave, offset VSP were acquired. Initial analysis of the P-wave volume shows good delineation of the algal mound structure but no obvious indications of internal variations in lithology. The PS-wave data is relatively good quality as well and has potentially better vertical resolution within the reservoir zone. The PS-wave data also shows the algal mound structure and possibly offers a glimpse into the internal lithology of the algal mound.

Introduction

The reservoirs in this region are typically mounds of algal (Ivanovia) limestone associated with organic-rich black dolomitic shale and mudstone rimming evaporite sequences of the Paradox Formation of the Hermosa Group (Ismay zone). Net pay is on the order of 3 m – 15 m but occasionally reaches a net thickness of 30 m. Porosities typically vary from 5% to 20%. The goal of this project is to detect reliably stratigraphic features that are on the order of 200 to 1000 acres. These features have little structural expression. The mounds are surrounded and overlain by massive anhydrite. The reservoir properties of these mounds are not homogeneous throughout. From the standpoint of reservoir development of an existing algal mound field, the critical factors lie in predicting the porosity, permeability, internal mound geometries and fluid content of the

mounds. While well information and production data are useful to understand some of these variations, they cannot alone be used to make more accurate descriptions of the salient reservoir parameters between well control.

Data Acquisition

Acquisition of these data utilized both P-wave and S-wave vibrators into three-component geophones. Four AHV-IV vibrators were used for the P-wave source effort while a single Mertz M18 was used for the S-wave portion. Two orthogonally oriented S-wave sources were used at each source location oriented approximately N315°E and N225°E (or N045°E). The change in source orientation for one of the S-wave sources was due to the direction of travel of the vibrator with respect to the source line direction. The horizontal geophones were oriented N180°E and N270°E for the x and y components respectively. Polarity convention and S-wave source orientation were carefully checked for each location to ensure consistency in the final products.

The geophone spacing was 220 feet with line spacing of 660 feet. Source points were 220 feet apart along diagonal lines spaced every 1,320 feet. The entire record spread was fixed and live for all sources.

Data Processing

Processing and analysis for this study was done to obtain additional information about the lithologic variations within the reservoir. The P-wave source and vertical geophone data were processed using conventional time processing techniques that included surface-consistent deconvolution, refraction and reflection statics, DMO and FK time migration. The horizontal geophone data for the same P-wave sources were processed using a similar flow with the significant addition of a receiver rotation to a radial and transverse orientation, S-wave detector statics estimation and CCP binning. Limited-azimuth PS-wave volumes were produced for both the radial and transverse components and evaluated for azimuthal anisotropy using a 2C x 2C Alford rotation and layer stripping methodology. The S-wave source and horizontal geophone data were processed in the principal S1/S2 orientations as determined from the PS-wave data. Again, a similar flow to the P-wave data was utilized.

Data Analysis

The primary method used for locating and delineating the algal mound structures involves the interpretation of key events above and below the reservoir and mapping the time thickness between the two. These events are known as the lower Ismay and Desert Creek formations. Figure 2(a) shows the interpretation of these events on the P-wave and PS-wave data. Figure 4 shows a map of the isochron thickness from the P-wave, clearly outlining the algal mound feature. The internal structure, however, is not apparent

The interpretation of these data also includes comparing isochron thickness maps from the P, PS and SS data volumes between the Ismay and Desert Creek formation picks. The top and base picks for the algal mound structure in Figure

2(b) on the PS-wave data shows an apparent higher resolution than the P-wave data over the same interval. This is probably due to the shorter wavelengths of PS-wave data.

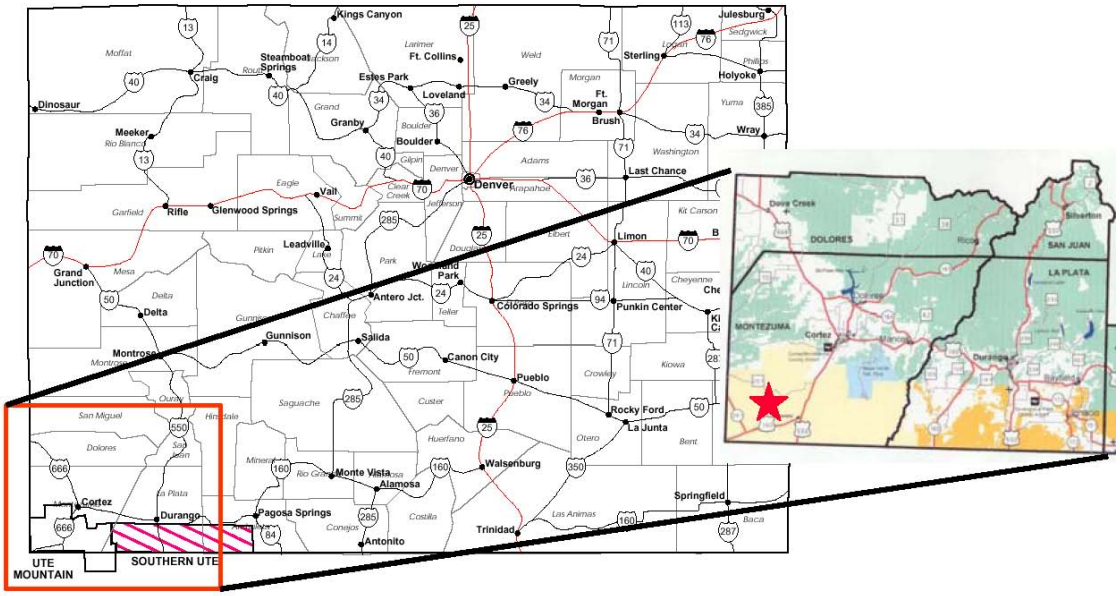

Figure 1. Survey location map in the Paradox Basin in southwestern Colorado.

Azimuthal anisotropy was also measured for the PS-waves over two layers. The first analysis layer included the events above the reservoir zone and is referred to as the overburden layer. The second analysis layer included the zone of interest. The overburden results are shown in Figure 4. The S-wave splitting is very weak over the entire survey area for the overburden as well as over the zone of interest. Peak distribution of percent anisotropy is around 1%, with a maximum of 2% difference in the fast and slow S-waves. While Figure 4 does show a regional NW/SE pattern, there does not appear to be a strong correlation of S-wave splitting attributes with the zone of algal mound buildup.

Conclusions

Preliminary analysis of the P-wave data volume confirms that the geometry of the algal mound buildup can be determined quite clearly. The PS-wave data correlates well with many of the P-wave reflection and the general shape of the algal mound can be identified. While noisier, the PS-wave data shows signs of potentially improved resolution within the reservoir. With this improved resolution it is hoped that a detailed Vp/Vs can be determined leading to a better understanding of the internal lithologic variations in the algal mound. This information combined with the SS-wave surface seismic and VSP data should provide additional confidence in the interpretation.

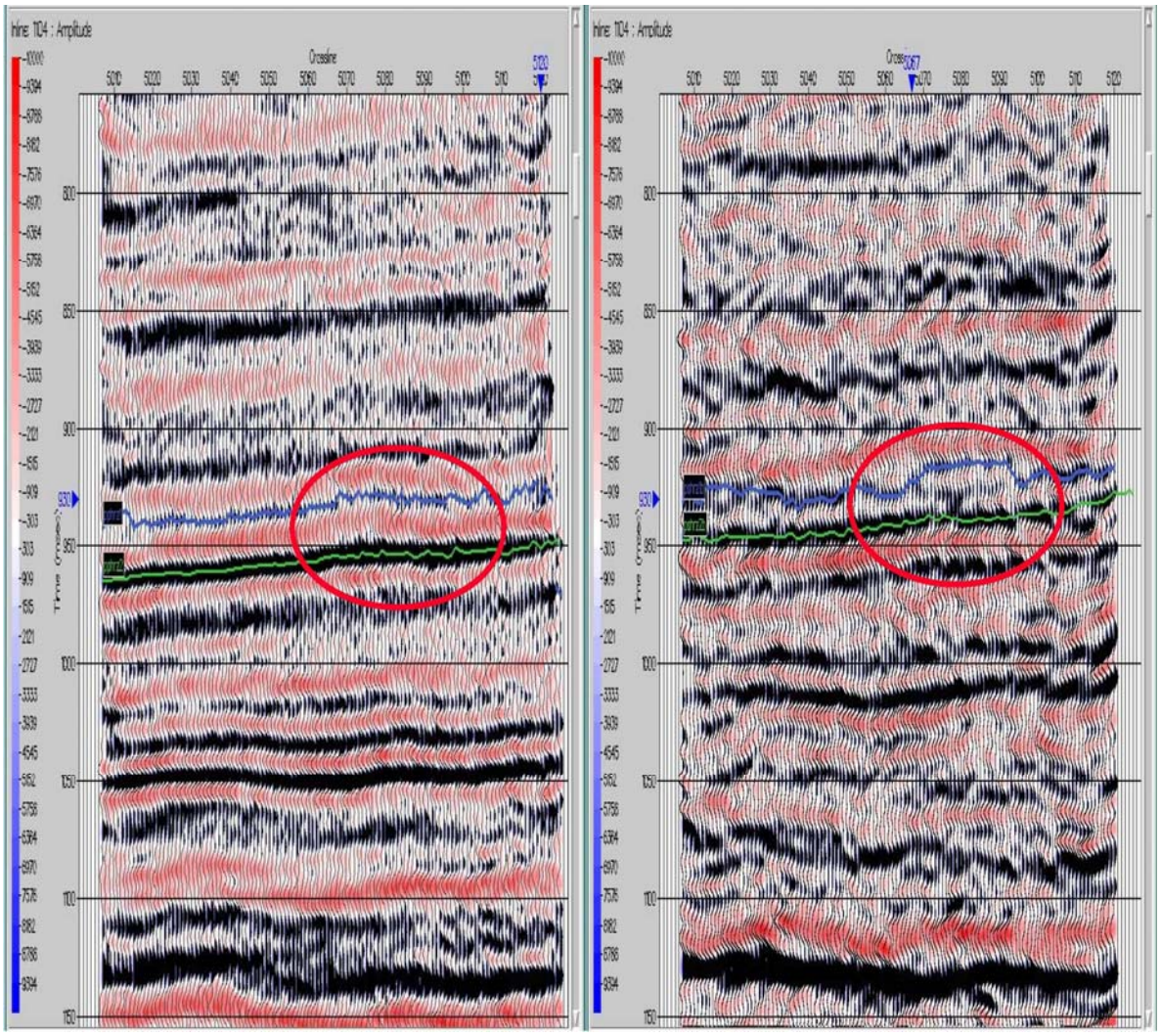

(a) **(b)**

Figure 2. (a) P-wave line extracted from 3D volume with top and base reservoir horizons. (b) PS-wave line extracted from 3D volume with equivalent top and base horizons. The red ovals indicate the approximate location of the algal mound buildup.

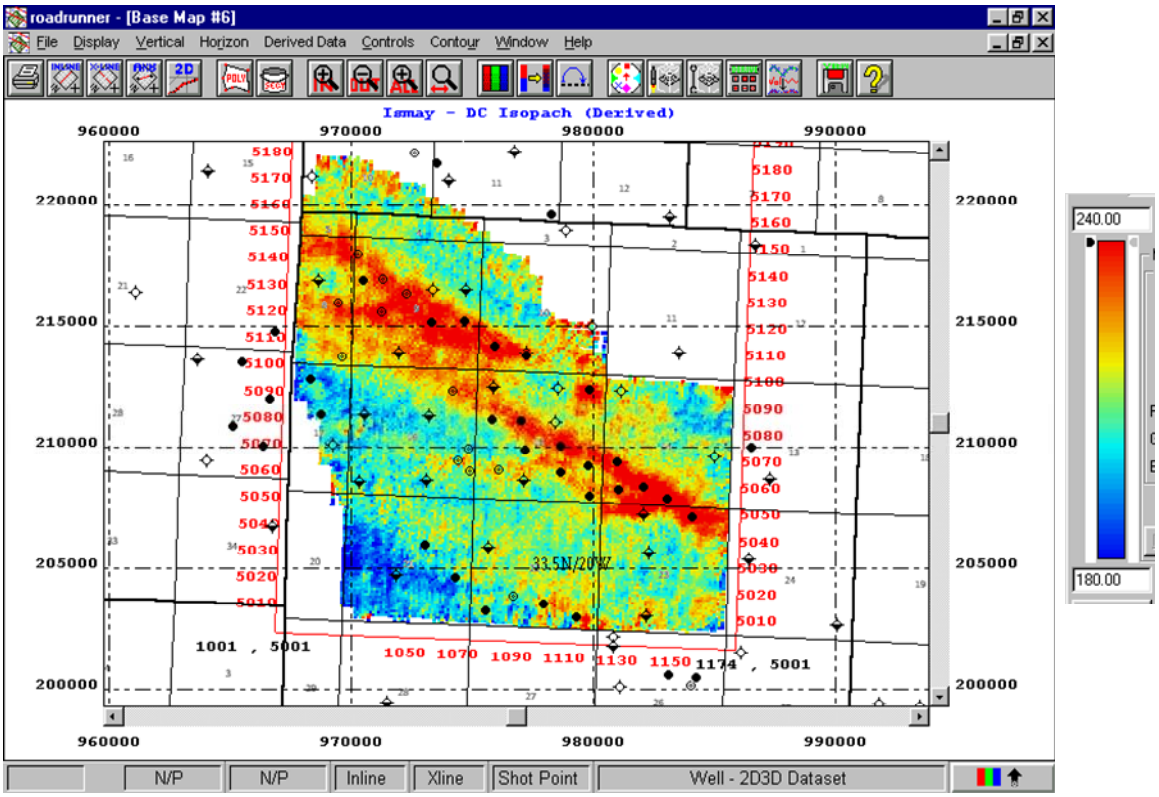

Figure 3. Map showing the isochron thickness between the Ismay and Desert Creek horizons and associated well control. Hot colors represent thickening of the reservoir and show the outline of the algal mound feature quite clearly.

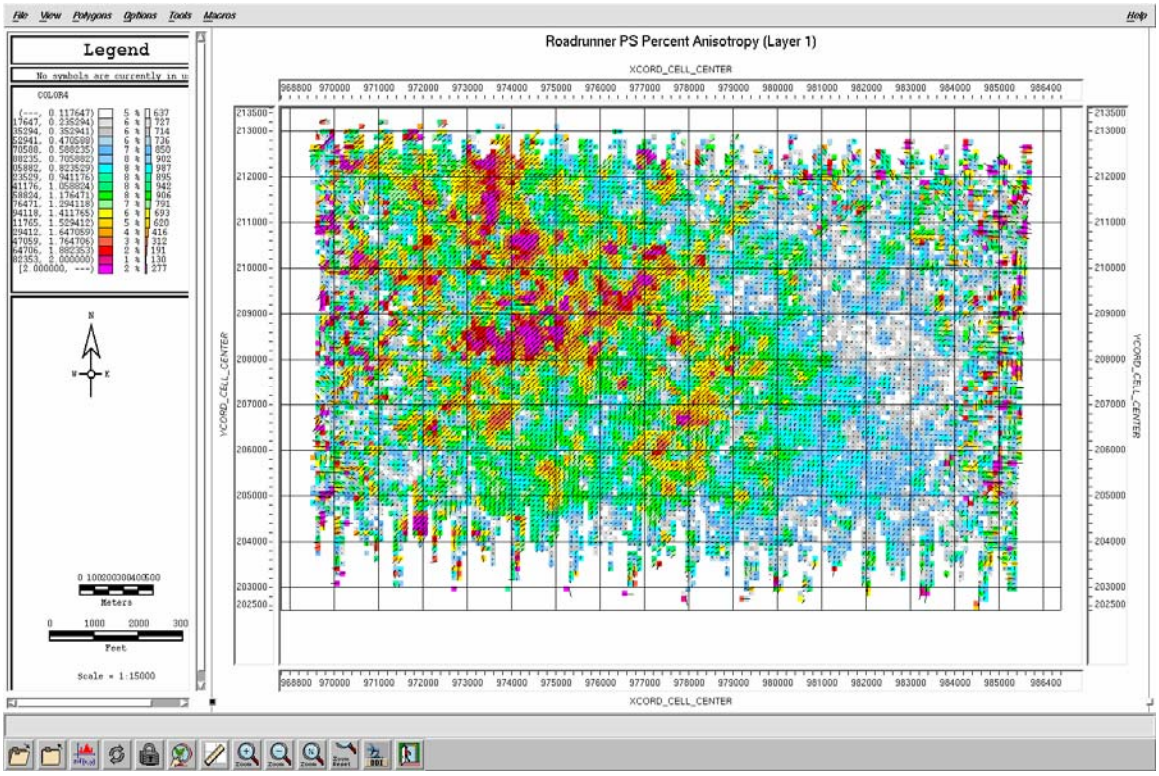

Figure 4. Map showing the S-wave azimuthal anisotropy for the overburden layer above the reservoir. Hot colors represent larger anisotropy measurements, up to 2%, with superimposed vectors indicating the direction of the fast S-wave direction. These anisotropy values are relatively small but still show a potentially interesting negative correlation pattern (NE/SW trend) of weaker anisotropy over the algal mound feature (as shown in Figure 3)